# TRANSPORT STUDIES OF ONE DIMENSIONAL ORGANIC CONDUCTORS

by

Kell Mortensen

DTU December 1979

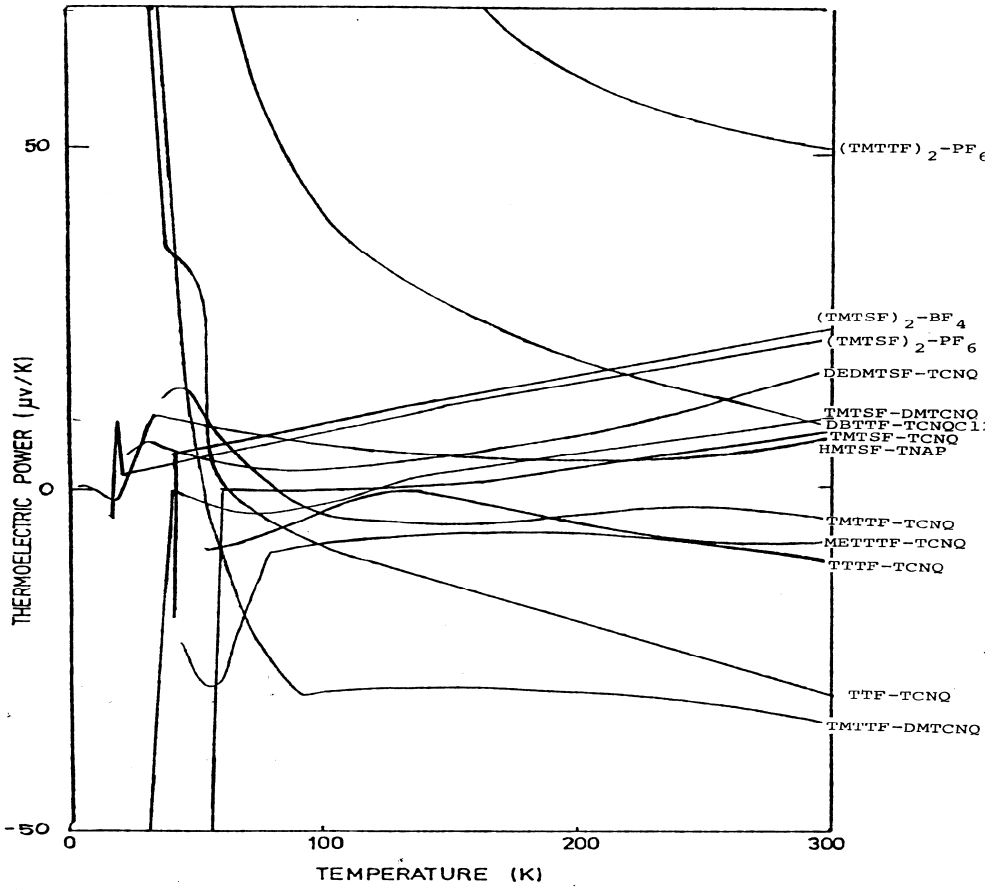


PhD (Lic.Techn) Thesis.
Supervisor, Professor Niels I. Meyer
Co-supervisor, Dr. Claus S. Jacobsen

# TRANSPORT STUDIES OF ONE DIMENSIONAL ORGANIC CONDUCTORS

by

Kell Mortensen

December 1979

## PREFACE

The present thesis is written for partiel fulfilment of the conditions for obtaining the Technical Licentiate Degree (corresponding to Ph.D.). The subject of the work has been studies of highly conducting organic single crystals. The licentiate study was performed at Physics Laboratory III, The Technical University of Denmark, in the period from February 1977 to December 1979.

Organic conductors has been the subject of great international activity during the last decade. One of the most interesting discussions going on in the period of time, while I made this thesis work, was concentrated on the attempt to understand the conduction mechanism in these new synthetic materials. In the present report, I have given special attention to the conductivity and thermoelectric power. The latter parameter has been studied experimentally in a number of compounds. Numerical calculations have been done, assuming electron scattering due to interaction with phonons.

## ACKNOWLEDGEMENTS

First of all, I wish to thank my co-supervisor, Dr. Claus S. Jacobsen, for his great support and encouragement all the way through the work. Likewise I thank Dr. Klaus Bechgaard, H.C. Ørsted Institute, for great support and for supply of samples. I appreciate very much valuable discussions with Dr. Hans J. Pedersen and I would like to thank my supervisor, Professor N.I. Meyer for great help and interests during the work.

Acknowledgements should go to several others from the staff of Physical Laboratory III and the associated workshop. Furthermore I thank Dr. J.R. Andersen, Risø, and Dr. P. Delhaes, Talence-France, for valuable cooperation and supply of samples. Finally I express my gratitude to Ms. Birgit Olsen for preparing all the figures and to Ms. Margot Frederiksen for her careful typing of the manuscript.

The economical basis for my work was a scholarship from the Technical University of Denmark.

Kell Mortensen

ABSTRACT

Studies of transport properties of single crystals of quasi-one-dimensional organic conductors are presented. In particular, the DC-conductivity and the thermoelectric power are treated. Measurements of the temperature dependent thermopower between 4 and 300 K are given for a number of derivatives of the prototype TTF-TCNQ. For the highly conducting compounds, the thermopower has a linear temperature dependence, indicative of coherent conduction. From the slope of S versus T, the bandwidth and charge transfer has been evaluated. For compounds of smaller conductivity, the thermopower results indicate diffusive conduction to occur. Below the phase-transition, the data indicate dominance of impurities. The phase-transition temperatures are clearly marked by anomalies in the S versus T curves.

Numerical calculations of the transport coefficients are presented for TTF-TCNQ, assuming single particle behaviour. The electron scattering is calculated for first and second order coupling to intermolecular modes, and for first order coupling to intramolecular modes.

TABLE OF CONTENT


| | | page |
|---|---|---|
| I | INTRODUCTION | 1 |
| 1.1 | Physics of One-Dimensional Systems | 2 |
| 1.2 | Organic Charge Transfer Salts, e.g. TTF-TCNQ | 6 |
| 1.3 | The Metallic State of TTF-TCNQ | 7 |
| 1.4 | Scope of the Present Work | 11 |
| II | QUASI-ONE-DIMENSIONAL TIGHT BINDING BAND MODEL | 12 |
| 2.1 | One-Dimensional Tight Binding Model | 12 |
| 2.2 | Periodic Modulation of the Transfer Integral | 15 |
| 2.3 | Including Inter-Chain Coupling | 17 |
| III | TRANSPORT COEFFICIENT IN ONE-DIMENSIONAL METALS | 22 |
| 3.1 | The Boltzmann Equation | 22 |
| 3.2 | General Transport Coefficients | 23 |
| 3.3 | Bethe-Sommerfeld Expansion of Transport-Integrals | 28 |
| 3.4 | Two Conduction Bands | 30 |
| 3.5 | Multiple Scattering Processes | 32 |
| 3.6 | Transport Parameters in One-Dimensional Tight Binding Band | 34 |
| IV | SCATTERING MECHANISM IN ORGANIC METALS | 39 |
| 4.1 | Electron-Phonon Interaction in TTF-TCNQ | 40 |
| 4.2 | Electron Coupling to External Modes | 41 |
| 4.3 | One-Phonon Hamiltonian | 42 |
| 4.4 | First-Order Scattering by Acoustic Modes | 46 |
| 4.5 | Two-Phonon Hamiltonian | 52 |
| 4.6 | Transport Properties for Second-Order Electron-Phonon Scattering | 56 |
| 4.7 | Coupling to Internal Modes | 59 |
| 4.8 | Scattering by All First Order Electron-Phonon Interaction | 73 |
| 4.9 | Electron-Electron Interaction | 76 |
| 4.10 | Influence of Lattice Defects and Impurities | 78 |
| V | PHONON DRAG | 84 |
| 5.1 | Resistivity | 84 |
| 5.2 | Thermopower | 86 |

| | | |
|---|---|---|
| VI | TRANSPORT PROPERTIES IN THE NON-METALLIC REGIME | 91 |
| 6.1 | Conductivity | 93 |
| 6.2 | Thermopower | 94 |
| VII | TECHNIQUE USED FOR THERMOPOWER MEASUREMENTS | 104 |
| VIII | THERMOPOWER MEASUREMENTS ON ORGANIC CHARGE TRANSFER SALTS | 114 |
| 8.1 | Thermopower of TTF-TCNQ | 114 |
| 8.2 | Thermopower of some Alkylated derivatives of TTF-TCNQ and TSF-TCNQ: TMTSF-TCNQ, DEDMTSF-TCNQ, TMTTF-DMTCNQ, TMTSF-DMTCNQ and TMTSF-DMTCNQ-MTCNQ | 121 |
| 8.3 | Decomposition of Transport Parameters in TMTSF-DMTCNQ and TMTTF-DMTCNQ | 135 |
| 8.4 | Thermopower of the Salts $(TMTSF)_2X$, $X = PF_6^-$, $AsF_6^-$, $SbF_6^-$, $NO_3^-$, $BF_4^-$, derived from Tetramethyltetraselenafulvalene (TMTSF) | 140 |
| 8.5 | Thermopower of $(TMTTF)_2PF_6$ | 148 |
| 8.6 | Thermopower of HMTSF-TNAP | 150 |
| 8.7 | Thermopower of TTTF-TCNQ and METTF-TCNQ | 155 |
| 8.8 | Thermopower of DBTTF-$TCNQCl_2$ | 156 |
| IX | SUMMARY AND CONCLUSION | 162 |

# CHAPTER I

## INTRODUCTION

In the last decade there has been a large amount of interest in metallic systems that exhibit quasi-one-dimensional electronic properties. Work on 1D conductors has been the subject of several proceedings of conferences |1-5| and summer schools |6-9|, and there have been several reviews in the field |10-15|. The crystals themselves are, of course, three dimensional, but the microscopic structure consists, to a greater or lesser extent, of a collection of weakly coupled, highly conducting chains.

One dimensional metals are of interest because they are expected to exhibit unusual physical properties. One example is the occurence of an intrinsic instability towards the formation of a periodic lattice distortion, the Peierls instability |18|. An interesting aspect of the Peierls distortion is that the superlattice wavevector is determined by the details of the Fermi surface and may bear no simple relation to the lattice periodicity. When the distortion in that way is incommensurate with the lattice, there is no prefered spatial location for the distortion, and hence the phase is free to move through the solid. Further, since the lattice is coupled to the charge density, the periodic lattice distortion is equivalent with a charge density wave (CDW). Thus the collective motion can carry a current, the sliding CDW. This is the mechanism of Fröhlich superconductivity |22|. When the distortion on the other hand is commensurate with the underlying lattice, it will have a preferred position and is unable to move without surmounting an energy barrier. The CDW is said to be pinned. The material is then insulating or semiconducting. Besides commensurability with the lattice, impurities and defects can also pin the CDW.

Another, and probably the most important reason for the intense studies of quasi-one-dimensional conductors is that it to a certain extent is possible for the chemists to synthesize 1D materials with desired physical properties.

A number of materials exhibiting quasi-one-dimensional properties have in the past decade been discovered. One class of com-

pounds is the mixed valence platinum complexes of cyanide or oxalate, including the well known salt $K_2Pt(CN)_4Br_{0.3}\cdot 3H_2O$, usually abbreviated to KCP. The planar arrangement of cyanide anions around the Pt cation allows regular stacking and overlap between the atomic platinum orbitals on adjacent ions, thus forming metallic b nds along the stacking axis. Another important group of materials discovered in the recent years is the polymers of sulphur-nitrogen $(SN)_x$, and of doped polyacetylene $(CH)_x$. Probably the most completely studied group of quasi 1D compounds is the organic conductors consisting of various charge transfer salts. The conduction bands in these organic metals are derived from overlap between $\pi$ electron orbitals of the planar molecules stacked one on top of another. The subject of this thesis is different compounds of this class of quasi 1D materials, all derivatives of the prototype tetrathiofulvalene-tetracyanoquinodimethanide (TTF-TCNQ).

## 1.1 PHYSICS OF ONE-DIMENSIONAL SYSTEMS

If we consider a system that contains an electron gas in equilibrium and we then slightly change the potential which the electrons experience, the result will be a change in the electron density. This density change is usually described by a response function $\chi$, giving the proportionality between the amplitude of the charge density change ($\delta\rho$), and the potential change (v):

$$\delta\rho = -\chi \cdot v \qquad (1.1)$$

Thus the total energy change for the electron system as a result of the potential v, is

$$\delta\varepsilon = -\tfrac{1}{2}\chi \cdot v^2 \qquad (1.2)$$

Generally, the linear equations (1.1) and (1.2) are only valid for simple harmonic oscillating potentials. Therefore, Fourier transformation is always necessary. Then taking the q-component of a given lattice potential

$$v(q) = v_q \cos qr \tag{1.3}$$

one can derive the response function by using second order perturbation theory |23|. The result takes the form

$$\chi_q = \sum_k \frac{f(k) - f(k+q)}{\varepsilon_{k+q} - \varepsilon_k} \tag{1.4}$$

which is known as the Lindhard-function. The sum in (1.4) is over the different values of the wave vectors k for the Bloch states. f(k) is the Fermi-Dirac distribution function and $\varepsilon_k$ is the energy of the electron with momentum $\hbar k$.

Now consider the situation where the potential $v_q$ is derived from displacement $u_q$ of phonon mode q coupled to the electron system through the Hamiltonian (see Chapter IV):

$$H_{ep} = N^{-\frac{1}{2}} \sum_q \sum_k g_q \, c^+_{k+q} \, c_k \, (a_q + a_{+q}) \tag{1.5}$$

$c^+_k(c_k)$ and $a^+_q(a_q)$ are the fermion and boson creation (annihilation) operators, respectively, and $g_q$ is a coupling parameter. In this case, |14|

$$v_q = g_q u_q |2M\omega_q/\hbar|^{\frac{1}{2}} \tag{1.6}$$

where M is the ionic mass and $\omega_q$ is the frequency of the phonon q. If the decrease of energy in the electron system, eq. (1.2), due to a periodic lattice distortion is larger than the elastic energy in the phonon mode q, given by

$$E_q = \tfrac{1}{2}M(\omega_q u_q)^2 \tag{1.7}$$

the ground state of the coupled electron-phonon system has a finite, static amplitude in the phonon mode q. Using equations (1.2), (1.6)

and (1.7), the instability criterion becomes

$$2g_q^2/\hbar\omega_q > 1/\chi_q \tag{1.8}$$

This is the basic condition for a state characterized by a periodic lattice distortion of wavevector q. Besides the coupling parameter $g_q$, the susceptibility, $\chi_q$, is a crucial function. Large values of $\chi_q$ arise for systems where, at a particular value of q, there are many occupied electron-states separated from many unoccupied states by q for which the denominator in (1.4) is close to zero. This corresponds to coupling across the Fermi surface.

In the case of a three dimensional free electron gas, there are only two degenerate states connected by the q-mode (see Fig. 1.1). In a one dimensional metal, on the other hand, the Fermi surface consists of planes at $-k_F$ and $+k_F$. Thus the number of states coupled by the $q=2k_F$ mode diverge. Now the Fermi surface is only sharp at $0^oK$, and taking thermal smearing into account, one will get the temperature dependence |24|

$$\chi_{q=2k_F} \sim \tfrac{1}{2} N(\varepsilon_F) \ln (\varepsilon_F/k_BT) \tag{1.9}$$

where $N(\varepsilon_F)$ is the density of states at the Fermi level $\varepsilon_F$, and $k_B$ is the Boltzmann constant. From (1.9) it appears that the static lattice distortion only occurs below some characteristic temperature $T_p$.

In a regular lattice, a displacement of the ions is opposed by elastic forces that holds the ions in place. The presence of a periodic lattice distortion will, however, produce an additional force on the ions via the charge density change, and thereby modify the phonon frequency to |25|

$$\omega_q = \omega_q^o \left[1 - 2g_q^2 \chi_q(T)/\hbar\omega_q^o\right]^{\frac{1}{2}} \tag{1.10}$$

$\omega_q^o$ being the undressed frequency. Hence for a one-dimensional metal, the frequency of the $q=2k_F$ mode decreases and goes to zero for some low temperature. This behaviour, known as the Peierls instability is illustrated in Fig. 1.2.

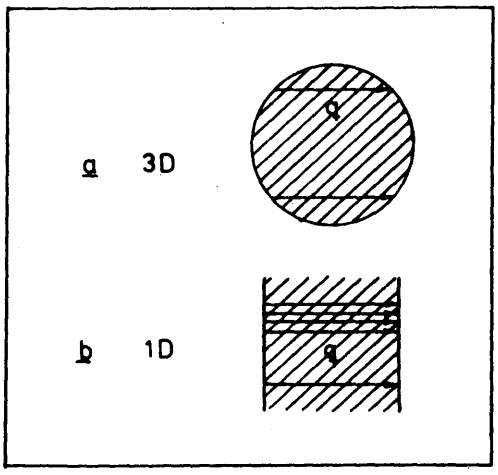


Fig. 1.1. The Fermi surface of a free electron gas. a For three dimensions and b for one dimension. For a given perturbation of wave vector q, only two equal energy states on the FS are coupled in 3D, whereas a set of planes of degenerate states are coupled in 1D.

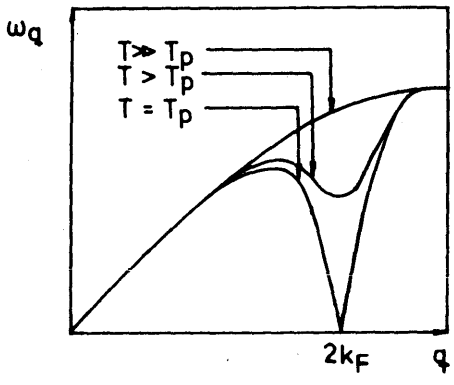


Fig. 1.2 Developement of giant Kohn anomaly in acoustic phonon branch.

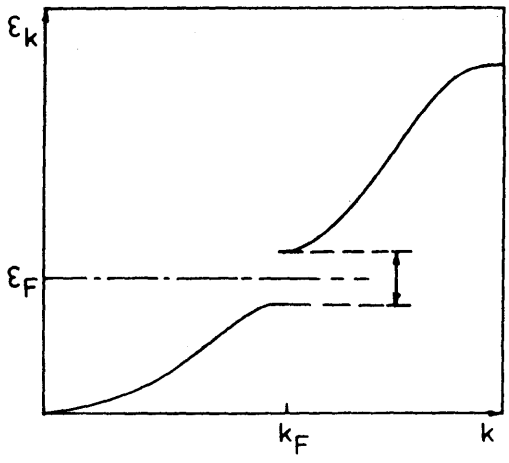


Fig. 1.3 Peierls gap in the energy band at the Fermi level.

In the structural aspects, the Peierls instability is expected to give rise to the following behaviour: At low temperature the static distortion will cause a well defined three dimensional superlattice. At higher temperatures the transverse order may be lost due to thermal disorder. This is the region of the giant Kohn anomaly due to Peierls fluctuations. At still higher temperatures the superlattice will gradually disappear, as the peak in the Lindhard function becomes less pronounced.

The low temperature 3D superlattice will cause a gap in the electronic energy spectrum at the Fermi level, the Peierls gap, thus leaving the material as a semiconductor. Above the 3D-1D transition temperature, the phase of the lattice distortion is pinned only by properties of the single chain. If the CDW is incommensurate with the primitive lattice, there is no preferred position. The phase is then free to move through the material. This Fröhlich mode can clearly carry a current. In a real system the phase will tend to be fixed by impurities, lattice defects or by interchain coupling. Also when the superlattice period is a multiplum (n) of the primitice lattice constant, i.e. is commensurate with the lattice, the CDW will have a prefered position. The CDW is then unable to move without surmounting an energy barrier, $E_{pinning}$, dependent of the order of commensurability (n), |26|

$$E_{pinning} \sim (E_g^2/\varepsilon_F)(E_g/W)^{n-2} \qquad (1.11)$$

where $E_g$ is the Peierls gap and W is the electronic bandwidth.

## 1.2 ORGANIC CHARGE TRANSFER SALTS, e.g. TTF-TCNQ

TTF-TCNQ is a charge-transfer complex formed from the almost planar TTF radical cation and TCNQ radical anion. The amount of charge transfer is 0.59 |27|. The highest occupied electronic states of these molecules are $\pi$-MO's, which means that the wave functions are extended in the direction perpendicular to the plane of the molecule (Fig. 1.5) |28|. The TTF and TCNQ molecules are in the crystalline structure (Fig. 1.6) arranged in segre-

gated stacks along the b-axis. Thereby they form a rather large overlap between the π-orbitals of adjacent molecules in the stacking direction, whereas the interstack overlap is rather small. Thus the material is highly anisotropic and does in fact exhibit many characteristics of one dimensional systems, e.g. the Peierls instability |27|. TTF-TCNQ is therefore usually designated quasi-one dimensional.

All other organic metals that have been prepared have in the same way conduction bands derived from the overlap between π electron orbitals. In some cases the molecules used are simple derivatives of the TTF or TCNQ molecules, e.g. the alkylated compounds |29| which will be discussed in chapter VIII. In other cases one radical is replaced by another organic molecule, e.g. NMP-TCNQ |30|, or by an inorganic molecule, e.g. $(TMTSF)_2-PF_6$ |31| which also will be discussed below. In the latter compound the acceptor molecules do not take part in the formation of conduction bands.

## 1.3 THE METALLIC STATE OF TTF-TCNQ

Among the immediate reasons for the extended research activities in the field of quasi-one-dimensional conductors was the report of a giant conductivity peak in TTF-TCNQ |32|. This large conductivity originally was proposed to be a result of fluctuations toward a superconducting state. Coleman et al. |32| ascribed the state to be of the BCS-type, whereas Bardeen |33| marked that the fluctuations rather were toward the Peierls-Fröhlich state. Since then, more detailed calculations have been attempted in order to explain the conductivity enhancement. Allender et al. |34| used mean field theory to explain the transition into an insulating state as a result of the charge density waves being pinned to the crystal lattice. However, their theory was unable to account for the observed magnitude of the conductivity enhancement. Anderson et al. |35| remarked that the observed magnitude required a mean field temperature of several hundreds degrees rather than the 60K used by Allender et al., Lee, Rice and Anderson |26| thereafter proposed a detailed Ginzberg-Landau model for the metal-insulator

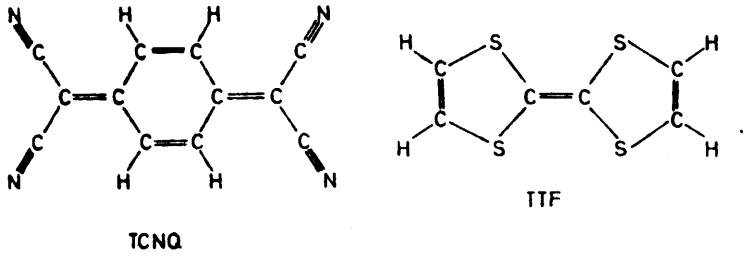


Fig. 1.4 Molecular constituents of TCNQ and TTF.

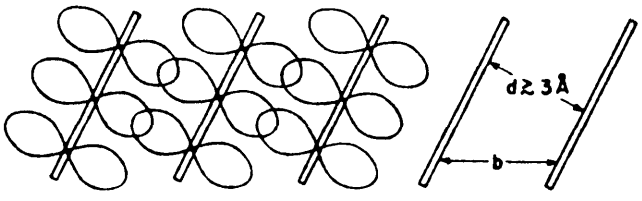


Fig. 1.5 Overlap of π-orbitals on adjacent (TCNQ-) molecules, forming conduction bands. |12|.

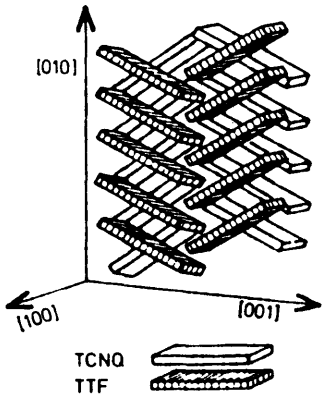


Fig. 1.6 Structure of TTF-TCNQ, showing a herring-bone stacking.

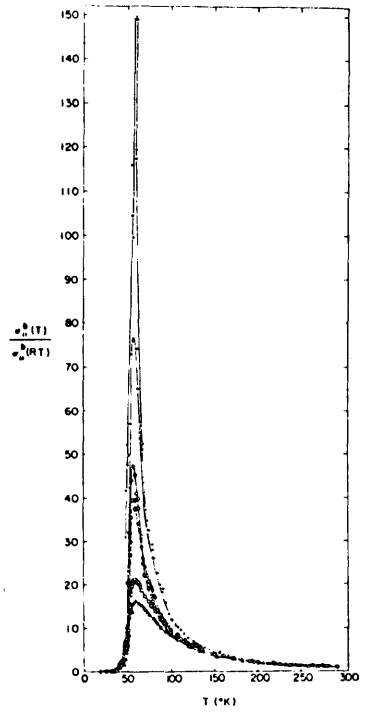


Fig. 1.7 Normalized b-axis conductivity of TTF-TCNQ as a function of temperature |41|.

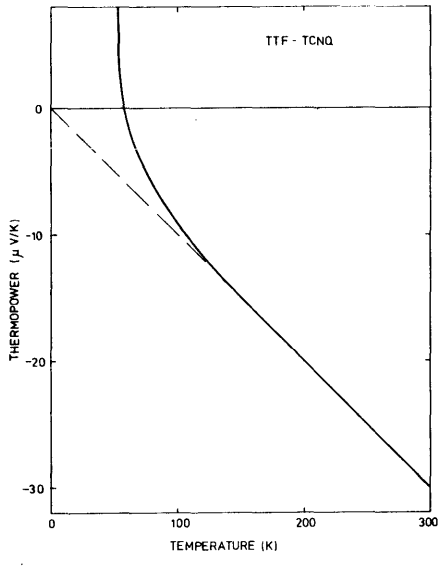


Fig. 1.8 Thermopower of TTF-TCNQ |39 and the present work|.

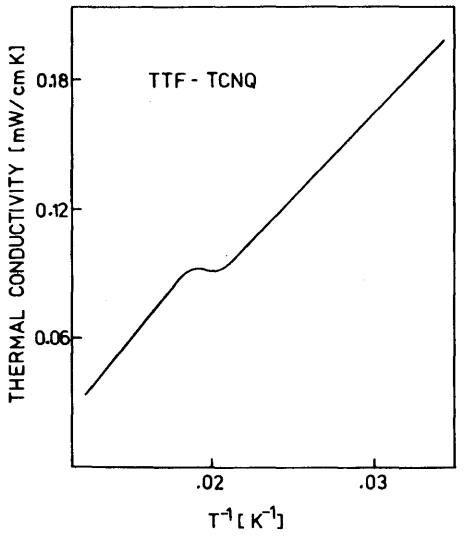


Fig. 1.9 Thermal conductivity of TTF-TCNQ |37|.

transition, which was attributed to three-dimensional ordering of the CDW. The giant conductivity was supposed to arise from sliding CDWs, which could also account for the strongly frequency dependent conductivity and the fall off in the IR range |36|. Support for the model of collective transport in TTF-TCNQ is given by the diffuse X-ray scattering |27|, showing fluctuations into an incommensurate CDW in the temperature range $58K < T < 150K$. However, the recent experiments by Andrieux et al. |153| are probably the best evidence of the fluctuating collective mode. By using high pressure, Andrieux et al. were able to achieve 3:1 commensurability of the periodic distortion with the lattice. The associated commensurability pinning did in fact cause a substantial drop in conductivity.

Nevertheless, there is still considerably scepticism concerning collective transport in TTF-TCNQ, and many attempts are made to reconcile the experimental data with single particle theory. In contrast to the conductivity, a varity of other transport phenomena appear to be consistent with an independent-particle picture. For example, the thermal conductivity (Fig. 1.9) follows approximately the Wiedeman-Franz law |37|. Using the free electron Lorenz number, the decrease in thermal conductivity at 55K yields an electrical conductivity some 25 times the room-temperature value, in fairly good agreement with the $T^{-2.3}$ -law noted empirically |38|. The thermopower (Fig. 1.8) as well is in accordance with a single-particle theory |39|. The high -temperature value is typical for a metallic system, so is the linear temperature dependence. If superconducting fluctuations were essential, we would expect a rather reduced absolute value. DC-Hall effect measurements also confirm single particle conductivity, as $R_H \simeq 1/ne$, where n is the concentration of electrons per molecule on the TCNQ chain |40|.

However, both the thermopower and Hall effect reveal deviations from the simple metallic behaviour below 150K. These deviations could be due to some collective transport mechanism. Thus we believe that the transport in TTF-TCNQ should be divided into three regions: Above 150K, TTF-TCNQ is a simple 1D metal containing independent carriers. In the region $54K < T < 150K$, both single particle motion and collective fluctuations may take part

in the electrical transport, but the degree of collective to single particle motion is rather dependent of the crystal quality. Below 54K, TTF-TCNQ is a semiconductor with an activated number of carriers.

## 1.4 SCOPE OF THE PRESENT WORK

Conduction in one dimensional chains must be extremely sensitive to imperfections, defects and impurities. It is therefore plausible that the measurement of a giant conductivity peak would be observed only in nearly perfect crystals. The thermopower, however, is a zero-current transport measurement and would not be limited by breaks in the chains, assuming that most of the temperature drop occurs across the unbroken regions. Hence, the TEP is one of the best experimentally determined intrinsic parameters.

In the present work we discuss the thermopower and conductivity for some organic quasi-one-dimensional conductors. The work contains two parts, a theoretical and an experimental treatment of the thermopower S) and the conductivity ($\sigma$) for compounds of the family of TTF-TCNQ. The theoretical discussions deal with single particle transport mechanism only. Based on different models known from the literature, the metallic conductivity and thermopower have been calculated numerically for TTF-TCNQ, and the results are compared with experimental data. The expected transport behaviour of semiconductors is treated in view and some simplified considerations for transport in systems dominated by strong Coulomb correlation are described. In Chapter VII the technique used for TEP measurements is described, and in Chapter VIII the experimental thermopower data for a series of organic charge transfer salts are presented. The results are discussed on the basis of the preceeding theoretical calculations. In order to understand the transport properties, we also include the experimental dc-conductivities |51|.

## CHAPTER II

## QUASI-ONE-DIMENSIONAL TIGHT BINDING BAND MODEL

Before discussing the transport properties of the organic quasi-one-dimensional systems, it is useful to understand the electronic band structure that emerges from the crystal structure, in some more detail |28, 42-44|.

The microscopic interactions of molecules in a solid may be obtained from molecular orbital (MO) calculations of their electronic wave functions. A particular useful MO technique for large organic molecules is the extended Hückel Method |28|. By this method, MO's are constructed from linear combinations of atomic Slater orbitals. The solid-state analogue of the extended Hückel method is the tight-binding approximation in which Bloch wave-functions, $\psi_k$, for the crystal are formed from linear combinations of molecular orbitals $\phi_j$ |45|.

$$\psi_k(r) = \sum_{\ell} \phi(r-\ell) e^{ik\ell} \qquad (2.1)$$

where k is the wave vector.

Application of the extended Hückel Method reveals that the highest occupied states of large and planar organic molecules are π-MO's, formed from linear combinations of atomic $p_z$ functions, where z is the direction normal to the plane of the molecule. In the conducting organic systems, the molecules stack in segregated acceptor and donor colums, and the π-orbital cause a relatively large overlap in the stacking direction (Fig. 1.5). In terms of the transfer integrals, these overlaps will be denoted $t_F$ and $t_Q$ for the donor and acceptor stacks respectively. In the absence of any coupling between the stacks, we would get two independent conduction bands.

However, in general one should also include interstack overlap, although they are expected to be small compared to the intrastack overlap.

### 2.1 ONE-DIMENSIONAL TIGHT BINDING MODEL

In the absence of any coupling between molecules beyond the

nearest neighbor intrastack interaction, the tight binding Hamiltonian is in the form

$$H = -t_Q \sum_{i\sigma} \left[ (c^Q_{i\sigma})^+ (c^Q_{i+1,\sigma}) + h.c. \right]$$

$$-t_F \sum_{i\sigma} \left[ (c^F_{i,\sigma})^+ (c^F_{i+1,\sigma}) + h.c. \right]$$

$$+ \varepsilon_o \sum_{i\sigma} (c^Q_{i,\sigma})^+ c^Q_{i\sigma} \qquad (2.2)$$

where $c_i^+$ and $c_i$ are the creation and annihilation operators, t is the intrastack transfer integral and $\varepsilon_o$ is essentially the electron affinity of the acceptor molecule (Q) relative to the ionization potential of the donor (F) |42|. In order to calculate the electron dispersion function, equation (2.2) must be Fourier transformed:

$$H = -t_Q \sum_{k,\sigma} \left[ (c^{Q1}_{k,\sigma})^+ c^{Q2}_{k,\sigma} e^{ikr} + h.c. \right]$$

$$-t_F \sum_{k\sigma} \left[ (c^{F1}_{k,\sigma})^+ c^{F2}_{k,\sigma} e^{ikr} + h.c. \right]$$

$$+ \varepsilon_o \sum_{k\sigma} (c^Q_{k,\sigma})^+ c^Q_{k,\sigma} \qquad (2.3)$$

The energy spectrum resulting from this Hamiltonian separates into two independent bands connected to each kind of molecular stack,

$$\varepsilon_F = -2t_F \cos kb \qquad (2.4a)$$

$$\varepsilon_Q = -2t_Q \cos kb + \varepsilon_o \qquad (2.4b)$$

where k is the wave number corresponding to the chain direction. Detailed calculations of the transfer integrals for TTF-TCNQ lead to a "normal" TCNQ band ($t_Q > 0$) and an "inverted" TTF band ($t_F < 0$), as shown in Fig. 2.1 |28| . The system charge neutrality requires that the two bands intersect at the Fermi momentum $k_F$, thus $k_F$ is related to the charge transfer $\rho$, through

$$k_F b = \pi\rho/2 \tag{2.5}$$

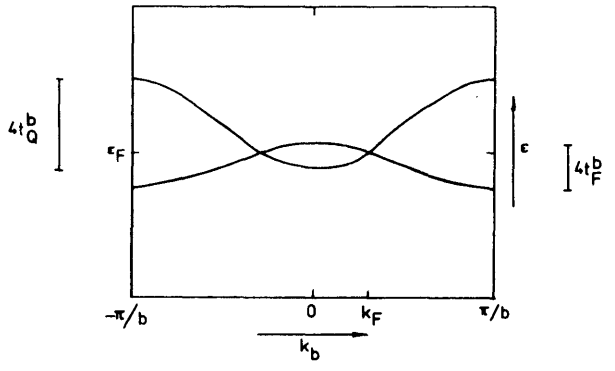


Fig. 2.1 Schematic band structure for an organic charge transfer salt containing two independent molecule-stacks.

The density of states for these cosine-bands is calculated to

$$N(\varepsilon) = \frac{dN}{dk}\frac{1}{d\varepsilon/dk} = \frac{N}{\pi}\frac{1}{|t|}\{1 - \cos^2 kb\}^{-\frac{1}{2}} \tag{2.6}$$

as $dN/dk = 2Nb/\pi$. It is often suitable to rewrite (2.6) in terms of the energy. If for simplification we choose the energy-origin as $\varepsilon(k=0) = 0$, we get $N(\varepsilon)$ in the form

$$N(\varepsilon) = 2N/\pi\ [\varepsilon(w-\varepsilon)]^{-\frac{1}{2}} \tag{2.7}$$

where $w = 4t$ is the bandwidth.
The equations (2.4) lead in the reciprocal space lattice to constant-energy surfaces that are planar and parallel. These surfaces have an energy-independent area, a fact of importance for the transport properties. For a compound with crystal structure like that of TTF-TCNQ, the area of the energy-surface is given by

$$\mathcal{S}(\varepsilon) = \mathcal{S}(\varepsilon_F) = 2 \times \frac{2\pi}{a} \times \frac{2\pi}{c/2} = \frac{16\pi^2}{ac} \tag{2.8}$$

The unit cell is here chosen to include only one of each molecule. Actually, this is not the proper Wigner-Seitz cell, which must include two of each molecules because of the alternating tilt arrangement in the crystal structure (Fig. 1.6). With this comment in mind, however, it is in the transport calculations advantageous to use the cell leading to eq. (2.8).

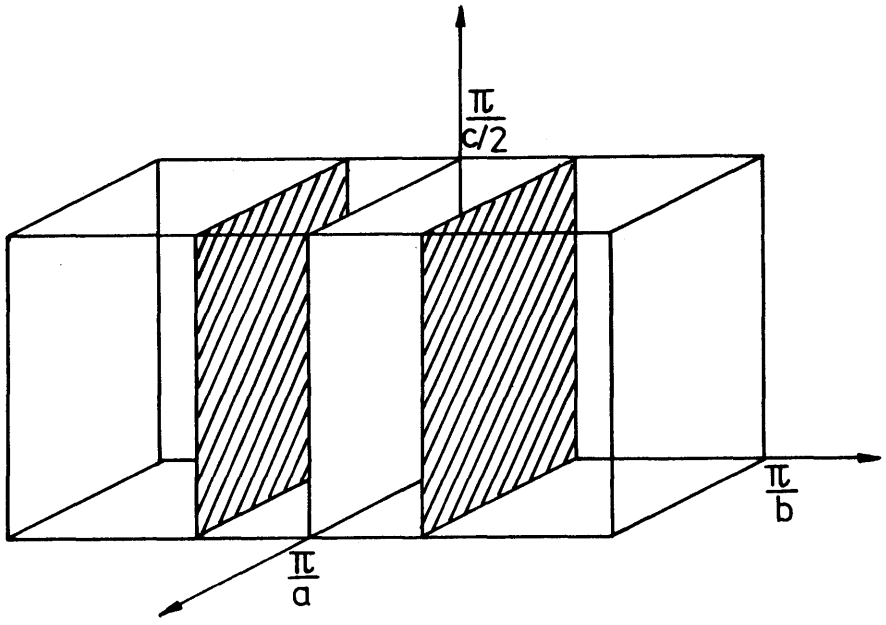


Fig. 2.2 Fermi surface in 1D metal (TTF-TCNQ)

## 2.2 PERIODIC MODULATION OF THE TRANSFER INTEGRAL

If the intrachain transfer integral is periodically modulated for some reason, e.g. by the electronic interaction with the phonon system leading to the Peierls distortion, the conduction band will split into two or more bands. We will as an example make a calculation for a trimerized chain, which can be taken as a rough approach to the Peierls distortion in TTF-TCNQ. Generally, such calculations can only be done analytically when the modulation is commensurate with the lattice.

The tight binding Hamiltonian of this trimerized system is given by (See fig. 2.3b)

$$H = \sum_{\ell} t(a_{\ell}^{+}b_{\ell}+b_{\ell}^{+}a_{\ell}+b_{\ell}^{+}c_{\ell}+c_{\ell}^{+}b_{\ell}) + \sum_{\ell}(t-\delta)(c_{\ell}^{+}a_{\ell+1}+a_{\ell+1}^{+}c_{\ell}) \tag{2.9}$$

In the Fourier transformed representation, this can be written

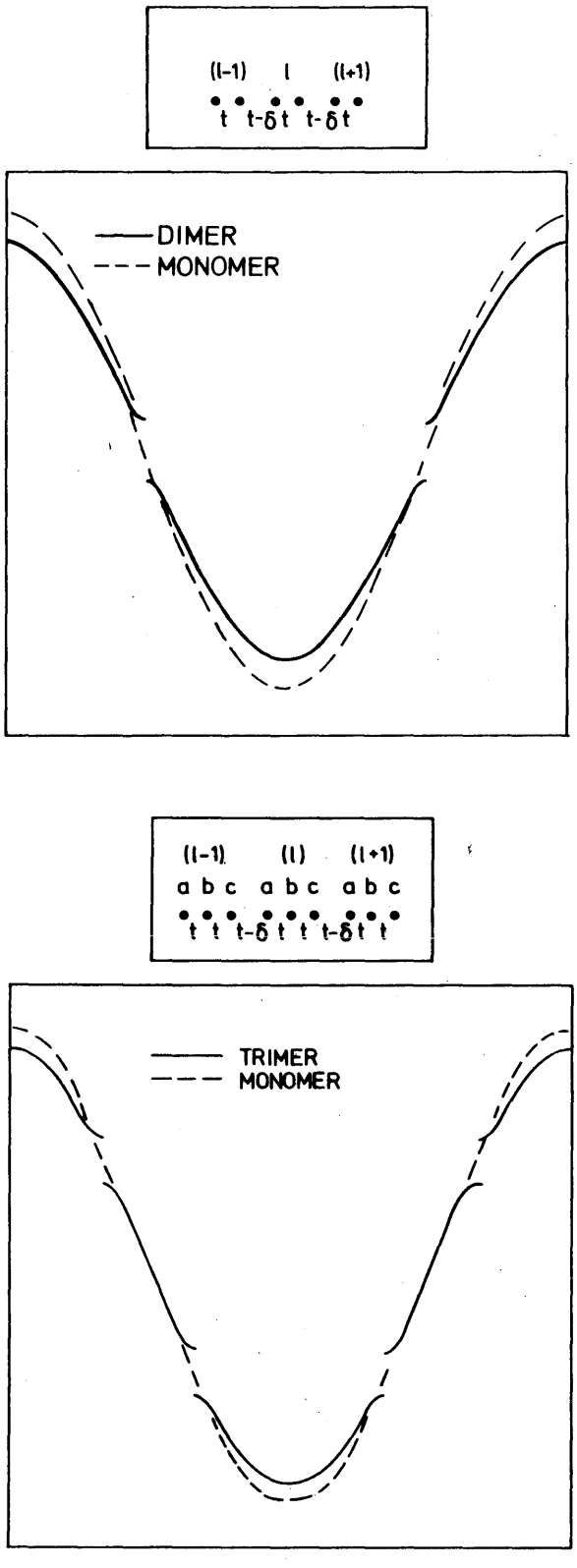


Fig. 2.3 Tight binding bands of dimerized and trimerized chains. t = -100 meV and $\delta$ = -22 meV.

$$H = \sum_k (a_k^+ b_k^+ c_k^+) \begin{pmatrix} 0 & t & (t-\delta)e^{-i3kb} \\ t & 0 & t \\ (t-\delta)e^{i3kb} & t & 0 \end{pmatrix} \begin{pmatrix} a_k \\ b_k \\ c_k \end{pmatrix} \qquad (2.10)$$

leading to the electron energy

$$\varepsilon_k = \omega \cos\left[\tfrac{1}{3}\mathrm{Arccos}(u\cos 3kb) + j2\pi/3\right], \quad j = 1,2,3 \qquad (2.11)$$

where

$$\omega = 2\{(2t^2 + (t-\delta)^2)/3\}^{\frac{1}{2}}$$

$$u = 3\sqrt{3}\, t^2(t-\delta)/\left[2t^2 + (t-\delta)^2\right]^{3/2}$$

The energy equation (2.11) corresponds to a splitting of the regular tight binding band into three bands separated with a gap of the order of $\delta$. In Fig. 2.3 an example is shown, with $t = -100$ meV and $\delta = -22$ meV. We also show the result for a dimerized band with the same magnitude of t and $\delta$.

## 2.3 INCLUDING INTER-CHAIN COUPLING

The interchain coupling will destroy the simple planar shape of the Fermi surface. The actual form depends primarily on the relative transfer integrals between neighbouring molecules, and is therefore very sensitive to the crystal structure.

### TTF-TCNQ

We will shortly look at the Fermi surface in a system with crystal structure like that of TTF-TCNQ. Conventionally, the nearest neighbour transfer integrals are denoted |44|

$$t_{F_1F_2}(0,1,0) = t_{F_2F_2}(0,1,0) \equiv t_F \qquad (2.12a)$$

$$t_{Q_1Q_1}(0,1,0) = t_{Q_2Q_2}(0,1,0) \equiv t_Q \qquad (2.12b)$$

$$t_{F_1Q_1}(\tfrac{1}{2},-1,0) = t_{F_2Q_2}(\tfrac{1}{2},1,0) \equiv t^a_{FQ} \qquad (2.12c)$$

$$t_{F_1F_2}(0,\tfrac{1}{2},\tfrac{1}{2}) \equiv t^c_F \qquad (2.12d)$$

$$t_{Q_1Q_2}(0,\tfrac{1}{2},\tfrac{1}{2}) \equiv t^c_Q \qquad (2.12c)$$

$$t_{F_1Q_2}(-\tfrac{1}{2},-\tfrac{1}{2},-\tfrac{1}{2}) = -t_{Q_1F_2}(-\tfrac{1}{2},-\tfrac{1}{2},-\tfrac{1}{2}) \equiv \nu \qquad (2.12f)$$

where $F_i$ and $Q_i$ denotes the molecular wave functions referring to Fig. 2.4. The transfer integral between donor and acceptor molecules situated in the same b-c plan along the a axis vanish as a result of opposite symmetry of the TTF-|46| and the TCNQ-wave function |47| :

$$t_{F_1Q_1}(\tfrac{1}{2},0,0) = t_{F_2Q_2}(\tfrac{1}{2},0,0) \equiv 0 \qquad (2.12g)$$

(The finite conductivity measured in the a-direction must thus mainly be via the $t^a_{FQ}$-integral). Shitzkovsky et al. |44| showed that the tight binding energy matrix resulting from these transfer integrals, eq. (2.12 ), is only reducible when $\nu = 0$. In that case, $\varepsilon(k)$ is given by

$$\varepsilon(k_a k_b, k_c) =$$

$$\left[(t_F+t_Q)\cos k_b b + 2(-t^c_F+t^c_Q)\cos(\tfrac{1}{2}k_b b)\cos(\tfrac{1}{2}k_c c) + \tfrac{1}{2}\varepsilon_o\right] \pm$$

$$\left[\{(t_F-t_Q)\cos k_b b + 2(-t^c_F-t^c_Q)\cos(\tfrac{1}{2}k_b b)\cos(\tfrac{1}{2}k_c c) - \tfrac{1}{2}\varepsilon_o\}^2 + \right.$$

$$\left. 16(t^a_{FQ})^2 \sin^2(k_b b)\cos^2(\tfrac{1}{2}k_a a)\right]^{\frac{1}{2}} \qquad (2.13)$$

where $\varepsilon_o$ is the ionization potential discussed in connection with eq. (2.2), and determines the charge transfer, as |44|

$$\varepsilon_o = 2(t_F - t_Q)\cos(\pi\rho/2) \qquad (2.14)$$

Only when the $t^a_{FQ}$-integral further is neglected, the Fermi Surface will extend across the whole Brillouin Zone (Fig. 2.5).

Eg. (2.13) is then reduced to the two bands

$$\varepsilon(k_a,k_b,k_c) = \begin{cases} 2t_F\cos k_b b - 2t_F^c\cos(\tfrac{1}{2}k_b b)\cos(\tfrac{1}{2}k_c c) \\ 2t_Q\cos k_b b - 2t_Q^c\cos(\tfrac{1}{2}k_b b)\cos(\tfrac{1}{2}k_c c) + \varepsilon_o \end{cases} \qquad (2.15)$$

both independent of $k_a$. Including $t_{FQ}^a$ causes the FS to contract and should result in a rather small FS when this parameter is large compared to $t_F^c$ and $t_Q^c$. A rough example is shown in Fig. 2.6 |44|. Including further the $\nu$-parameter destroys the otherwise rather high symmetry between electron and hole surfaces. In addition, there is no longer overlap between the electron and hole surfaces, and the FS degenerates into pockets of electrons and holes |44|, Fig. 2.7.

Thus, the organic charge transfer salts are very sensitive to the magnitude of interchain coupling. If these are not negligible compared to the intrachain coupling, the compounds will be semimetallic or semiconducting rather than metallic.

HMTSF-TCNQ |43|

Discussing the shape of the Fermi surface for TTF-TCNQ it was seen that the transfer integral between chains leads to non-planar surfaces. The integrals between alike chains ($t_F^c$, $t_Q^c$) resulted in a large FS and hence a metallic density of states, whereas the integrals between unlike chains ($t_{FQ}^a$, $\nu$) caused a covalency gap, i.e. a vanishing density of states at the Fermi level.

In compounds with structure like that of HMTSF-TCNQ, the neighbours are unlike in both directions perpendicular to the stacking direction |48| . Therefore, one would expect a vanishing FS and a semiconducting behaviour, in contrast to experiments |49|. A phenomenological model explaining this apparent paradox has been deduced by Weger |43|. The relatively short Se-N distance in HMTSF-TCNQ may cause the two center integrals interacting with an excited state of HMTSF, and displace the TCNQ energy level. Rough calculations lead then to a 1D metallic

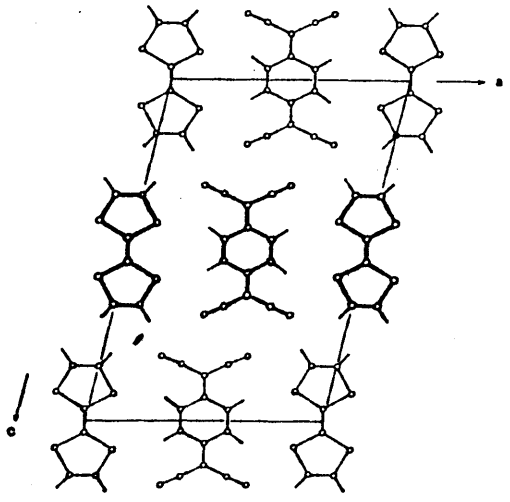

Fig. 2.4 A view normal to the a-c plan of TTF-TCNQ.

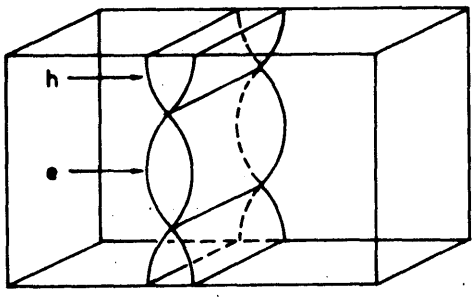


Fig. 2.5 Fermi surface for the case of $t_F^c$, $t_Q^c \neq 0$ and $t_{FQ}^a = \nu = 0$.

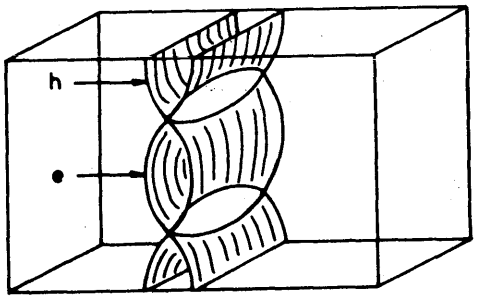


Fig. 2.6 Fermi surface for the case of $t_F^c$, $t_Q^c$, $t_{FQ}^a \neq 0$ and $\nu = 0$.

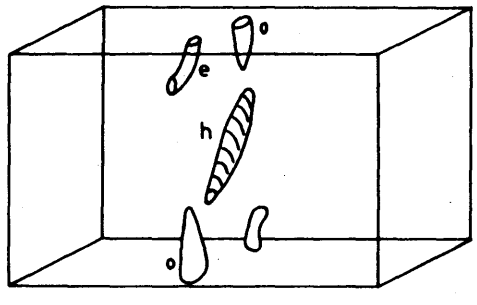


Fig. 2.7 Fermi surface for the case of $t_F^c$, $t_Q^c$, $t_{FQ}^a$, $\nu \neq 0$.

high-temperature state, and a 3D semimetallic low-temperature state, in good agreement with experiments.

CHAPTER III

## TRANSPORT COEFFICIENTS IN ONE-DIMENSIONAL METALS

A number of experimental high-temperature properties of TTF-TCNQ were in chapter I attributed to an independent particle behaviour. In connection to that we will in the present chapter assume that the electrical transport properties may be described within the framework of conventional linearized Boltzmann theory.

### 3.1 THE BOLTZMANN EQUATION |52|

The local distribution function is in equilibrium determined by use of Fermi-Dirac statistics

$$f_k^o(\bar{r}) = \{1 + \exp([\varepsilon_k - \varepsilon_F]/k_B T)\}^{-1} \tag{3.1}$$

where $\varepsilon_F$ is the Fermi-energy and $k_B$ the Boltzmann constant. However, in the presence of applied fields and temperature gradients, the distribution function will deviate somewhat from the equilibrium value

$$f_k(r) = f_k^o(r) + g_k(r) \tag{3.2}$$

In steady-state the rate of change in $f_k$ must be zero. Now, this rate is caused by three physical effects: diffusion, external fields and scattering of carriers from one state to another. By use of Liouville's theorem, this leads in the presence of an electrical field (E), to

$$v_k \nabla_r f_k - \hbar^{-1} eE \nabla_k f_k = \partial f_k/\partial t|_{sc} \tag{3.3}$$

where -e is the carrier charge and $v_k = (1/\hbar)\nabla_k \varepsilon_k$ is the velocity, and sc stand for the change in $f_k$ due to scattering. In the region of "linear transport theory", it is assumed that $g_k/f_k^o << 1$. To first order in $g_k$, eq. (3.3) then gets the form

$$v_k \frac{\partial f_k^o}{\partial T} \nabla_r T - v_k e E \frac{\partial f_k^o}{\partial \varepsilon_k} = \left.\frac{\partial f_k}{\partial t}\right|_{sc} \tag{3.4}$$

which is the linearized Boltzmann equation. When this equation has been solved, the macroscopic current densities of charge and heat can be calculated from their respective definitions:

$$J = -2 \int e\, v_k\, f_k\, dk \tag{3.5a}$$

$$Q = 2 \int (\varepsilon_k - \varepsilon_F)\, v_k\, f_k\, dk \tag{3.5b}$$

Generally the problem in solving the Boltzmann equation is the complexity of the scattering term, which involves all occupied states. Roughly it is given by the difference between electron transition rate into the state k, and electron transition rate out of k. In integral form this should be written

$$\left.\frac{df_k}{dt}\right|_{sc} = \int \left[P(k',k) f_{k'} (1-f_k) - P(k,k') f_k (1-f_{k'})\right] \cdot dk' \tag{3.6}$$

where the first term represents the scattering into k and the second the scattering out of k. $P(k_1,k_2)$ is the probability of transition from the state $k_1$ to the state $k_2$, by any kind of scattering mechanism. The scattering term, eq. (3.6), can not in general be simplified further, but for certain types of interactions it can be shown that the scattering is in the form

$$\frac{\partial f_k}{\partial t} = - \frac{f_k - f_k^o}{\tau_k} \tag{3.7}$$

where $\tau_k$ then is called the relaxation time.

## 3.2 GENERAL TRANSPORT COEFFICIENTS |52|

In the relaxation time approximation (3.7) the Boltzmann-equation is given in the form

$$-v_k \frac{\varepsilon_k - \varepsilon_k}{T} \left(\frac{\partial f_k^o}{\partial \varepsilon_k}\right) \nabla_r T - v_k e \frac{\partial f_k^o}{\partial \varepsilon_k} E = - \frac{f_k - f_k^o}{\tau_k} \tag{3.8}$$

where $\partial f_k^o/\partial T$ has been deduced. Thus, the steady-state distribution becomes

$$f_k = f_k^o + \tau_k v_k \left(-\frac{\partial f_k^o}{\partial \varepsilon_k}\right)\left[\frac{\varepsilon_k-\varepsilon_F}{T}\ (-\nabla_r T) - eE\right] \qquad (3.9)$$

In equilibrium there is by definition no electrical or heat flow. Therefore the $f_k^o$-term of (3.9) must vanish when used in (3.5). The steady-state transport integrals are thereby

$$J = -2\int e\tau_k v_k v_k\left[\frac{\varepsilon_k-\varepsilon_F}{T}\ (-\nabla_r T) - eE\right](-\frac{\partial f_k^o}{\partial \varepsilon_k})\,d^3k \qquad (3.10a)$$

$$Q = 2\int(\varepsilon_k-\varepsilon_F)\tau_k v_k v_k\left[\frac{\varepsilon-\varepsilon_F}{T}(-\nabla_r T) - eE\right](-\frac{\partial f_k^o}{\partial \varepsilon_k})\,d^3k \qquad (3.10b)$$

which should be expressed in the general form

$$J = e^2 K_o E + (e/T)K_1(-\nabla_r T) \qquad (3.11a$$

$$Q = eK_1 E + (1/T)K_2(-\nabla_r T) \qquad (3.11b)$$

since E and $\nabla_r T$ are independent of the momentum. The coefficients in (3.11) can all be expressed in the common way

$$K_n = 2\int(\varepsilon-\varepsilon_F)^n\ \tau_k v_k v_k(-\frac{\partial f_k^o}{\partial \varepsilon_k})\ d^3k \qquad (3.12)$$

which in general are tensors. It is normally advantageous to transform these transport integrals from being over a volume in k-space into an integration over surfaces of constant energy:

$$d^3k \to (\frac{1}{2\pi})^3 \int\frac{d\sigma}{|d\varepsilon_k/\partial k|}\ d\varepsilon_k \qquad (3.13)$$

by which

$$K_n = 2/(2\pi)^3 \iint(\varepsilon_k-\varepsilon_F)^n\ \tau_k v_k v_k\ \frac{d\sigma}{|d\varepsilon_k/dk|}\ (-\ \frac{\partial f_k^o}{\partial \varepsilon_k})\ d\varepsilon_k \qquad (3.14)$$

In a one-dimensional metal the energy-surfaces are independent of $\varepsilon_k$, as discussed in chapter 2 (eq. 2.8). The transport tensor

$K_n$ then has only a finite component in the chain-direction, given by

$$K_n = \frac{2}{\hbar} \frac{\mathcal{S}}{(2\pi)^3} \int (\varepsilon_k - \varepsilon_F)^n \tau_k v_k (- \frac{\partial f_k^o}{\partial \varepsilon_k}) d\varepsilon_k \qquad (3.15)$$

as $|d\varepsilon_k/dk| = \hbar v_k$.

Electrical conductivity

The electrical conductivity is defined by the relation

$$J = \sigma E \qquad (3.16)$$

for a specimen at constant temperature ($\nabla_r T = 0$). Hence, from (3.11) and (3.15) we have

$$\sigma = e^2 K_o = \frac{2e^2}{\hbar} \frac{\mathcal{S}}{(2\pi)^3} \int \tau(\varepsilon_k) v(\varepsilon_k) (- \frac{\partial f_k}{\partial \varepsilon_k}) d\varepsilon_k \qquad (3.17)$$

which is an integral over the single electron states. It is often suitable to elucidate the macroscopic $\sigma$ as a sum of the conductivity distributions from each single electron state, by rewriting (3.17) to the form

$$\sigma = \int \sigma(\varepsilon_k) d\varepsilon_k \qquad (3.18)$$

Thermal conductivity

The thermal conductivity of the electron system will not be discussed in detail in this work. However, in relation to the later discussion concerning thermopower in systems with more than one scattering mechanism, it is advantageous to make a few comments. The thermal conductivity ($\kappa$) is defined for a specimen in an open electric circuit, to prevent any electrical current flowing through it:

$$Q = \kappa (-\nabla_r T)_{J=0} \qquad (3.19)$$

Thus, from (3.11)

$$\kappa = T^{-1} (K_2 - K_1^2/K_o) \qquad (3.20)$$

The "correction" $K_1^2/K_o$, which results from setting the current and not the field to zero, is negligible compared to $K_2$ in common metallic systems. Thus

$$\kappa \simeq T^{-1} K_2 \tag{3.21}$$

In terms of (3.18), this should be written

$$\kappa \simeq T\left(\frac{k_B}{e}\right)^2 \int \left(\frac{\varepsilon_k-\varepsilon_F}{k_B T}\right)^2 \sigma(\varepsilon_k)\, d\varepsilon_k \tag{3.22}$$

Thermoelectric power

The general transport equations (3.11) show that there are interacting effects between the electrical and the thermal currents, the thermo-electric effects. One of these is the thermopower, also named as the Seebeck-effect after T.J. Seebeck (1770-1831). It is defined by the ratio of electric field to thermal gradient in the absence of electric currents:

$$E = S \nabla_r T \Big|_{J=0} \tag{3.23}$$

Hence S is in terms of the general transport coefficients (3.11) given by

$$S = -(eT)^{-1} K_1/K_o \tag{3.24}$$

However, in the Boltzmann theory leading to (3.11) and (3.24) only the dynamics of the electron system is taken into account. The phonon system is assumed to be in equilibrium. But when there is a thermal gradient over a specimen there is certainly a flow of phonons from the hot to the cold end. Such a phonon-flow will drag charge carriers and thereby make an additional thermoelectric effect, the phonon-drag TEP($S_g$). In a later chapter we will discuss this term explicitly, whereas only the "diffusive" TEP (3.24) will be treated in the present and subsequent chapters.

In terms of the single electron state conductivity distribution, the thermopower can by use of (3.24), (3.15) and (3.18) be

written in the form

$$S = -\frac{k_B}{e}\int \frac{\varepsilon_k-\varepsilon_F}{k_BF}\ \frac{\sigma(\varepsilon_k)}{\sigma}\ d\varepsilon_k \tag{3.25}$$

which is the Kubo-Greenwood formula given by Fritzsche |53|.

We will in addition to the thermopower mention another thermoelectric effect: The Peltier effect, $\Pi$. This is in a way conjugated to the Seebeck effect. By sending an electric current through a specimen in the absence of a thermal gradient, there will be a flow of heat:

$$Q = \Pi \cdot J|_{\nabla_r T=0} \tag{3.26}$$

By use of (3.11), we find

$$\Pi = e^{-1}\ K_1/K_o \tag{3.27}$$

The Peltier coefficient appears to have a rather simple physical explanation. If (3.27) is rewritten in terms of (3.18) $\Pi$ gets the form

$$\Pi = -\int \frac{\varepsilon_k-\varepsilon_F}{e}\ \frac{\sigma(\varepsilon_k)}{\sigma}\ d\varepsilon_k \tag{3.28}$$

Hence $\Pi$ is identified as the energy carried by the electrons per unit charge. By combination of (3.24) and (3.27) we further get the Kelvin relation between S and $\pi$

$$S = \Pi/T \tag{3.29}$$

From the expressions (3.25) and (3.28) we notice that the sign of S and $\Pi$ are determined by whether the dominating conduction mechanism takes place above or below the Fermi-level. This will in most situations lead to negative values for systems with less than half filled band (electron-like) and positive values for systems of more than half filled band (hole-like). However, a further discussion must include a specific band, e.g. tight

binding band, and also specific kind of scattering mechanism, as $\sigma(\varepsilon) \sim -\tau(\varepsilon) \cdot d\varepsilon/dk \cdot df/d\varepsilon$.

## 3.3 BETHE-SOMMERFELD EXPANSION OF THE TRANSPORT-INTEGRALS

The integrals appearing in the linearized transport equations (chapter 3.2) do not in general represent known functions. They are consequently evaluated either numerically or by expansion into power series. Often the latter method is preferred in order to explain the transport behaviour in terms of simple physical pictures.

In simple metallic systems the distribution is highly degenerated, i.e.

$$k_B T/\varepsilon_F << 1 \tag{3.30}$$

The transport integrals can then be treated by Bethe-Sommerfeld expansion, by which the integrals are expanded with $k_B T/\varepsilon_F$ as parameter. In the general form, we have |54|:

$$\int_0^\infty \Phi(\varepsilon_k)\left(-\frac{\partial f_k^o}{\partial \varepsilon_k}\right) d\varepsilon_k = \tag{3.31}$$

$$\Phi(\varepsilon_F) + 2c_2 (k_B T)^2 \left.\frac{d^2\Phi}{d\varepsilon_k^2}\right|_{\varepsilon_F} + \ldots$$

All odd terms in the power series vanish and the even terms are given by

$$c_{2r} = \sum_{s=0}^{\infty} (-1)^s/(s+1)^{2r} \tag{3.32}$$

Usually it is not necessary to include terms beyond the second power

$$\int_0^\infty \Phi(\varepsilon_k)\left(-\frac{df_k}{d\varepsilon_k}\right) d\varepsilon_k \simeq \Phi(\varepsilon_F) + \frac{\pi^2}{6} (k_B T)^2 \Phi''(\varepsilon_F) \tag{3.33}$$

In the case of electrical conductivity, we identify the Φ-function in (3.17) with

$$\Phi(\varepsilon_k) = \frac{2e^2}{\hbar} \frac{\mathcal{S}}{(2\pi)^3} \tau(\varepsilon_k) v(\varepsilon_k) = \sigma_o(\varepsilon_k) \tag{3.34}$$

which we denote $\sigma_o$. This should not be confused with the $\sigma(\varepsilon_k)$ term defined in (3.18)

$$\sigma(\varepsilon_k) = \sigma_o(\varepsilon_k)(-df_k^o/d\varepsilon_k) \tag{3.35}$$

Including only the first non-vanishing term in the B-S expansion of $\sigma$, we hence get

$$\sigma = \sigma_o(\varepsilon_F) = \frac{2e^2}{\hbar} \frac{\mathcal{S}}{(2\pi)^3} \tau(\varepsilon_F) v(\varepsilon_F) \tag{3.36}$$

Similarly the thermal conductivity becomes

$$\kappa = \frac{\pi^2}{3} T\sigma_o(\varepsilon_F) = \frac{e^2}{\hbar} \frac{\mathcal{S}}{12\pi} T\tau(\varepsilon_F) v(\varepsilon_F) \tag{3.37}$$

By combining the approximations for $\sigma$ (3.36) and $\kappa$ (3.37), the Wiedemann-Franz law may be deduced

$$\kappa = \left[\frac{\pi^2}{3}\left(\frac{k_B}{e}\right)^2\right] T \sigma \tag{3.38}$$

where the prefactor is the Lorenz number.

The approximation leads to a somewhat more complicated expression for the thermopower. From (3.25), (3.35) and (3.33), S gets the form |55|

$$S = -\frac{\pi^2}{3} \frac{k_B}{e} k_B T \left.\frac{d\ln\sigma_o(\varepsilon_K)}{d\varepsilon_k}\right|_{\varepsilon_F} \tag{3.39}$$

which requires detailed knowledge of the scattering mechanisms for the single particle states. The equation (3.39) is known as the Mott-Jones expression. By use of the definition of $\sigma_o$ (3.34) and $v_k$ (3.3 ) we can rewrite (3.39) to the form |39|

$$S = -\frac{\pi^2}{3} \frac{k_B}{e} k_B T \left[\frac{\varepsilon_k''}{(\varepsilon_k')^2} + \frac{\tau'(\varepsilon_k)}{\tau(\varepsilon_k)}\right]_{\varepsilon_F} \tag{3.40}$$

where the derivatives of $\varepsilon_k$ are with respect to the momentum k. It appears from this expression that the TEP is made up of two terms: One reflecting the band structure, and one the energy-dependence of the scattering time. The former term $(\varepsilon_k''/\varepsilon_k'^2)$ could be somewhat temperature dependent as a result of shifts in bandwidth and charge transfer with temperature. However, based on the diffuse X-ray experiments, we do not expect this effect to be appreciable in the organic metals. Dependent on the dominating scattering mechanism, on the other hand, the latter term in (3.40), $\tau'/\tau$, may change somewhat with T. An experimental observed deviation from linearity, $S \sim T$, is therefore primarily to be associated with the electronic scattering mechanism.

## 3.4 TWO CONDUCTION BANDS

The results deduced in the preceding treatment have all been general and valid for any uncorrelated system within the Bloch theory, and they are independent of the number of bands representing the carriers. It is often desirable, however, to study the intrinsic transport parameters connected to a single band, e.g. the band of a specific kind of chains in the solid. It is therefore suitable to describe the coefficients for a general system in terms of these intrinsic paramaters |56|.

The general transport coefficients ($K_n$) given in chapter 3.2 are by definition integrations over the single particle states. They may therefore be separated directly into parts for the individual bands (i),

$$K_n = \sum_i K_n^{(i)} \tag{3.41}$$

The conductivity is essentially equal to $K_o$. Thus

$$\sigma = \sum_i \sigma_i \tag{3.42}$$

with $\sigma_i$ equal the conductivity of the i'th band.

The thermopower is a little more complicated as it is a ratio of two coefficients of the type $K_n$. But using the formula (3.25), we get

$$S = -\frac{k_B}{e}\int \frac{\varepsilon_k-\varepsilon_F}{k_BT}\ \frac{\sum_i \sigma_i(\varepsilon_k)}{\sigma}\ d\varepsilon_k$$

$$= \sum\frac{\sigma_i}{\sigma}\ (-\frac{k_B}{e})\int \frac{\varepsilon_k-\varepsilon_F}{k_BT}\ \frac{\sigma_i(\varepsilon)}{\sigma_i}\ d\varepsilon_k \qquad (3.43)$$

which shows that the total thermopower is a result of a conductivity weighted sum of the intrinsic band values:

$$S = \sum_i (\sigma_i/\sigma)S_i \qquad (3.44)$$

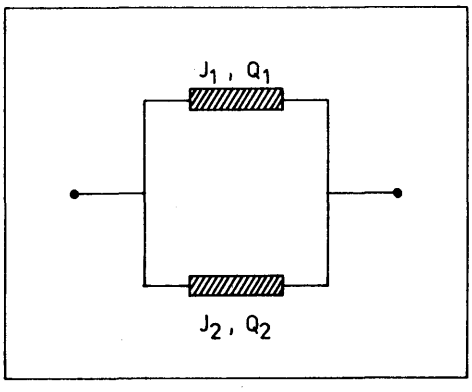


Fig. 3.1 Schematic diagram of two conduction bands.

The approximate thermal conductivity given in (3.21) is, as the electrical conductivity, given essentially by a general transport coefficient ($K_2$). Thus

$$\kappa \simeq \sum_i \kappa_i \qquad (3.45)$$

However, in a more detailed treatment based on the correct definition (3.20), one finds that the macroscopic $\kappa$ involves both the electrical conductivity and the thermopower besides the thermal conductivity itself. After some reorganization like that in (3.43), one arrives at

$$\kappa = \sum_i \left[\kappa_i - T\,\sigma_i S_i\,(S-S_i)\right] \qquad (3.46)$$

In many of the complex organic metals, e.g. TTF-TCNQ, both of the molecule types are organized to form highly conducting chains. If these chains are effectively decoupled, we saw in chapter 2 that they form two independent bands: The donor band

(D) and the acceptor band (A). Hence, the measured conductivity and thermopower in these systems are composed of the intrinsic values as

$$\sigma = \sigma_D + \sigma_A \tag{3.47a}$$

$$S = \sigma_D/\sigma \cdot S_D + \sigma_A/\sigma \cdot S_A \tag{3.47b}$$

## 3.5 MULTIPLE SCATTERING PROCESSES

### The Nordheim-Gorter rule and the Matthiessen's rule

Although the charge carrier scattering processes have not yet been discussed in details at all, it is natural in this place to make some remarks concerning situations where there are several different scattering processes going on at the same time, e.g. electron-phonon and electron-impurity scattering.

In order to deduce some simple relations between each scattering process and the macroscopic transport behaviour, we must use some more or less restrictive assumptions. [For a detailed discussion, see ref. 57] . Beyond the Bloch-condition the matrix elements for scattering of the independent electrons must be a function of the carrier energy only, and should not explicitly depend on the wavevector k. Further the charge carrier scattering mechanisms must be entirely independent of one another. Then the relaxation time approximation is valid for each of the scattering terms (i). In the Boltzmann transport equation (3.4), the scattering term hence becomes

$$\frac{df_k}{dt} = - \Sigma \frac{f_k - f_k^o}{\tau_i} \tag{3.48}$$

and thus, the resulting time of relaxation is defined by

$$\tau^{-1} = \sum_i \tau_i^{-1} \tag{3.49}$$

Provided that $\tau$ is only slightly energy dependent so that the Bethe-Sommerfeld expansion is valid, the conductivity must be

proportional to $\tau$. Thus the resistivity $\rho = 1/\sigma$ is related to $\tau$ as

$$\rho \sim \tau^{-1} = \sum_i \tau_i^{-1} \tag{3.50}$$

If we now define the specific resistivity ($\rho_i$) due to a single type of scattering process solely, we will get

$$\rho = \sum_i \rho_i \tag{3.51}$$

which is the Matthiessen's Rule. The same result could be deduced from rather crude arguments. But as it is seen, eq. (3.51) is only true under certain special circumstances |58|.

Provided validity of the Wiedeman-Franz law (3.38), an equivalent rule can be deduced concerning the thermal resistivity (w) (equal to the reciprocal of thermal conductivity):

$$w = \sum_i w_i \tag{3.52}$$

Hence the electrical and thermal resistivities depend on the absolute scattering due to each particular mechanism present. This contrast with the characteristic of thermopower, in which the magnitude of the intrinsic contributions depends on the relative scattering, as seen below: By defining the macroscopic resistivity dependence of the energy level, corresponding to the conductivity in eq. (3.36)

$$\rho_o(\varepsilon) = 1/\sigma_o(\varepsilon) \tag{3.53}$$

we can rewrite the Mott-Jones formula (3.39) to

$$S = \frac{\pi^2}{3} \frac{k_B}{e} k_B T \frac{1}{\rho_o}(\varepsilon_F) \left.\frac{d\rho_o}{d\varepsilon}\right|_{\varepsilon_F} \tag{3.54}$$

Now, utilizing the Matthiessen rule leads to

$$S = \sum_i \frac{\rho_i}{\rho} S_i \tag{3.55}$$

an expression originally derived by Nordheim and Gorter |59|, who studied effects of small impurity concentrations on the TEP. The formula (3.55) could also be deduced by inspection of the model shown in Fig. 3.2, which is based on the Matthiessen rule and the Wiedemann-Franz law. The element (i) must have a temperature drop which relative to the mascroscopic drop is given by

$$\Delta T_i = \frac{w_i}{w} \Delta T \tag{3.56}$$

The induced thermoelectric potential is therefore

$$\Delta v_i = S_i \left(\frac{w_i}{w} \Delta T\right) \tag{3.57}$$

which lead to the total termopower given by the Kohler formula |60|

$$S = \sum_i \frac{w_i}{w} S_i \tag{3.58}$$

Using the Wiedemann-Franz law, this expression leads to (3.55)

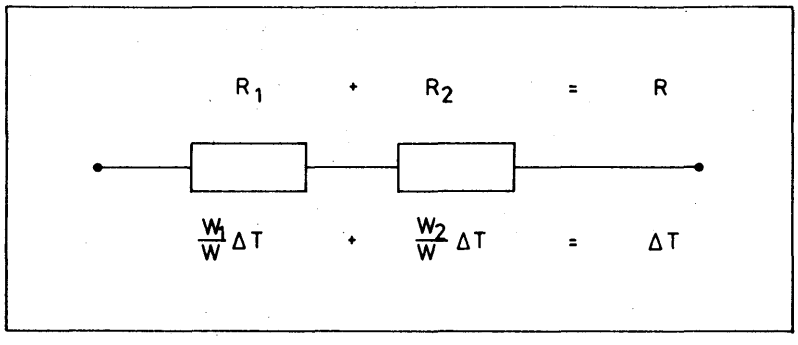


Fig. 3.2 Schematic outline of a two-scattering mechanism.

## 3.6 TRANSPORT PARAMETERS IN ONE-DIMENSIONAL TIGHT BINDING BAND

In chapter 2 it was shown that the conduction bands in the absence of any interchain coupling can be expressed as simple cosine bands

$$\varepsilon(k) = \frac{W}{2}(1 - \cos kb) \tag{3.59}$$

where w is the bandwidth and b the intrachain lattice constant. The Fermi Surface is in this model parallel planes, corresponding to true one-dimensionality. In the present chapter the main transport parameters will be expounded on the basis of this model. The crystal structure is assumed to be of a type where both acceptor and donor molecules form conducting chains, and the unit cell consists of one of each molecule (see chapter 2.1). The coefficients deduced below are the intrinsic parameters corresponding to individual chains.

Electrical conductivity

The general one-dimensional transport-theory discussed above lead in the tight binding band model to the conductivity (3.17)

$$\sigma = \frac{4}{\pi}\frac{e^2}{\hbar^2}\frac{b^2}{V}\int \tau(\varepsilon)\left[\varepsilon(W-\varepsilon)\right]^{\frac{1}{2}}\left(-\frac{df^o}{d\varepsilon}\right)d\varepsilon \tag{3.60}$$

where the Fermi surface expression (2.8) and the dispersion relation (3.59) has been utilized. In the Bethe-Sommerfeld approximation (3.36) this reduces to

$$\sigma \simeq \frac{4}{\pi}\frac{e^2}{\hbar^2}\frac{b^2}{V}\tau(\varepsilon_F)\left\{\varepsilon_F(W-\varepsilon_F)\right\}^{\frac{1}{2}} \tag{3.61}$$

The Fermi-energy is determined by the amount of charge transfer; $\varepsilon_F = \varepsilon(k_F = \pi\rho/2b)$. Thus

$$\sigma \simeq \frac{2}{\pi}\frac{e^2}{\hbar^2}\frac{b^2}{V}\tau(\varepsilon_F)\cdot W \sin\left(\frac{\pi\cdot\rho}{2}\right) \tag{3.62}$$

Since the scattering time generally is inversely proportional to the density of states, eq. (3.62) and (2.6) suggests that $\sigma$ is proportional to the second power of the bandwidth.

The charge carrier density (n) for a specific kind of chain is in the present formalism given by

$$n = \rho/(\tfrac{1}{2}V) \tag{3.63}$$

The mobility must then be in the form

$$\mu = \frac{2}{\pi} \frac{e}{\hbar^2} \frac{b^2}{\rho} \tau \{\varepsilon_F (W-\varepsilon_F)\}^{\frac{1}{2}} \qquad (3.64)$$

In the organic materials the bandwidths are usually rather small, i.e. not orders of magnitude larger than the thermal energy. The expansion of the transport integrals is therefore somewhat erroneous. In Fig. 3.3 the analytical expression (3.61) is compared with a numerical calculation of (3.60), assuming the scattering time to be energy-independent. It appears that the analytical expression leads to excessive conductivity at high T. This is a result of the non-vanishing Fermi-factor near the band-edges. The rather narrow bands demand further a detailed knowledge of the relaxation time, as it may vary strongly within a range of $k_B T$.

Thermoelectric power

The integral-form of the thermopower, S, in the tight binding band model is probably best given in terms of the conductivity

$$S = - \frac{k_B}{e} \int_0^W \frac{\varepsilon-\varepsilon_F}{k_B T} \frac{\sigma(\varepsilon)}{\sigma} d\varepsilon \qquad (3.65)$$

where $\sigma(\varepsilon)$ and $\sigma$ is given by (3.60). The analytical formula is derived using (3.40) and (3.59)

$$S = - \frac{\pi^2}{6} \frac{k_B}{e} \frac{k_B T}{\varepsilon_F} \left[ \frac{W-2\varepsilon_F}{W-\varepsilon_F} + 2\varepsilon_F \frac{\tau'}{\tau}\Big|_{\varepsilon_F} \right] \qquad (3.66)$$

This may, as well as the conductivity, be rewritten in terms of the charge density |61|

$$S = - \frac{2\pi^2}{3} \frac{k_B}{e} \frac{k_B T}{W} \left[ \frac{\cos \pi\rho/2}{\sin^2 \pi\rho/2} + \frac{W}{2} \frac{\tau'}{\tau}\Big|_{\varepsilon_F} \right] \qquad (3.67)$$

In the organic compounds, the charge transfer is always less than one: $\rho \leq 1$. Hence, the donor-chain exhibits a positive TEP due to the band-structure contribution, whereas the acceptor-chain exhibits a negative value.

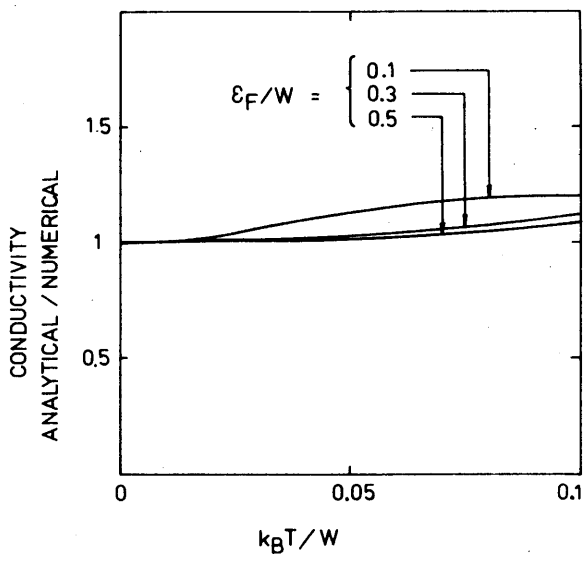


Fig. 3.3 Ratio of analytical to numerical calculation of tight binding conductivity versus relative temperature.

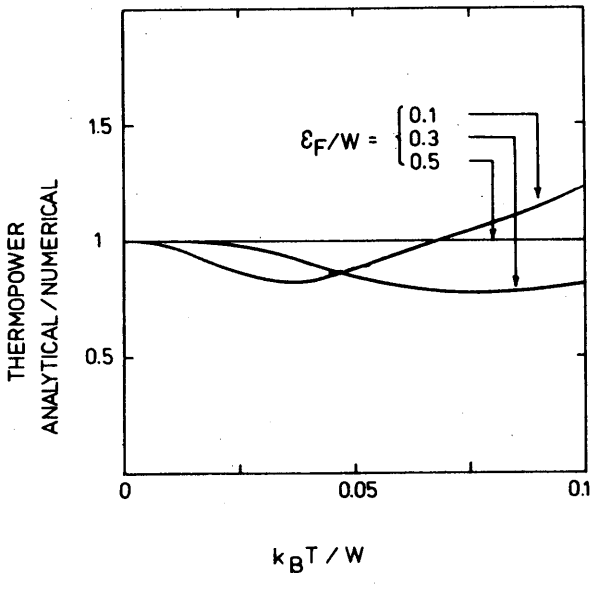


Fig. 3.4 Ratio of analytical to numerical calculation of tight binding thermopower versus relative temperature.

In Fig. 3.4 we show the analytical calculations compared to the numerical for different values of $\varepsilon_F$. The plot corresponds to the conductivity plot showed in Fig. 3.3

## CHAPTER IV

## SCATTERING MECHANISM IN ORGANIC METALS

It appears from the discussion in chapter 3 that the transport properties are distinctly affected by the time of relaxation, $\tau$. We will in the present chapter discuss different possible single particle scattering models. Since TTF-TCNQ has been most extensively investigated, there exist more data for this material than for any other organic metal. The calculations will therefore mainly be related to TTF-TCNQ, but most of the results are general for all the compounds. Comparison with experimental transport data should not be taken too serously below 100-150K, as fluctuations into charge density wave states may be important in this region. Furthermore it should be noticed that all calculations presented are based on "constant-volume", whereas experimental data normaly are for "constant pressure". In the frequently used resistivity approximation

$$\rho = \rho_o + \rho_1 \cdot T^{\alpha} \qquad (4.1)$$

$\alpha \sim 2.3$ under ambient pressure. In the case of constant volume, however, $\alpha$ is somewhat different, depending on which volumen used |62|. For example the resistivity is quasi-linear in T, when the 60K-volumen is employed |63|.

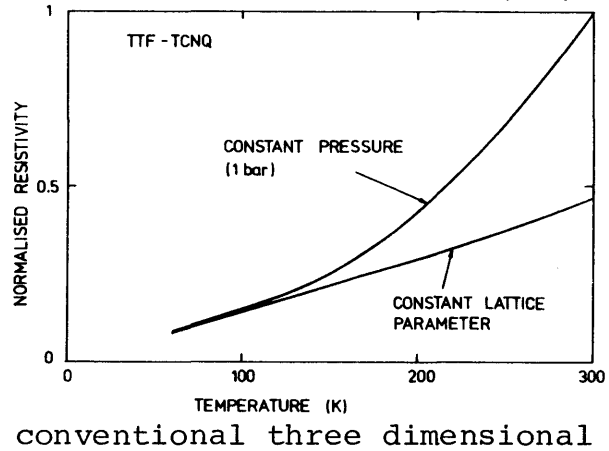


Fig. 4.1 Normalized resistivity of TTF-TCNQ. |63|

In conventional three dimensional metallic systems the electrical conductivity is mainly limited by electron-phonon interactions. During the last few years the discussion about single-particle resistivity in the highly conducting organic crystals has been focused on such interactions. But beyond the first order coupling of the electrons to the acoustic modes, well

known from 3D metals, the discussions concerning the present compounds have included both the first and second order coupling to the acoustic as well as the optical and rotational (libronic) modes. In the present part we will therefore mainly concentrate on e-ph interactions, whereas electron-electron interactions will be reviewed superficially. Finally a short discussion concerning lattice defects will be given.

## 4.1 ELECTRON-PHONON INTERACTION IN TTF-TCNQ

The TTF-TCNQ unit cell consists of four molecules. With 3 translational and 3 rotational degrees of freedom for each molecule, 24 branches arise to the intermolecular phonon spectrum. Of these, 3 are acoustic and the remaining 21 optical. With respect to the highly conducting direction he acoustic branches are denoted as the longitudinal (LA) mode, the transverse ($TA_c$) mode with displacements principally along the $c^*$-direction, and the transverse ($TA_a$) mode with displacement along $a^*$. Among the 21 optical modes, some correspond to translational movements of the individual molecules, others to rotational motions (librons) round the $\eta$, $\zeta$ and $\xi$-axis defined in Fig. 4.2, and the rest are mixtures of translations and rotations

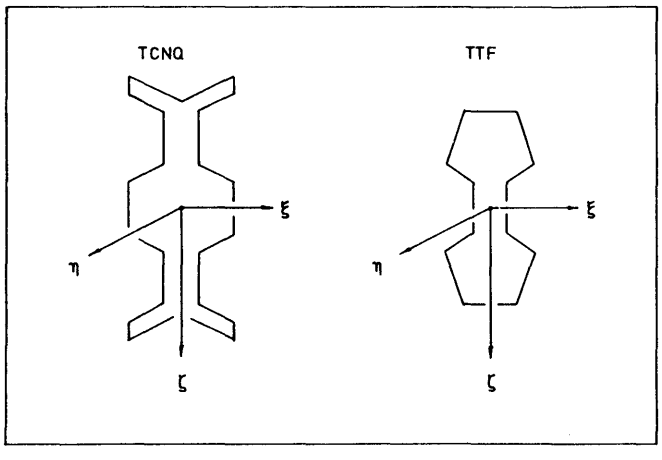


Fig. 4.2 Definition of the molecular axis |64|.

Besides these intermolecular motions, the external modes, there are phonons based on the intramolecular motions, the internal modes. In TCNQ there are 54 such normal modes, and in TTF, there are 36. |65|

The electron coupling to these phonons will be calculated by use of the usual tight-binding Hamiltonian |66|

$$H = \sum_j \varepsilon_j c_j^+ c_j + \sum_{ij} (t_{i,j} c_j^+ c_i + h.c.) + \sum_{n,q} (b_n^+(q) b_n(q) + \tfrac{1}{2}) \qquad (4.2)$$

The summation is taken over the molecules i and j, the phonon wave vector q and the phonon branch n. The first two terms in (4.2) give the total energy for the charge carriers, and the third term the total energy for the phonons, all in the absence of interactions between electrons and phonons.

The coupling of electrons to the external modes will be taken to occur via modulation of the tight binding transfer integral. The coupling to the intramolecular modes will be taken to occur via modulation of the energy of the conducting electron molecular orbital. The interaction is therefore contained in the two first terms of (4.2).

## 4.2 ELECTRON COUPLING TO EXTERNAL MODES

As already mentioned, the coupling between electrons and external phonons is assumed to occur via modulation of the neighbouring intrachain transfer integrals. The Hamiltonian of interest is then from eq. (4.2):

$$H_{e,ph}^{ex} = \sum_{j,i=j\pm1} \{t_{ij} c_j^+ c_i + h.c.\} \qquad (4.3)$$

To obtain the coupling parameters, we may assume that the vibrational amplitudes are small. Hence, the transfer integrals can be expanded into power-series of the displacement u:

$$t_{i,j} = t^o + \left(\frac{dt^o}{du}\right)(u_i - u_j) + \frac{1}{2}\left(\frac{d^2 t^o}{du^2}\right)(u_i - u_j)^2 + \ldots. \qquad (4.4)$$

where $t^o$ is the equilibrium transfer integral. The interaction-Hamiltonian can now be decomposed into power-series of u. The first and second order Hamiltonians are thus:

$$H_1 = \sum_{j,i=j\pm1} \left[\frac{dt^o}{du}(u_i-u_j)c_j^+c_i + h.c.\right] \tag{4.5}$$

$$H_2 = \sum_{j,i=j\pm1} \frac{1}{2}\left[\frac{d^2t^o}{du^2}(u_i-u_j)^2c_j^+c_i + h.c.\right] \tag{4.6}$$

As it will be shown below, eq. (4.5) include all electron interactions where only one external phonon contribute to the process. Correspondingly eq.(4.6) affects electron scattering by two phonons simultaneously. $H_1$ and $H_2$ are therefore indicated as one-phonon and two-phonon Hamiltonians, respectively.

## 4.3 ONE-PHONON HAMILTONIAN

The electron annihilation (creation) operators in eq. (4.2) are connected to the Bloch-state operators through

$$c_{j\sigma}^{(+)} = N^{-\frac{1}{2}} \sum_k e^{(-)ijkb} c_{k\sigma}^{(+)} \tag{4.7}$$

By quantization of the displacement operators u in terms of the phonon-annihilation ($a_q$) and -creation operators ($a_q^+$) |67|

$$u_j = \sum_q \left\{\frac{\hbar}{2MN\omega_q}\right\}^{\frac{1}{2}} \{a_q e^{ijqb} + a_q^+ e^{-ijqb}\} \tag{4.8}$$

the one-phonon interaction Hamiltonian becomes

$$H_1 = \sum_n \sum_{j=\pm1} \frac{dt}{du}\left\{\frac{\hbar}{2MN^3}\right\}^{\frac{1}{2}} \sum_{k\sigma} e^{-inkb} c_{k\sigma}^+ \sum_{k\sigma} e^{i(n+j)kb} c_{k\sigma}$$

$$\cdot\{\sum_q \omega_q^{-\frac{1}{2}} [a_q e^{i(n+j)qb} + a_q^+ e^{-i(n+j)qb}] -$$

$$\sum_q \omega_q^{-\frac{1}{2}} [a_q e^{inqb} + a_q^+ e^{\quad}]\} \tag{4.9}$$

By first sight this seems rather complicated. However, conservation of total momentum during the scattering process and the assumption that the e-p interaction can not change spin, excludes most of the terms in (4.9) from being active. The effective Hamiltonian is then reduced to |66|.

$$H_1 = \sum_{q,k,\sigma} \frac{dt}{du} \left\{\frac{\hbar}{2MN\omega_q}\right\}^{\frac{1}{2}} f_1(k,q)\ (a_q + a_{-q}^+) c_{k+q}^+ c_k \qquad (4.10a)$$

where

$$f_1(k,q) = -2i(\sin kb - \sin(k+q)b) \qquad (4.10b)$$

The electron scattering time due to this first order interaction with external phonons can now be derived by usual second order perturbation theory. We will assume that the phonon energy is negligible compared to the electron energy, i.e. elastic scattering. The principle of microscopic reversibility is then sufficient to proceed:

$$P(k,k') = P(k',k) \qquad (4.11)$$

P is the transition probability. Eq. (3.6) lead then to the scattering term in the form:

$$\frac{g_k}{\tau_k} = \int P(k,k+q)\ [f^o_{k+q} - f^o_k\ ]dk \qquad (4.12)$$

The transition probability can be deduced by use of the Golden Rule

$$P(k,k+q) = \frac{2\pi}{\hbar}\left|\langle k+q, n_q \pm 1 | H_1 | k, n_q \rangle\right|^2 \cdot N_\sigma(\varepsilon_{k+q}, k+q) \cdot \delta(\varepsilon_{k+q} - \varepsilon_k) \qquad (4.13)$$

where $N_\sigma(\varepsilon_k, k)$ is the density of states in the final state, thus corresponding to a specific spin and wave number. $N_\sigma(\varepsilon_k, k)$ must

therefore be a quarter of the density of states $N(\varepsilon_k)$ discussed in chapter 2 (2.6):

$$N_\sigma(\varepsilon_k,k) = \frac{N}{2\pi}\{\varepsilon_k(W-\varepsilon_k)\}^{-\frac{1}{2}} \tag{4.14}$$

The $\delta$-function in (4.13) in a 1D-tight binding band is only finite for k+q=-k+g where g is a reciprocal lattice vector: i.e.

$$q = -2k + n \cdot 2\pi/b \tag{4.15}$$

n is in a "normal"-band (t<0) zero for electrons with energy less than W/2 (Normal-process), and one for electrons with energy larger than W/2 (Umklapp-process). (See Fig. 4.3). The opposite relation is valid for an inverted band (t>0).

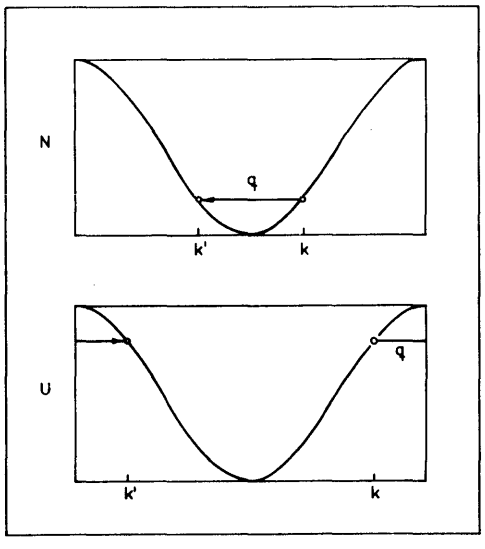


Fig. 4.3 Transition possibilities in an elastic scattering process in an 1D tight binding band, a Normal-process and b. Umklapp-process.

The Fermi-Dirac functions involved in the scattering expression (4.12), should thus be coupled as

$$f^o_{k+q} = f^o_{-k} = f^o_k \tag{4.16}$$

and then

$$f_k - f_{k+q} = (f_k - f^o_k) - (f_{-k} - f^o_{-k}) = g_k - g_{-k} = 2g_k \tag{4.17}$$

The scattering time may therefore be reduced to

$$\tau^{-1}(\varepsilon_k) = \frac{2}{\hbar} \frac{N}{[\varepsilon_k(w-\varepsilon_k)]^{\frac{1}{2}}} \; M_1^2(k,-k) \tag{4.18}$$

where $M_1$ is the one-phonon matrix element

$$M_1(k,-k) = \langle -k,\ n_{q=-2k} \pm 1 | H_1 | k,\ n_{q=-2k} \rangle \tag{4.19}$$

Inserting the interaction Hamiltonian (4.10) gives the form (for phonon emission)

$$M_1(k,-k) = \left(\frac{dt}{du}\right)^2 \frac{\hbar}{2MN\omega_q} \; f_1^2(k,-k) \cdot [2n_q+1] \Big|_{q=-2k} \tag{4.20}$$

The scattering time for the electrons due to first-order coupling to external phonons is now given by

$$\tau^{-1}(\varepsilon_k) = 64\hbar \left(\frac{dt}{du}\right)^2 \frac{1}{MW^2} [\varepsilon_k(w-\varepsilon_k)]^{\frac{1}{2}} \left. \frac{2n_q+1}{\hbar\omega_q} \right|_{|q|=2k} \tag{4.21}$$

The corresponding tight-binding band mobility is obtained from eq. (3.64) and (4.21)

$$\mu = \frac{1}{32\pi} \frac{e}{\hbar^3} \frac{b^2MW^2}{\rho} \left(\frac{dt}{du}\right)^{-2} \left. \frac{\hbar\omega_q}{2n_q+1} \right|_{|q|=2k_F} \tag{4.22}$$

which reduces to

$$\mu \simeq \frac{1}{64\pi} \frac{e}{\hbar^3} \frac{b^2MW^2}{\rho} \left(\frac{dt}{du}\right)^{-2} \left. \frac{(\hbar\omega_q)^2}{k_BT} \right|_{|q|=2k_F} \tag{4.23}$$

when the phonon energy is small compared to $k_BT$. In this high-temperature region the mobility has a 1/T-behaviour. This is the well known situation in conventional 3D metals. However, both the phonon energy and the coupling constant in (4.23) may also change somewhat with changing temperatures, due to thermal contraction resulting in a more rigid lattice.

Deviation from the 1/T-law can therefore be expected, even if the electron scattering is mainly a result of one-phonon interactions.

In order to investigate the thermoelectric behaviour due to the first order e-p scattering, detailed knowledge of the phonon-dispersions are needed. Using the analytical approximation (3.66) and the expression (4.21) for $\tau$ gives the thermopower

$$S = -\frac{2\pi^2}{3}\,\frac{k_B}{e}\,\frac{1}{\omega_q}\,\frac{d\omega_q}{d\varepsilon_k}\Bigg|_{|q|=2k_F} \cdot k_B T \qquad (4.24)$$

We note that the bandstructure part of the thermopower has been cancelled by a corresponding term in the energy-derivative of the relaxation time, actually the density of states. Therefore the thermopower is a measure of the $2k_F$-phonon dispersion relative to the electron dispersion. This is perhaps better seen by writing (4.24) in the form

$$S = -\frac{4\pi^2}{3}\,\frac{k_B}{e}\,\frac{k_B T}{\{\varepsilon_F(W-\varepsilon_F)\}^{\frac{1}{2}}}\,\frac{d\omega_q/d(qb)}{\omega_q}\Bigg|_{qb=\pi\rho} \qquad (4.25)$$

## 4.4 FIRST-ORDER SCATTERING BY ACOUSTIC MODES

The main electronic scattering processes due to first order interaction with external phonons are probably the scattering by the acoustic modes. It has been emphasized that the rotational displacements (librons) may couple more effectively to the electrons in the organic systems based on large planar molecules with extended $\pi$-orbitals, than the ordinary phonons [68]. However, by symmetry arguments, the coupling of electrons to such libronic modes are only second-order processes in TTF-TCNQ [69].

The properties of the acoustic modes in TTF-TCNQ are known from inelastic neutron scattering experiments (see Fig. 4.4) [70,71].

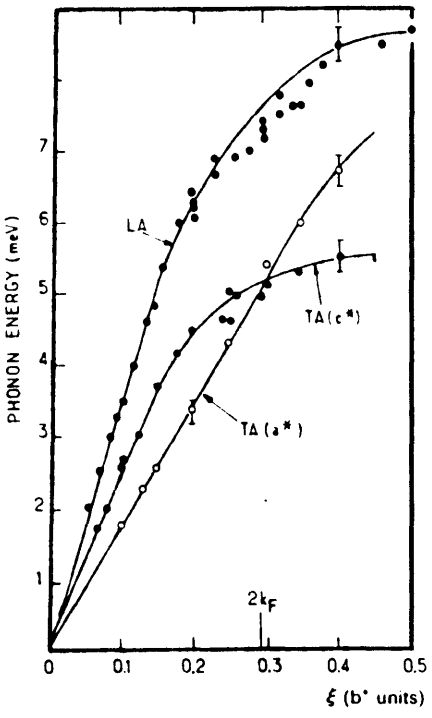


Fig. 4.4 Dispersion curve in deuterated TTF-TCNQ for modes propagating along the chain direction, T = 300K |71|.

The phonon energy corresponding to $|q|=2k_F$ is therefore known. At room temperature the energy of the longitudinal LA mode is 7.5 meV, while the transverse modes TA($c^*$) and TA($a^*$) both are 5 meV, approximately. The TA($a^*$) vibration differs from the others in that the molecules move in their own plane so that it does not change the intermolecular distances in the chain, but still it does produce a change in the transfer integral. However, by symmetry, the overlap is an extremum in the equilibrium position, resulting in a vanishing first order e-p interaction |72|.

Both the LA and the TA($c^*$) phonon branches show a Kohn-anomaly below 150 K |70|, thus suggesting strong first-order coupling to the electrons. Based on an Extended Hückel method, Berlinsky et al. have calculated the e-p coupling constant corresponding to the LA-mode for a half-filled tight binding band |28|. For the TCNQ-molecule, they find

$$\left|\frac{dt}{du}\right|_{LA} = 0.17 \text{ eV/Å} \qquad (4.26)$$

With the $2k_F$-phonon energy equal to 7.3 meV, the electronic bandwidth, 0.5 eV, and a charge transfer of 0.59, the scattering time (4.21) becomes

$$\tau_{TCNQ}(LA) = 2.3\times10^{-14} \text{ sec} \qquad (4.27)$$

This corresponds to the mobility (4.22): $\mu$=16.6 $cm^2/Vs$ |73|. Assuming an $\omega_q \sim q$ dispersion relation, which is in fairly good agreement with Fig. 4.4, the thermopower (4.24) becomes, S=-79,2 $\mu V/k$. If numerical methods based on (3.60) and (3.65) were used instead of the B-S approximations, the calculated values would be 16.7 $cm^2/Vs$ and -73,9 $\mu V/k$ for $\mu$ and S respectively. The energy-dependent scattering-time enclosed in these integrations is shown in Fig. 4.5.

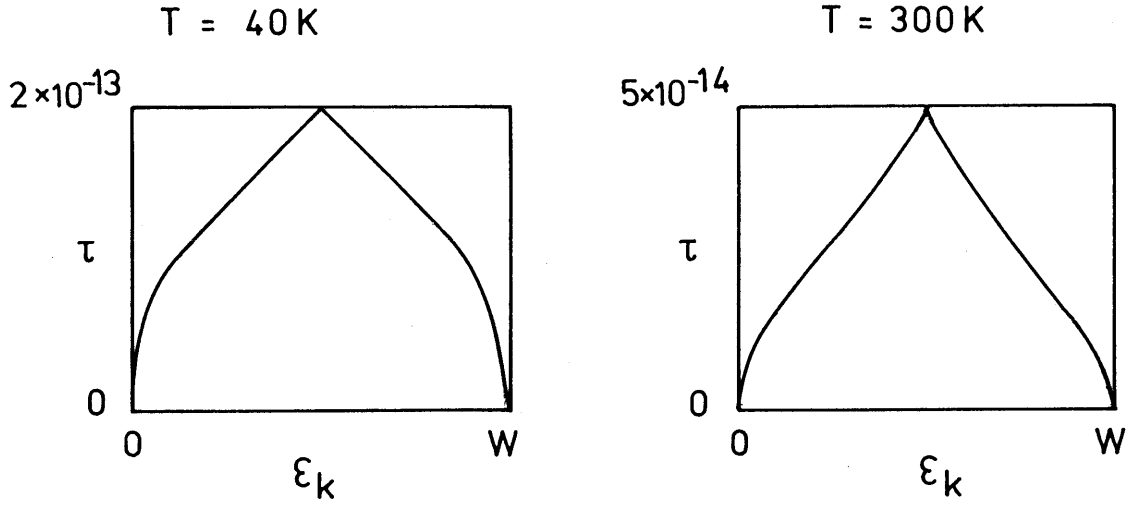


Fig. 4.5 Electronic scattering time due to first order e-p interaction with the LA mode.

Since the molecules in TTF-TCNQ are tilted, the transverse TA($c^*$) vibration will also result in an alternation in the intermolecular spacing b. The rate of change of the overlap due to motion along $c^*$ may be estimated by assuming that the component along the chain will affect t corresponding to the effect of the LA vibration |72|. The angle between the plane of the molecule and the plane perpendicular to b is $34^o$ |50|. Thus

$$\left.\frac{dt}{du}\right|_{TA_c} = \left.\frac{dt}{du}\right|_{LA} \tan 34^{o} = 0.11 \text{ eV/Å} \qquad (4.28)$$

resulting in a scattering time equal to $2.3\times10^{-14}$ sec. The mobility and thermopower calculated numerically for both of the acoustic modes are summarized in Table 4.1.

Table 4.1 Transport properties in the TCNQ-chain assuming scattering by acoustic modes at 300K

| Mode | dt/du (eV/Å) | $\hbar\omega(q=2k_F)$ (meV) | $\mu$ ($cm^2$/Vs) | S ($\mu$V/K) |
|---|---|---|---|---|
| LA | 0.17 | 7.4 | 16.7 | -73.9 |
| TA($c^*$) | 0.11 | 4.8 | 16.8 | -74.2 |
| LA+TA($c^*$) | | | 8.4 | -74.0 |

$\mu$ and S are calculated numerically, based on the equations (4.21), (3.60) and (3.65).

The values corresponding to scattering by LA and TA($c^*$) phonons should be compared with the experimentally found mobility and thermopower for TTF-TCNQ, equal to 3.9 $cm^2$/Vs and -28 $\mu$V/K, respectively. The mobility is the sum of the values on the TTF- and the TCNQ-chain. No matter what the role is of the individual chains, we can therefore conclude that unless the e-p coupling is enhanced essentially compared with the Berlinsky calculations, the electron scattering solely due to first order interaction with acoustic modes cannot account for the transport properties. A further discussion will be given in 4. The qualitative temperature behaviour of the mobility is seen from (4.23) to be in agreement with the behaviour corresponding to a constant volume equal to the 60K-value, as pointed out by Cooper et al. |63|, Fig. 4.1. The $\sigma \sim T^{-2.3}$ rule observed at ambient pressure must therefore in this one-phonon picture be attributed as an additional $T^{-1.3}$-factor due to the contraction, resulting in a more rigid lattice, and thus an en-

hanced phonon energy with decreasing temperatures. In Fig. 4.6 the mobility is shown as a function of T and $\omega_q$. The phonon-dispersion is assumed to be $\omega_q \propto q$. The $\sigma \propto \omega_q^2$ approximation is seen to be good. Therefore, if the temperature (volume) dependence of the phonon-energy shall explain the $\sigma \propto T^{-2.3}$ rule, $\omega_q$ must

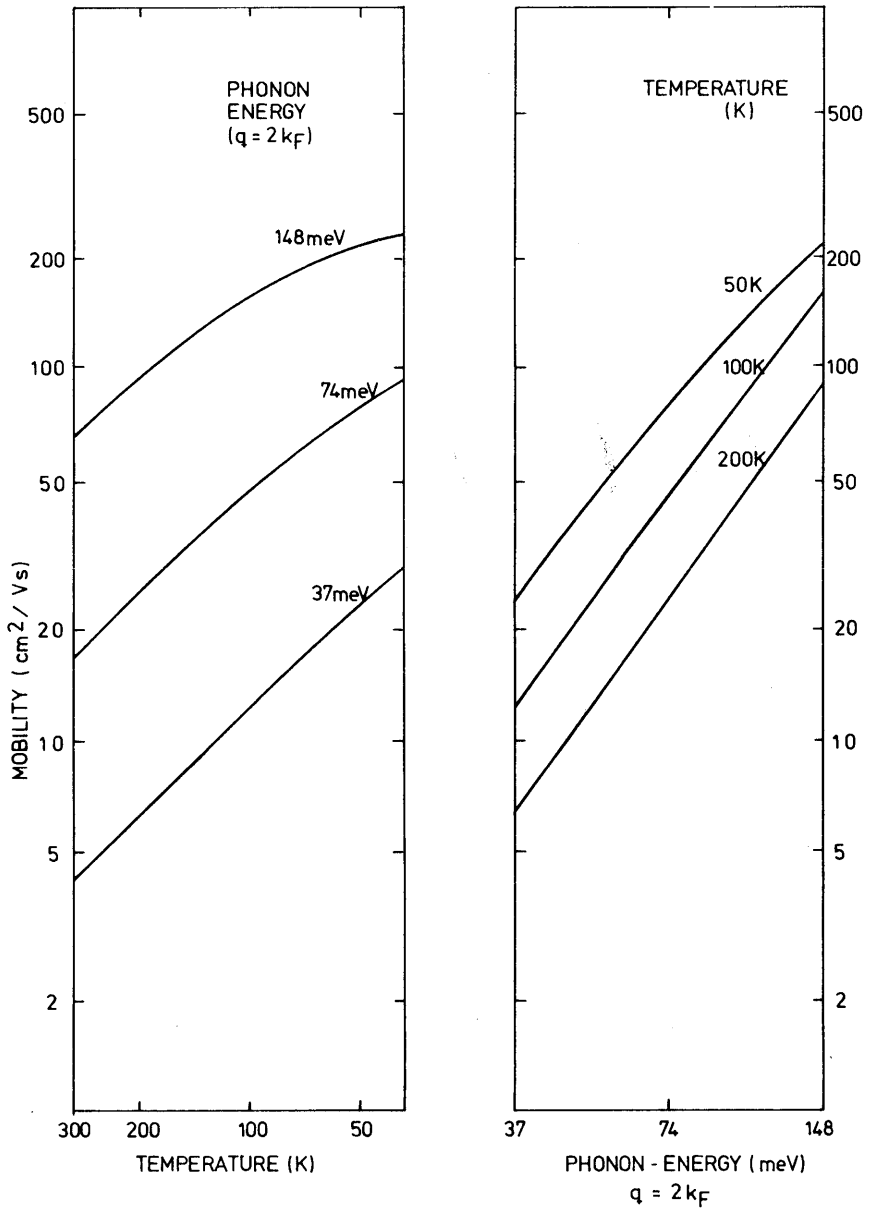


Fig. 4.6 Mobility of carriers in a tight binding band (W=0.5 eV, $\varepsilon_F$=0.1 eV) for first order coupling to acoustic modes, as a function of phonon-energy and temperature.

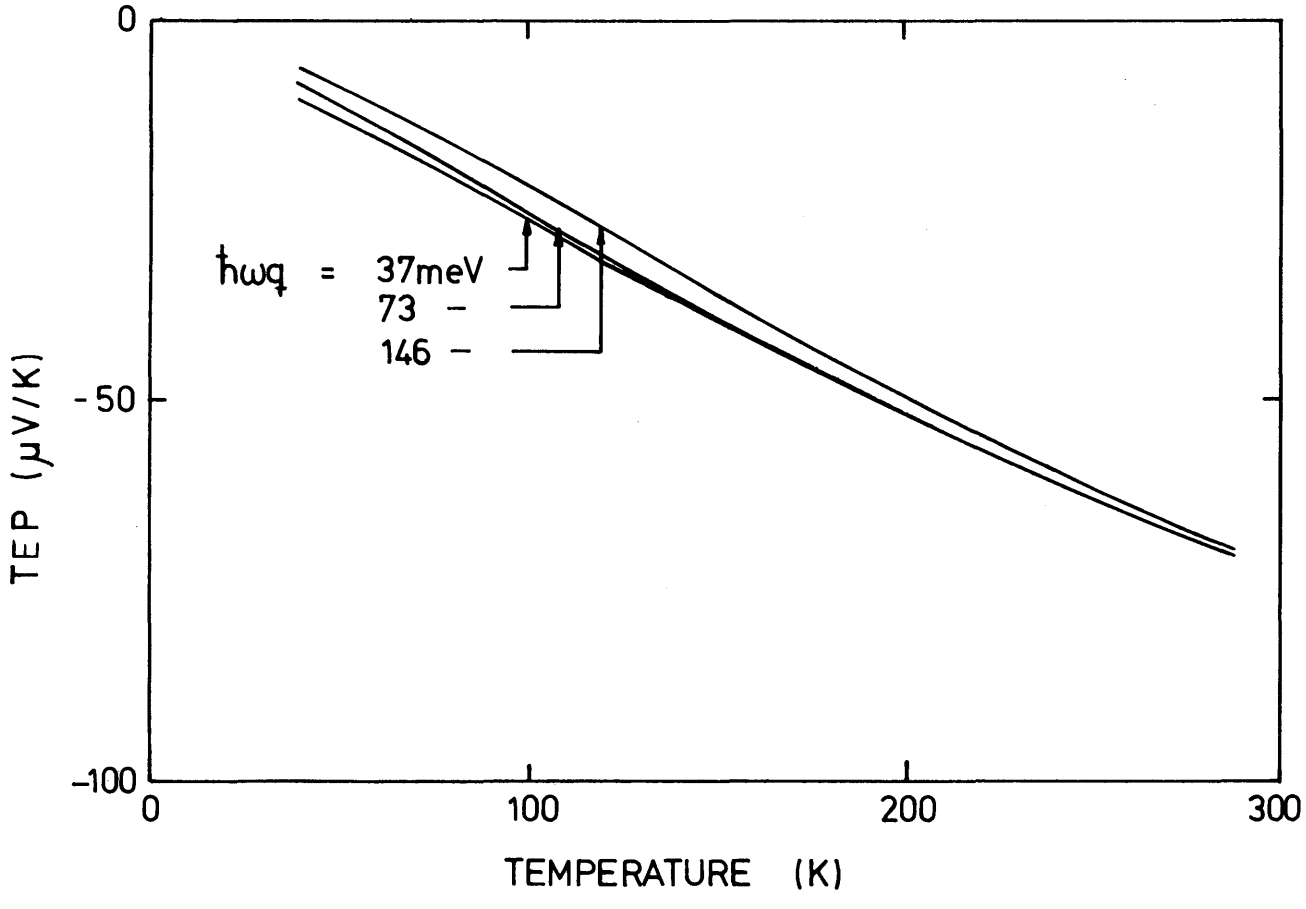


Fig. 4.7 Thermopower of carriers in a tight binding band (W=0,5 eV, $\varepsilon_F$=0.1 eV) for first order electron coupling to acoustic modes.

be doubled from room-temperature to 100K. This rather drastic effect is in agreement with the observed strong pressure dependence |74|. However, if the temperature-dependent constant-volume conductivity had been relative to a volume corresponding to a temperature of 200K, or higher, the experimental data are not the simple 1/T-form found by Cooper |62|. This controversy cannot be explained by the first-order e-p scattering model.

A change in the phonon-energy will not affect the intrinsic thermopower very much, since S is approximately independent of the absolute value of $\omega_q$ (4.25). This is illustrated in Fig. 4.7 , showing numerical calculations of the TEP. The values correspond to the mobility shown in Fig. 4.6. In a two-band model, however, this phonon-energy (pressure) independence of the TEP need not be correct. If the $\omega_q(P)$ dependences are different in the two chains, this will be reflected via the sum-rules (3.47).

## 4.5 TWO-PHONON HAMILTONIAN

Rewriting the quadratic coupling of the electrons to the lattice vibrations (4.6) in terms of phonon-operators is somewhat more complicated, although in principle similar to the linear term (4.5) and (4.10). In terms of the creation and annihilation operators, (4.6) immediately becomes

$$H_2 = \sum_n \sum_{j=\pm 1} \frac{1}{2} \frac{d^2t}{du^2} \frac{1}{N} \left\{\frac{\hbar}{2NM}\right\}^{\frac{1}{2}} \sum_{k,\sigma} e^{-inkb} c^+_{k\sigma} \sum_{k,\sigma} e^{i(n+j)kb} c_{k\sigma}$$

$$\left\{\sum_{q'} \omega_{q'}^{-\frac{1}{2}} \left[a_q e^{i(n+j)qb} + a_q^+ e^{-i(n+j)qb}\right] - \sum_q \omega_q^{-\frac{1}{2}} \left[a_q e^{inqb} + a_q^+ e^{-inqb}\right]\right\}^2 \qquad (4.29)$$

After some reorganizations and utilizing that only a few of the terms will remain after a matrix formation, the two-phonon Hamiltonian is reduced to |75|.

$$H_2 = \sum_{q,q',k} \frac{d^2t}{du^2} \frac{\hbar}{2MN[\omega_q \omega_{q'}]^{\frac{1}{2}}} f_2(k,q,q') \cdot$$

$$[a_q + a_{-q}^+][a_{q'} + a_{-q'}^+] c_{k+q+q'}^+ c_k \qquad (4.30a)$$

where

$$f_2(k,q,q') = \cos(k+q+q')b - \cos(k+q)b - \cos(k+q')b + \cos kb \qquad (4.30b)$$

This interaction-Hamiltonian involves beside the electron two phonons with wave-number q and q' respectively. Each phonon may be either created or annihilated. For each pairs of phonons, (q,q') there are therefore basically four different possible processes imaginable. The matrix element for scattering for charge carriers is consequently composed of the four terms:

i Absorption of both phonons

$$\{\langle k+q+q', n_q-1, n_{q'}-1 | H_2 | k, n_q, n_{q'}, \rangle\}^2 =$$

$$\left(\frac{d^2t}{du^2}\right)^2 \frac{\hbar^2}{4M^2N^2\omega_q\omega_{q'}} f_2^2(k,q,q') n_q n_{q'} \qquad (4.31a)$$

ii Emission of both phonons

$$\{\langle k+q+q', n_q+1, n_{q'}+1 | H_2 | k, n_q, n_{q'}, \rangle\}^2 =$$

$$\left(\frac{d^2t}{du^2}\right)^2 \frac{\hbar^2}{4M^2N^2\omega_q\omega_{q'}} f_2^2(k,q,q') (n_q+1)(n_{q'}+1) \qquad (4.31b)$$

iii and iv Absorption of one phonon ($q_1$) and Emission of the other ($q_2$), $q_1, q_2 = q, q'$

$$\{<k\ q_1\ q_2,\ n_{q_1}-1,\ n_{q_2}-1|H_2|k,n_{q_1},n_{q_2}>\}^2 =$$

$$\left(\frac{d^2t}{du^2}\right)^2 \frac{\hbar^2}{4M^2N^2\omega_{q_1}\omega_{q_2}} f_2^2(k,q_1,q_2)n_{q_1}(n_{q_2}+1) \tag{4.31c}$$

Assuming elastic scattering ($\hbar\omega_q << \varepsilon_k$) the phonon momentums are confined by the relation

$$k + q + q' = -k + n\cdot 2\pi/b \tag{4.32}$$

equivalent with (4.15). The probability that an electron is scattered out of the state k, is then, according to the Golden Rule:

$$P(k,-k) = \frac{\hbar}{4M^2N}\left(\frac{d^2t}{du^2}\right)^2 [\varepsilon_k(W-\varepsilon_k)]^{\frac{1}{2}} \sum_q \frac{f_2^2(k,q)}{\omega_q\omega_{q'}} (2n_q+1)(2n_{q'}+1) \tag{4.33a}$$

where q' is given by (4.32), and

$$f_2(k,q) \equiv f_2(k,q,q') = 2(\cos kb-\cos(k+q)b) \tag{4.33b}$$

The density of states utilized is that defined in eq. (4.14). Using the conventional transformation from summation to integration over the phonon-spectrum

$$\sum_q \rightarrow \int \rho_q d_q = \frac{N}{2\pi}\int d(qb) \tag{4.34}$$

The expressions (4.12) and (4.33) yield the scattering time

$$\tau_2^{-1}(\varepsilon_k) = \frac{\hbar}{4\pi}\left(\frac{d^2t}{du^2}\right)^2 \frac{1}{M^2} [\varepsilon_k(W-\varepsilon_k)]^{\frac{1}{2}} \cdot$$

$$\int \frac{f_2^2(k,q)}{\omega_q\omega_{q'}} (2n_q+1)(2n_{q'}+1)d(qb) \tag{4.35}$$

The integration-limits are dependent on the model used, e.g. neglecting Umklapp processes or not. Gutfreund and Weger |75| assumed that only phonons with momentum in the direction opposite of the charge carriers are effective in the scattering process. Their integration region is accordingly q |0,-2k|. Furthermore, they have an integration over q', in disagreement with the relation (4.32) |76|. Assuming that the phonon-momentum can be in both directions relative to the k-vector, the following limits are valid:

i, no Umklapp-processes allowed:

$$q \in \{-\pi/b,\ \pi/b-2k\} \tag{4.36a}$$

$$q' = -2k + q \tag{4.36b}$$

ii, including first order Umklapp processes:

$$q \in \{-\pi/b,\ \pi/b\} \tag{4.37a}$$

$$q' = -2k + n2\pi/b-q,\ n = 0,\pm 1 \tag{4.37b}$$

where the value of n in (4.37) allow the q'-momentum to be in the first Brillouin Zone.

In the high-temperature region ($k_B T >> \hbar\omega_q$), the scattering time due to second order electron-phonon interactions, is from eq. (4.35) approximately given in the form

$$\tau_2^{-1}(\varepsilon_k) \simeq \frac{1}{\pi\hbar}\ \frac{b}{M^2}\{\varepsilon_k(W-\varepsilon_k)\}^{-\frac{1}{2}}\ \left(\frac{d^2t}{du^2}\right)^2 \cdot (k_B T)^2 \int \left(\frac{f_2^2(k,q)}{\omega_q \omega_{q'}}\right)^2 dq \tag{4,38}$$

Assuming temperature independent phonon-frequencies, this scattering mechanism consequently results in a $T^{-2}$ behaviour of $\tau$, and hence a $T^2$-behaviour of the resistivity, in reasonable agreement with the experimental data for TTF-TCNQ at ambient pressure. The strong pressure-dependence, as well as the

deviation from the $T^2$-law, can in this two-phonon picture be accounted for on basis of the essentially fourth order dependence on the phonon frequencies (4.38).

## 4.6 TRANSPORT PROPERTIES FOR SECOND-ORDER ELECTRON-PHONON SCATTERING

The integration in the expression for $\tau$ (4.35) has generally no simple analytical solution. Further investigations based on the two-phonon scattering mechanism are therefore done numerically.

The second-order derivative of the overlap, $d^2t/du^2$, is not known in the organic crystals. Only for the rotational displacements (the librons) have values of the coupling term been estimated |75|. Gutfreund and Weger assumed that the amplitude of these thermal rotations at ambient temperature is such that the overlap decreases by roughly a factor of two. In terms of the angle of rotation ($\theta$), the second-order e-p coupling is in the form

$$\frac{d^2t}{du^2} = \frac{M}{I}\,\frac{d^2t}{d\theta^2} \tag{4.39}$$

I being the moment of inertia. Assuming the librons to be dispersion-less optical modes |77|

$$\hbar\omega_L(q) = \hbar\omega_L^o \sim 2.5\text{-}3.7 \text{ meV} \tag{4.40}$$

the amplitude of the thermal vibration is approximately $(k_BT/I\omega^2)$. The estimated coupling is thus

$$\frac{d^2t}{du^2} \sim 4 - 10 \text{ eV/Å}^2 \tag{4.41}$$

for the acceptor chain in TTF-TCNQ, with 4t=0.5 eV. Utilizing the lower limit $d^2t/du^2=4\text{eV/Å}^2$ and the libron energy equal to 4 meV, (4.35) results in a scattering time equal to $10^{-15}$ sec for electrons near the Fermi-level of the TCNQ-band. The corresponding mobility is

$$\mu_{RT} \sim 0.8 \text{ cm}^2/\text{Vs} \qquad (4.42)$$

Recalling that the coupling probably has been somewhat over-estimated, the libron-theory is seen to give a correct order of magnitude besides the nearly correct temperature dependence of $\mu$.

In Fig. 4.8 some numerical calculations of mobility for scattering mechanism dominated by second order coupling to the phonons are shown. The two curves represent coupling to i dispersion-less optical phonons (e.g. librons) and ii coupling to acoustic phonons with $\omega_q \propto q$. The phonon-energies corresponding to $q = -2k_F$ are equal for the two curves, as well as the derivatives $d^2t/du^2$. The results for the thermopower are given in Fig. 4.9. With the absence of experimental evidence of the coupling parameters in mind, the two situations represented in Fig. 4.8 and 4.9 show comparable transport behaviour. The conductivity is characterized by the approximately, $T^{-2}$-rule, and the possibility of explaining the strong pressure dependence via $\sigma \propto \omega_q^4$. The thermopower shows the $S \propto T$ behaviour known from metallic systems, and experimentally found in TTF-TCNQ. The room-temperature TEP are in both cases rather large, -55 $\mu$V/K and -82 $\mu$V/K for scattering by acoustic and optical modes, respectively. This indicate that the scattering term in the TEP-expression is not negligible compared to the band-term (3.40). The intrinsic thermopower is on the whole unaffected by changes in phonon-energy and coupling constants. A comparison with the experimental value, however, requires more detailed knowledge of the separate properties of the two conducting bands.

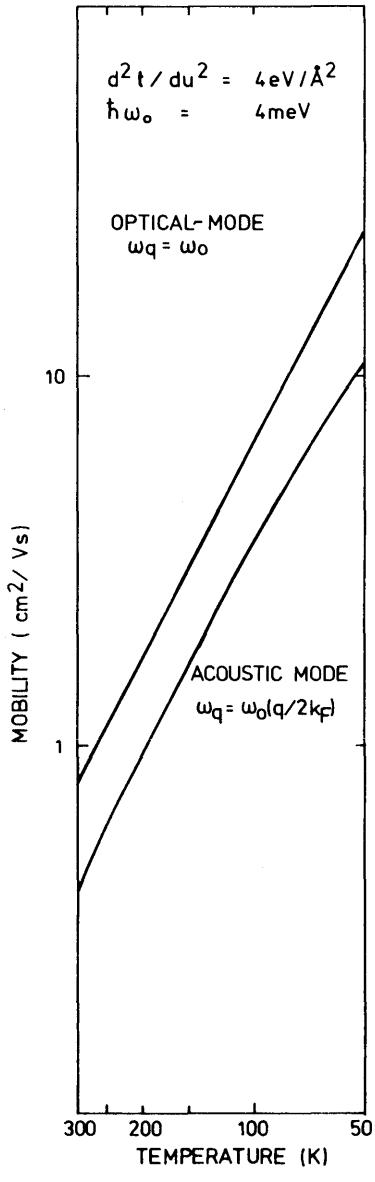


Fig. 4.8 Mobility of electrons in the TCNQ-band, for second-order e-p scattering.

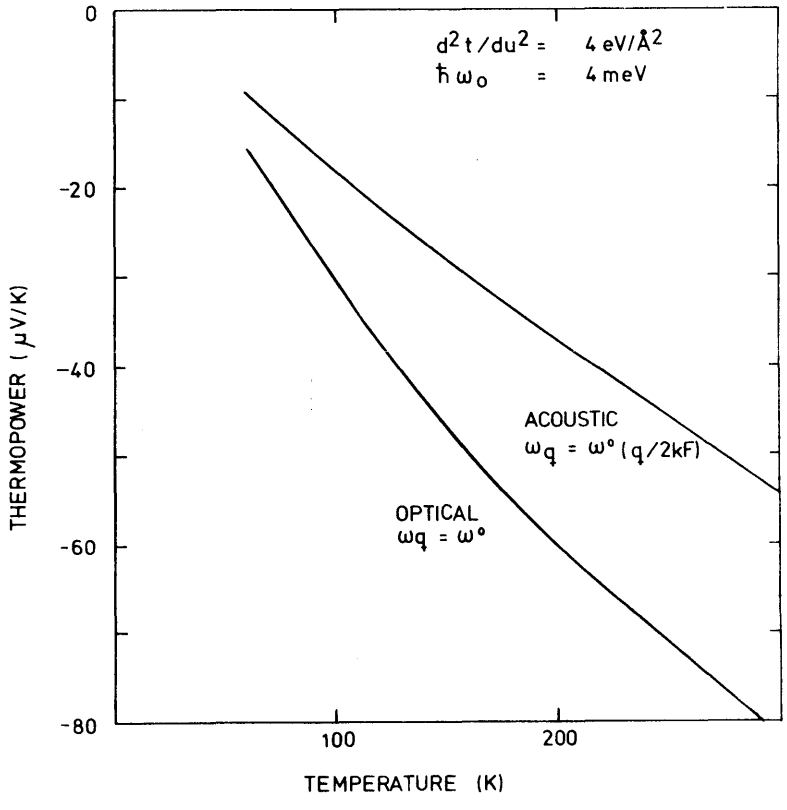


Fig. 4.9 Thermopower of electrons in the TCNQ-band for second-order e-p scattering.

## 4.7 COUPLING TO INTERNAL MODES

The interaction between charge carriers and the intramolecular vibrations is probably among the most intensively examined parameters in TTF-TCNQ. This is mainly a result of trying to explain the stabilization of the charge density wave in the organic conductors as a consequence of the intramolecular distortion |66|, rather than the more ordinary intermolecular distortion. This essential role of the internal modes arises, not because the individual intramolecular coupling strengths are particularly large, but because there are so many of them: 54 modes in TCNQ |78| and 36 in TTF |79|. Limiting the discussion to linear coupling, however, the number of interacting vibrations is by symmetry reduced to only 10 normal modes for the TCNQ-molecule |66| and 7 normal modes for the TTF-molecule |80|. These modes are shown in Fig. 4.10. But still this is a relative large number of vibrational modes.

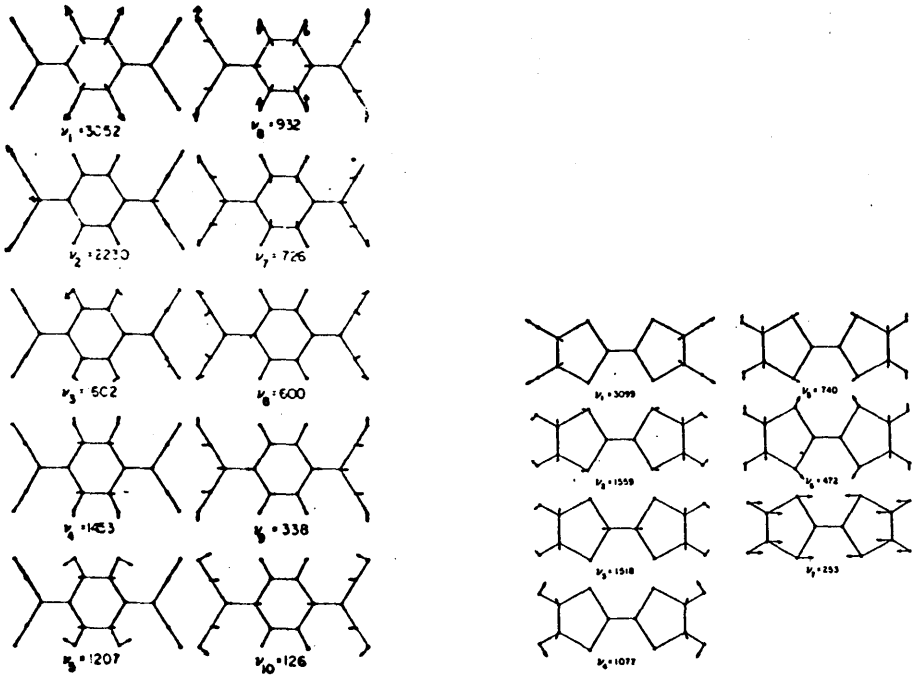

Fig. 4.10 Normal mode amplitudes for the $a_g$-symmetric modes in a TCNQ and b TTF.

A similar substantial role of these intramolecular vibrations could be expected on the single particle scattering |81|.

The mechanism of interaction between the electrons and the molecular vibrations is taken to occur by modulation of the conducting electron molecular orbital. Analogous to the expansion of the intermolecular overlap (4.4) the energy of the electronic state may be expanded. In terms of the dimensionless coordinates of the normal modes, $Q_n(j)$, corresponding to the symmetric vibration n and the monomer j, this lead to |82|

$$\varepsilon(\{Q_n(j)\}) = \varepsilon^o + \sum_{n,j} \frac{d\varepsilon}{dQ_n(j)}\bigg|_o Q_n(j) + \ldots \qquad (4.43)$$

The $Q_n(j)$'s are related to the lattice displacement vector $u_j$ of the atomic nuclei labeled j, via

$$Q_n(j) = A_{n,j}\, u_j \cdot \sqrt{M_j\, \omega_n/\hbar} \qquad (4.44)$$

where $A_n(j)$ is the transformation matrix leading to the normal coordinate representation, $M_j$ is the nuclei-mass and $\omega_n$ is the frequency of the normal mode n. From (4.43), we get the first-order electron-intramolecular vibrational Hamiltonian:

$$H = \sum_{n,j} \{(\frac{d\varepsilon}{dQ_n(j)})\ Q_n(j)\ c_j^+ c_j + h.c.\} \qquad (4.45)$$

Analogous to the discussion concerning the intermolecular modes, this Hamiltonian should be transformed into terms of creation and annihilation operators. While the electron operators are those given previously (4.7), the vibrational modes get the form

$$Q_n(q) = \frac{1}{\sqrt{N}} \sum_j Q_n(j)\exp[-iqR(j)] = 2^{-\frac{1}{2}}[a_q + a_{-q}^+] \qquad (4.46)$$

Thus, the Hamiltonian becomes

$$H = N^{-\frac{1}{2}} \sum_{n,q,k} [g_n \hbar\omega_n(q)][a_n(q) + a_n^+(-q)]c_{k+q}^+ c_k \qquad (4.47)$$

where the coupling constants $d\varepsilon/dQ_n(j)$, which are independent of j |66|, have been replaced by

$$\frac{d\varepsilon}{dQ_n} = \sqrt{2}\ q_n\ \hbar\omega_n \qquad (4,48)$$

The coupling constants in TTF-TCNQ are known from theoretical as well as experimental investigations |83|. The theoretical calculations have been based on a Complete Neglect of Differential Overlap (CNDO) type parameterization for the electronic structure and a Modified Valence Force Field (MVFF) approach for the vibrational modes. The experimental information on the magnitude of the coupling constants has been obtained from photoemission experiments in gaseous phase, and from polarized optical reflectance measurements in the solid state phase. The agreement between theory and experiments is rather good |83|.

TABLE 4.2 Values of $g_n$ and $\hbar\omega_n$ for TTF|80| and TCNQ |65|.

| MODE | TTF $g_n$ | TTF $\hbar\omega_n$ (eV) | TCNQ $g_n$ | TCNQ $\hbar\omega_n$ (eV) |
|---|---|---|---|---|
| 1 | 0.03 | 0.3843 | 0.00 | 0.3784 |
| 2 | 0.23 | 0.1933 | 0.13 | 0.2735 |
| 3 | 0.62 | 0.1882 | 0.49 | 0.2003 |
| 4 | 0.16 | 0.1335 | 0.20 | 0.1725 |
| 5 | 0.49 | 0.0918 | 0.22 | 0.1483 |
| 6 | 1.33 | 0.0585 | 0.20 | 0.1213 |
| 7 | 0.16 | 0.0314 | 0.24 | 0.08? |
| 8 | | | 0.20 | 0.0760 |
| 9 | | | 0.70 | 0.0418 |
| 10 | | | 1.54 | 0.0184 |

The energy of the intramolecular modes comes out to be of the order of the Fermi energy (Table 4.2). The electron scattering is therefore inelastic. Still, however, the relaxation time approximation is valid, since the matrix element for scattering

appears to depend solely on the initial state and the phonon-energy, assuming

$$\omega(-q) = \omega(q) \tag{4.49}$$

The interaction between electrons in the state k and phonons of the branch n, is essentially based on the following four mechanisms, illustrated in Fig. 4.11.

i Scattering out of k by absorption of a phonon.
ii Scattering into k by emission of a phonon
iii Scattering out of k by emission of a phonon
iv Scattering into k by absorption of a phonon.

In the derivation of the scattering time, we will assume the optical phonons to be dispersionless. From the Hamiltonian (4.47) it then follows that the matrixelement between the states k and k+q is equal to the matrixelement between k and -(k+q), provided everything else is the same. Thus the matrix-elements for the absorption processes i and iii are given by

$$\begin{aligned} M^2_{a,n} &= \{\langle k+q,\ n_n-1\ |H|\ k,n_n\rangle\}^2 \\ &= \{\langle -(k+q),\ n_n-1\ |H|\ k,n_n\rangle\}^2 \\ &= 1/N \cdot (g_n \hbar\omega_n)^2 \cdot n_n \end{aligned} \tag{4.50}$$

and correspondingly for the two emission processes ii and iv

$$\begin{aligned} M^2_{e,n} &= \{\langle k+q,\ n_n+1\ |H|\ k,n_n\rangle\}^2 \\ &= \{\langle -(k+q),\ n_n+1\ |H|\ k,n_n\rangle\}^2 \\ &= 1/N \cdot (g_n \hbar\omega_n)^2\ (n_n+1) \end{aligned} \tag{4.51}$$

$n_n$ is the number of phonons with energy $\hbar\omega_n$. Further, we will use relations concerning the distribution functions (3.2):

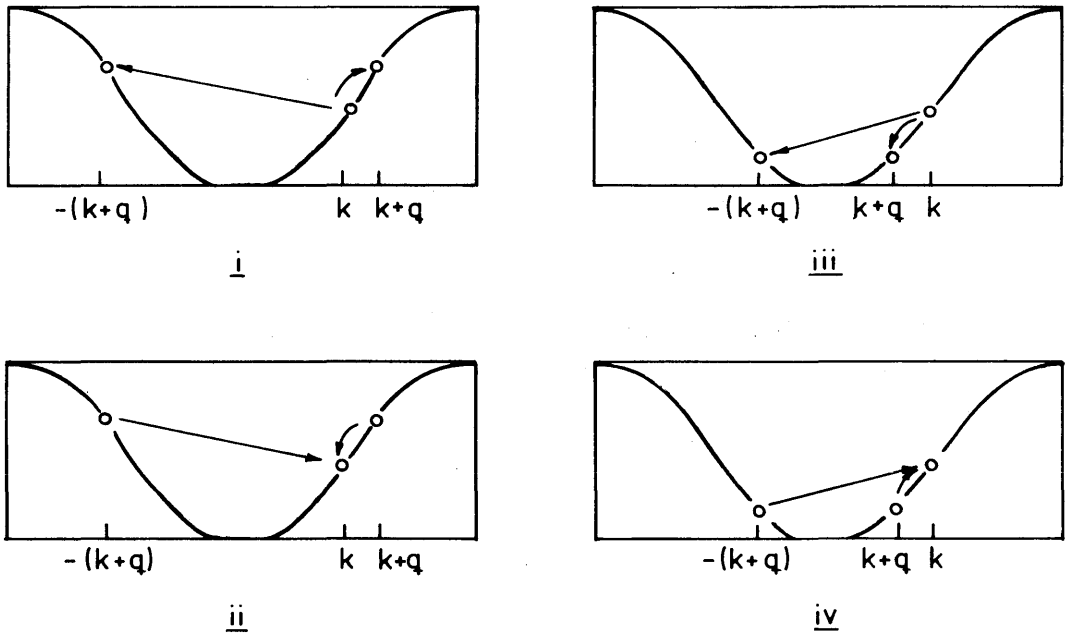


Fig. 4.11 Electron scattering by intramolecular vibrations, assuming $\omega_n(q) = \omega_n(-q)$. i Scattering out of the state k by absorbing a phonon q, ii scattering into k by emission of a phonon, iii scattering out of k by emission of a phonon, and iv scattering into k by absorption of a phonon.

$$f_k = f_k^o + g_k \tag{4.52a}$$

$$f_{k+q} = f_{k+q}^o + g_{k+q} \tag{4.52b}$$

$$f_{-(k+q)} = f_{k+q}^o - g_{k+q} \tag{4.52}$$

which are valid in one-dimensional systems. Thus the scattering term in the Boltzmann equation, due to the i-process is given by:

$$\left(\frac{g_k}{\tau}\right)_n^{(i)} = \frac{2\pi}{\hbar} M_{a,n}^2 N_\sigma(\varepsilon_{k+q}, k+q)\ h(W-\varepsilon_k-\hbar\omega_n)$$

$$\cdot\left[f_k(1-f_{k+q}) + f_k(1 - f_{-(k+q')})\right] \tag{4.53}$$

where the symmetry of the density of states (4.14) and the h(x) stepfuntion are utilized. From (4.14) and (4.52), the scattering term (4.52) reduces to

$$\left(\frac{g_k}{\tau}\right)_n^{(i)} = \frac{2}{\hbar}(g_n\hbar\omega_n)^2\, n_n \cdot h(W-\varepsilon_k-\hbar\omega_n)$$

$$\frac{(f_k^o + g_k)(1 - f_{k+q}^o)}{\left[(\varepsilon_k+\hbar\omega_n)(W-\varepsilon_k-\hbar\omega_n)\right]^{\frac{1}{2}}} \tag{4.54}$$

In a similar way the scattering term due to the ii-process becomes

$$\left(\frac{g_k}{\tau}\right)_n^{(ii)} = -\frac{2\pi}{\hbar} M_{e,n}^2 N_\sigma(\varepsilon_{k+q}, k+q)\ h(W-\varepsilon_k-\hbar\omega_n)$$

$$\cdot\left[f_{k+q}(1-f_k) + f_{-(k+q)}(1-f_k)\right] \tag{4.55}$$

reducing to

$$\left(\frac{g_k}{\tau}\right)_n^{(ii)} = -\frac{2}{\hbar}(g_n\hbar\omega_n)^2(n_n+1)\cdot h(W-\varepsilon_k-\hbar\omega_n) \cdot \frac{f^o_{k+q}(1-f^o_k-g_k)}{\left[(\varepsilon_k+\hbar\omega_n)(W-\varepsilon_k-\hbar\omega_n)\right]^{\frac{1}{2}}} \tag{4.56}$$

Combining these two processes, i and ii, gives the total interaction between the state k and the states with energy $\varepsilon_k+\hbar\omega_n$. After a few reorganizations, the sum of (4.54) and (4.56) becomes

$$\left(\frac{g_k}{\tau}\right)_n^{(i+ii)} = \frac{2}{\hbar}(g_n\hbar\omega_n)^2 \frac{h(W-\varepsilon_k-\hbar\omega_n)}{\left[(\varepsilon_k+\hbar\omega_n)(W-\varepsilon_k-\hbar\omega_n)\right]^{\frac{1}{2}}} \tag{4.57}$$

$$\cdot\left[n_n f^o_k(1-f^o_{k+q}) - (n_n+1)f^o_{k+q}(1-f^o_k)+n_n g_k(1-f^o_{k+q})+(n_n+1)g_k f^o_{k+q}\right]$$

By use of the form of the Fermi-Dirac distribution function

$$f^o_k \equiv f^o(\varepsilon_k) = 1/\left[\exp\left[(\varepsilon_k-\varepsilon_F)/k_BT\right]+1\right] \tag{4.58}$$

and the Bose-Einstein distribution function

$$n_n \equiv n(\hbar\omega_n) = 1/\left[\exp\left[\hbar\omega_n/k_BT\right]-1\right] \tag{4.59}$$

it is seen that the sum of the first two terms in the bracket of (4.57) vanishes, in accordance with the condition in thermal equilibrium

$$n_n f^o_k(1-f^o_{k+q}) - (n_n+1)f^o_{k+q}(1-f^o_k) \equiv 0 \tag{4.60}$$

Further, the distribution functions lead to the relations

$$n_n+1 = e^{(\hbar\omega_n/k_BT)} \cdot n_n \tag{4.61}$$

and

$$1 - f_k^o = e^{((\varepsilon_k-\varepsilon_F)/k_BT)} \cdot f_k^o \tag{4.62}$$

Hence the relaxation-time due to the i and ii processes is in the form

$$\left(\frac{1}{\tau}\right)_n^{(i+ii)} = \frac{2}{\hbar}(g_n\hbar\omega_n)^2 \, n_n \, \frac{1-f^o(\varepsilon_k+\hbar\omega_n)}{1-f^o(\varepsilon_k)} \, \frac{h(W-\varepsilon_k-\hbar\omega_n)}{[(\varepsilon_k+\hbar\omega_n)(W-\varepsilon_k-\hbar\omega_n)]^{\frac{1}{2}}} \tag{4.63}$$

Similarly, a relaxation time due to interaction between the state k and the states with energy $\varepsilon_k-\hbar\omega_n$, can be deduced. The process iii, where the electron is scattered out of k by emission of a phonon of the branch n, then becomes

$$\left(\frac{g_k}{\tau}\right)_n^{(iii)} = \frac{2}{\hbar}(g_n\hbar\omega_n)^2(n_n+1)(f_k^o+g_k)(1-f_{k+q}^o) \, \frac{h(\varepsilon_k-\hbar\omega_n)}{[(\varepsilon_k-\hbar\omega_n)(W-\varepsilon_k+\hbar\omega_n)]^{\frac{1}{2}}} \tag{4.64}$$

and the process iv, reverse of iii:

$$\left(\frac{g_k}{\tau}\right)_n^{(iv)} = -\frac{2}{\hbar}(g_n\hbar\omega_n)^2 \, n_n \, f_{k+q}^o(1-f_k^o-g_k) \, \frac{h(\varepsilon_k-\hbar\omega_n)}{[(\varepsilon_k-\hbar\omega_q)(W-\varepsilon_k+\hbar\omega_n)]^{\frac{1}{2}}} \tag{4.65}$$

After reductions by use of (4.58) to (4.60) the sum of the processes iii and iv is given by

$$\left(\frac{1}{\tau}\right)_n^{(iii+iv)} = \frac{2}{\hbar}(g_n\hbar\omega_n)^2 \frac{1-f^o(\varepsilon_k-\hbar\omega_n)}{1-f^o(\varepsilon_k)} \frac{h(\varepsilon_k-\hbar\omega_n)}{\left[(\varepsilon_k-\hbar\omega_n)(W-\varepsilon_k+\hbar\omega_n)\right]^{\frac{1}{2}}} \tag{4.66}$$

The resulting relaxation time for electrons in the state k, due to interactions with the intramolecular optical phonons of the mode n is finally given by the sum of (4.63) and (4.66). The effects of the h-functions is that they exclude contribution to the scattering when the phonon-energy is too large to keep electrons in the band, i.e. for the terms described in (4.63), h vanish when

$$\varepsilon_k + \hbar\omega_n > W \tag{4.67}$$

and correspondingly for (4.66), when

$$\varepsilon_k - \hbar\omega_n < 0 \tag{4.68}$$

The resulting relaxation time due to interaction with all the intramolecular vibrations is now given by summation of scattering terms described for each mode in (4.63) and (4.66). |84|

$$\tau^{-1}(\varepsilon_k) = \frac{2}{\hbar}\sum_n (g_n\hbar\omega_n)^2 \cdot \tag{4.69}$$

$$\left[(n_n+1)\cdot\frac{1-f^o(\varepsilon_k-\hbar\omega_n)}{1-f^o(\varepsilon_k)}\cdot\frac{h(\varepsilon_k-\hbar\omega_n)}{\left[(\varepsilon_k-\hbar\omega_n)(W-\varepsilon_k+\hbar\omega_n)\right]^{\frac{1}{2}}}\right.$$

$$\left. n_n\cdot\frac{1-f^o(\varepsilon_k+\hbar\omega_n)}{1-f^o(\varepsilon_n)}\cdot\frac{h(W-\varepsilon_k-\hbar\omega_n)}{\left[(\varepsilon_k+\hbar\omega_n)(W-\varepsilon_k-\hbar\omega_n)\right]^{\frac{1}{2}}}\right]$$

Before discussing the transport properties that emerges from the electron scattering by interaction with the intramolecular vibrations, it is useful to understand the effect of

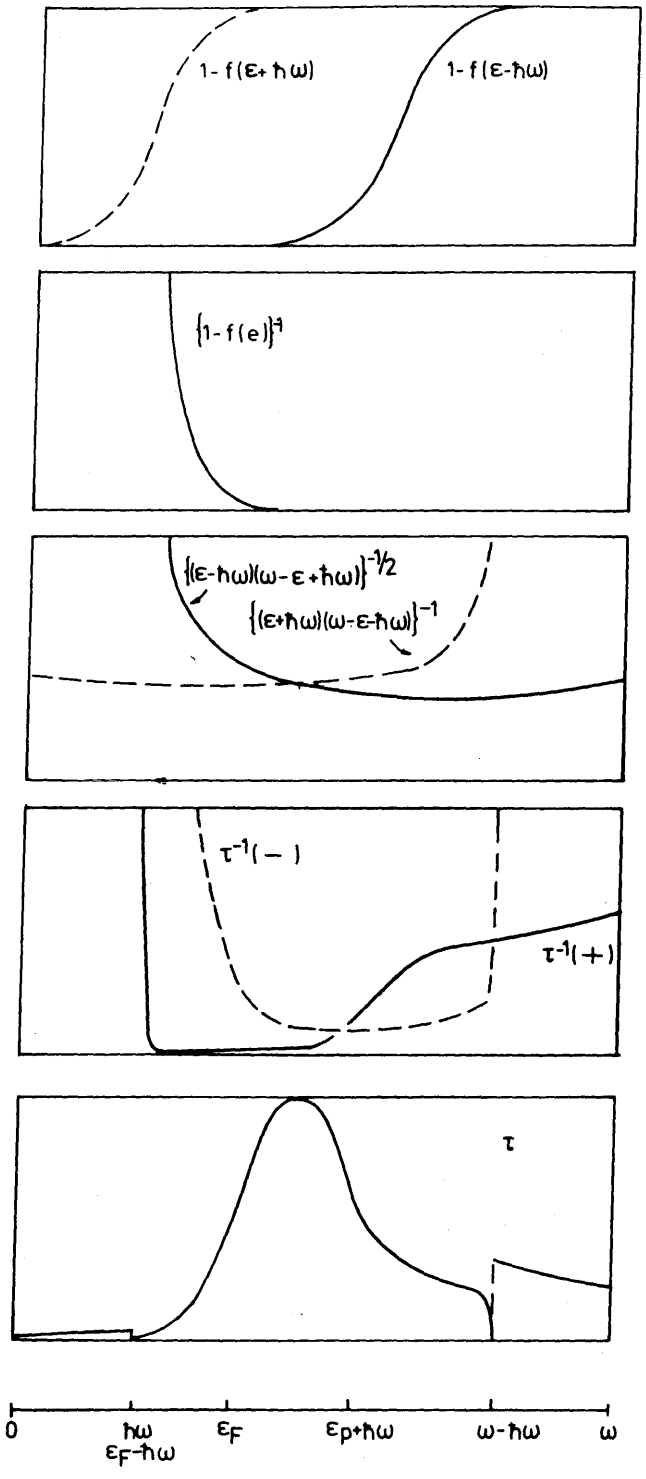


Fig. 4.12 Schematic illustration of the relaxation time ($\tau$) for a TCNQ-band with electrons scattered by one intramolecular mode.

each of the terms in (4.69). In Fig. 4.12, an illustrative example is given, showing the energy-dependence of the relaxation time for scattering by one mode. For a band like that of the acceptor chain in TTF-TCNQ, the illustration corresponds to approximately 250K, i.e. a typical temperature in the region discussed.

A characteristic behaviour of the scattering due to these high energy internal modes is seen to be a sharp drop in relaxation time when the various scattering mechanisms set in. That is for energies above $\hbar\omega_n$ for interaction with the states of energy $\varepsilon_k-\hbar\omega_n$, and below $W-\hbar\omega_n$. Further the magnitude of $\tau$ below $\varepsilon_F+\hbar\omega_n$ and above $\varepsilon_F+\hbar\omega_n$, by the terms $(1-f^o(\varepsilon_k\pm\hbar\omega_n))$, is substantially reduced compared to the value at the Fermi-level. The transport behaviour is therefore solely a matter of charge carriers confined to the regime, $|\varepsilon_F-\hbar\omega_n,\ \varepsilon_F+\hbar\omega_n|$. At high temperature, these limits are smeared out, whereas they may be rather sharp at low temperatures. Besides this, due to the relaxation time enclosed number of electrons taking part in transport mechanism, the conventional limits to a region of width $k_BT$ around $\varepsilon_F$ is substantial.

In Fig. 4.13, the individual terms resulting in a transport coefficient are shown for each of the single electron states in the conducting band. The present example is the thermopower of the TCNQ-band, including all 10 internal modes (Table 4.2). The energy and coupling coefficients for these modes are diagramatically shown in Fig. 4.13a. The resulting macroscopic thermopower is essentially equal to the integral of the curves in Fig. 4.13f. We recognize the structure of the relaxation time (Fig. 4.13b) as qualitatively equal to that discussed referring to Fig. 4.12. At both temperatures shown, this structure may be of great importance for the transport behaviour, in particular the thermopower. Thus numerical calculations are necessary when the effect of scattering due to intramolecular vibrations are investigated.

In Fig. 4.14 calculations of the mobility and thermopower for the TCNQ-chain are shown. The values of $\hbar\omega_n$ and $g_n$ used for the calculations are given in Table 4.2. The temperature dependence

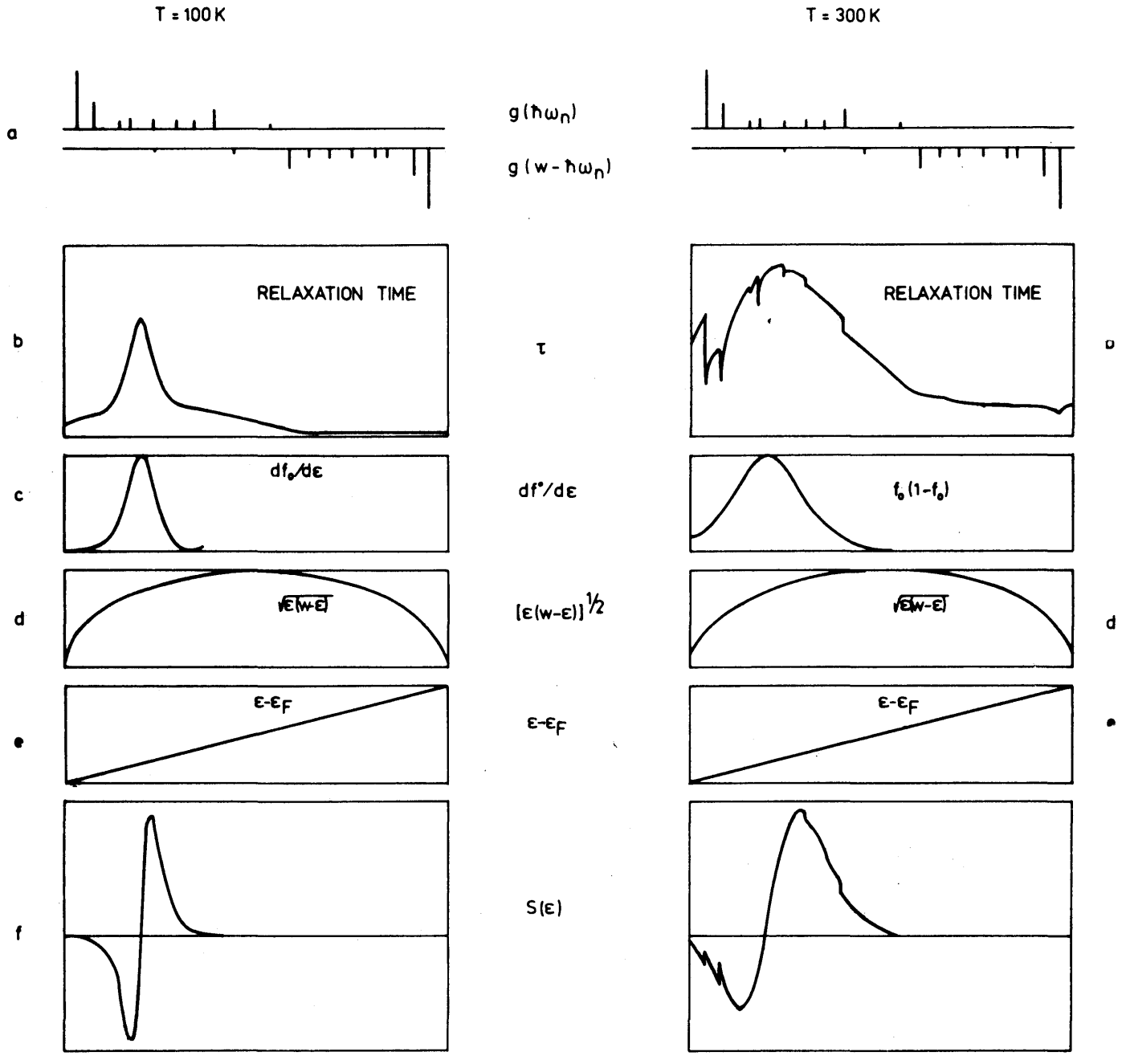


Fig. 4.13. Sketch of the terms resulting in the thermoelectric power: $S \propto - \int (\varepsilon-\varepsilon_F)\tau(\varepsilon)\left[\varepsilon(W-\varepsilon)\right]^{\frac{1}{2}} \left(-\frac{df}{d\varepsilon}\right) d\varepsilon$

a Energy and coupling constants of the internal modes interacting with the electrons

b the electron-scattering time, $\tau(\varepsilon)$

c the Fermi factor, $-df/d\varepsilon$

d Density of states $N(\varepsilon) \propto \left[\varepsilon(W-\varepsilon)\right]^{\frac{1}{2}}$

e $\varepsilon-\varepsilon_F$

f The product of b-e

of the mobility is seen to be in good agreement with the experimentally found $\mu \propto T^{2.3}$ behaviour at ambient pressure. The absolute room-temperature value of 13.5 $cm^2/Vs$ is however 2.3 times the value found experimentally in the best crystals. Further, the electron scattering by the internal vibrations can not account for the strong pressure dependence. The only pressure dependent parameters are the bandwidth W, and the charge transfer $\rho$, and none of these is able to explain the $\mu(P)$ behaviour.

With respect to the thermopower, we must know the intrinsic values of S and $\mu$ for both chains, unless one of them does not contribute to the transport at all. Based on the parameters given in Table 4.2 these values, besides the mobility for TCNQ already given, become $\mu(TTF) = 4.2$ $cm^2/Vs$, $S(TTF) = 16$ $\mu V/K$ and $S(TCNQ) = -38$ $\mu V/K$. The resulting thermopower for TTF-TCNQ is hence -26 $\mu V/K$, in good agreement with experiments. Also the quasi-linear temperature dependence (Fig. 4.14b) is in agreement with experiments.

In conclusion, however, we must, based on the mobility data, exclude the model of a scattering mechanism solely due to the interaction with intramolecular vibrations.

Table 4.3 Transport behaviour for TTF-TCNQ, when the carriers interact with the internal modes given in Table 4.2.

| | TTF* | TCNQ | TTF-TCNQ | experimental TTF-TCNQ |
|---|---|---|---|---|
| $\mu(cm^2/Vs)$ | 4.2 | 13.5 | 17.7 | 3 |
| $S(\mu V/K)$ | 16 | -38 | -26 | -30 |

* The mobility of TTF corresponds to conduction by holes, i.e. 0.59 carrier per molecule.

Fig. 4.14 Transport behaviour of carriers in the TCNQ-chain coupled to the internal vibrations (Table 4.2). a Mobility versus temperature b Thermopower versus temperature.

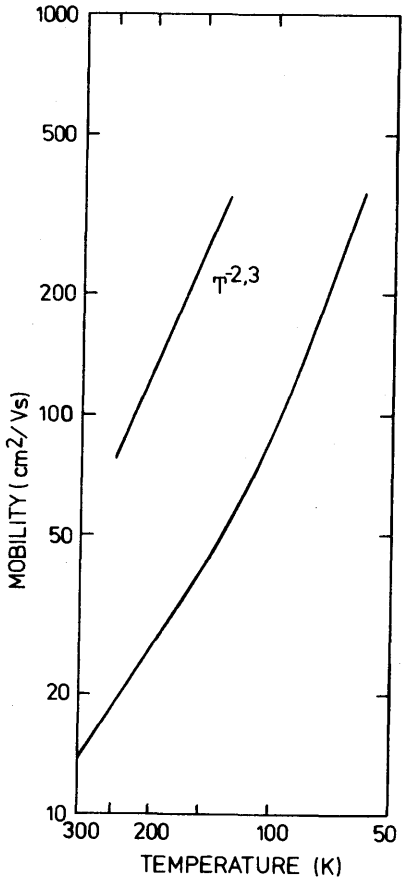


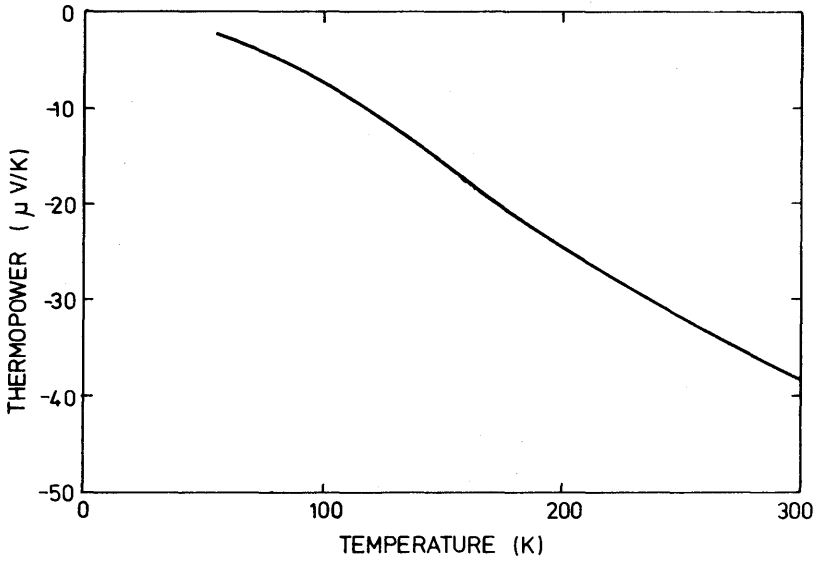

## 4.8 SCATTERING BY ALL FIRST ORDER ELECTRON-PHONON INTERACTIONS

From the previous discussion it appears that the best known parameters with regard to electron-phonon interactions, probably all concern first order interactions. In the present part the transport behaviour in TTF-TCNQ will be calculated on the basis of all these well-known first-order e-p interactions. The coupling constants and phonon energies utilized are given in Table 4.1 and 4.2 for the TCNQ-acoustic modes and for the internal optical modes, respectively. In the absence of data for the external modes of the TTF-chain, the values are taken to be the same as for TCNQ. The bandwidths used are 0.5 eV for the TCNQ- and 0.25 eV for the TTF-band |28|, and the charge-transfer is 0.59 electrons/molecule |85|.

In Fig. 4.15 and 4.16 numerical calculations of the mobility and thermopower are shown. The mobility is seen to be dominated by the TCNQ-chain, as expected from the experimental data of the thermopower |39| and Hall-effect |40|. Still, however, the first order e-p scattering gives a room-temperature mobility, which is too large.

On the other hand, the thermopower comes out to be in good agreement with the experimental data (Fig. 1.8 and 4.16c). The S(T) curve is not quite as linear as the one experimentally found, but has a slight curvature. That is mainly a result of the scattering properties in the TTF-chain: At high temperatures all modes contribute equally to the scattering process, whereas the external modes dominate at lower temperature (see also Fig. 4.15). From Fig. 4.16 it appears that the thermopower is a result of intrinsic terms of numerical values much larger than the resulting one. In a system where only one of the chains contributes to the transport-properties, we therefore on the basis of first order electron-phonon interaction would expect a rather enhanced thermopower. This is in fact the experimental reality in TTF-TCNQ. Taking doping experiments, for example, we may expect the conductivity of the doped chain to decrease because of static disorder, and therefore more or less bulk transport behaviour equal to the intrinsic values of the undoped chain |86|. Doping of TTF-TCNQ with TSF, in that way, results in an enhanced thermopower of approximately 5o% |87|, in good agreement with the model in discussion.

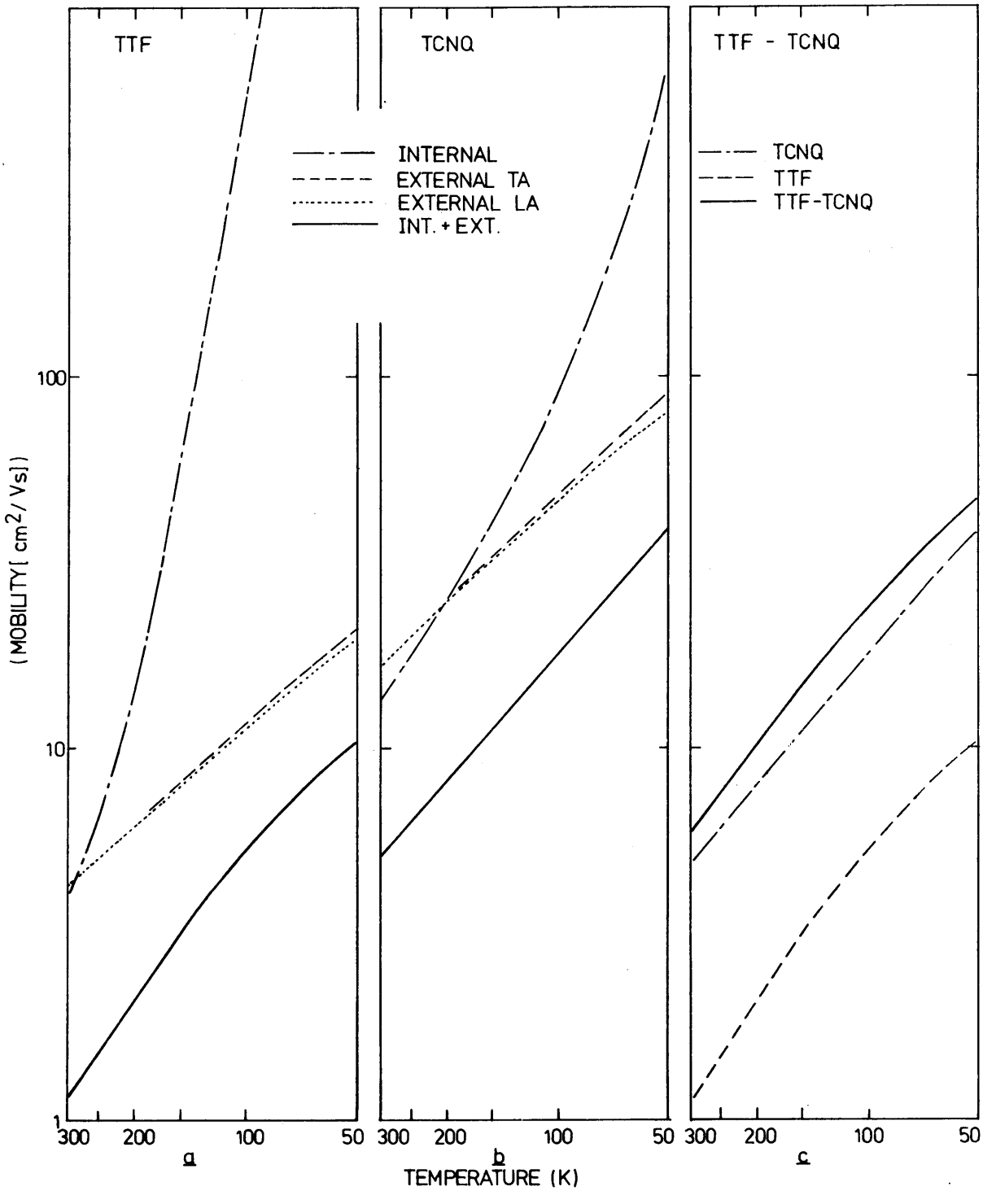


Fig. 4.15 Mobility of holes in TTF (a), and electrons in TCNQ (b), for first-order e-p scattering. c mobility of the charge carriers in TTF-TCNQ.

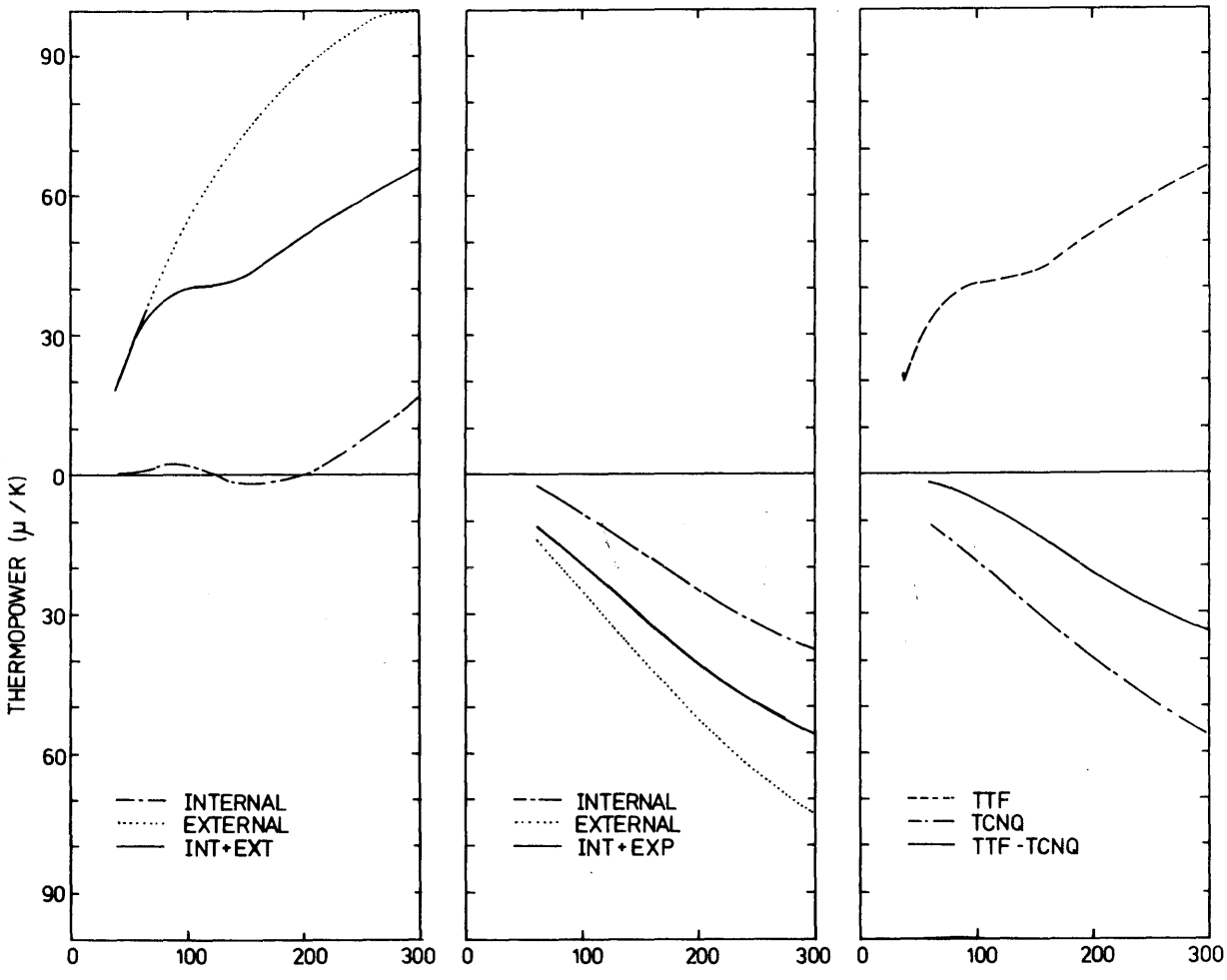


Fig. 4.16 Thermopower of the TTF-band (a), the TCNQ-band (b) and the TTF-TCNQ two-band system, when scattering is due to first-order e-p interactions.

Assuming the model to be essentially correct, the reduced mobility in the experiments may originate in some sort of lattice-defect scattering |81|. That would also explain the rather large variations in the observed $\sigma_{max}/\sigma(300K)$-ratio.

## 4.9 ELECTRON-ELECTRON INTERACTION |89,91|.

In the previous discussions concerning scattering mechanisms the electron-electron interaction has been completely ignored. This is in contrast to a number of proposed models that have used the enhanced susceptibility over the Pauli-value as evidence for strong Coulomb-coupling |88|. In fact, e-e interaction has also been proposed to account for the conductivity behaviour in TTF-TCNQ |89-91|.

In order to affect the conductivity, the e-e collisions must transfer momentum to the lattice. This may be done via i, Umklapp-processes or ii (provided a two-band model) via transfering momentum from high-mobility charge carriers in the one band, to low mobility carriers in the other. From the discussions in the previous parts, concerning electron-phonon interactions, the latter possibility of e-e scattering mechanism must be excluded in the TTF-TCNQ. Although the e-p relaxation time turned out to be larger in the TCNQ-band than in the TTF, the difference was not big enough to explain a drain of momentum from the acceptor-chain, via the donor-chain to the lattice. In one-chain systems like $(TMTSF)_2-PF_6$, for example a possibility of contribution to the resistivity from e-e interactions in the form of ii, by definition does not exist. Thus, scattering due to electron-electron interaction is only working via Umklapp processes.

A collision between an incident electron at the Fermi-level, with momentum $k_1 = k_F$ and a target electron of momentum $k_2$, must satisfy the momentum conservation law

$$k_1 + k_2 = k_1' + k_2' + g \qquad (4.70)$$

where g is a reciprocal lattice vector. In three dimensions the conductivity due to e-e processes is given by |92|

$$\sigma_{e-e} = \frac{e^2}{\hbar} \frac{1}{k_F \sigma_F} \left(\frac{\varepsilon_F}{k_B T}\right)^2 \qquad (4.71)$$

where $\sigma_F$ essentially is the e-e matrix element. The dominant factor in this expression is the $(k_B T/\varepsilon_F)^{-2}$ - term, which arises from the need to satisfy the Pauli-exclusion principle twice, once for the initial state of the electron, and once for the final. By use of the extended Born-approximation, the conductivity in a tight binding band model becomes |91|

$$\sigma_{e-e} = \frac{\pi^2 b}{2\, e^2 \hbar k_B^2} \frac{W^4\, \rho^3 \sin^4(\pi\rho/2)}{Q\, T^2} \qquad (4.72)$$

where Q is a function of the screening constant. The main factors to note in (4.72) are the dependencies on the bandwidth, $W^4$, and the charge-transfer, $\rho^3 \sin^4(\pi\rho/2)$. These factors could explain the large pressure dependence of the conductivity, and the deviation from the $T^{-2}$-dependence.

In strictly one-dimensional systems Umklapp-processes involve simultaneous jumps of two electrons from one side of the Fermi-surface to the other, i.e. $k_1=k_2=k_F$ and $k_1'=k_2'=-k_F$. But then from (4.70) we have that the scattering process can only occur in the case of <u>one</u> electron per molecule, because only in that case is $4k_F$ equal to an inverse lattice vector. It is well known that TTF-TCNQ under ambient pressure has 0.55-0.59 electrons per molecule. Therefore electron-electron scattering can not be the dominant mechanism of resistivity.

Furthermore, the final states in one dimension are entirely defined by the momentum relation (4.70) in contrast to two and three dimensions where the number of allowed final states introduced a $(k_B T/\varepsilon_F)$-factor. Therefore, e-e scattering vary only linearly with temperature in 1D. |93|

In conclusion, the e-e collisions can not be the dominant scattering mechanism in the highly conducting organic materials

like TTF-TCNQ. On the other hand, there is good evidence for a strong Coulomb correlation in the 1:2 salts with narrow, 1/4-filled bands, e.g. Qn $(TCNQ)_2$ |94,95|.

## 4.10 INFLUENCE OF LATTICE DEFECTS AND IMPURITIES

The rather large variations in the experimental conductivity behaviour in TTF-TCNQ, especially the $\sigma_{max}/\sigma_{RT}$-ratio, provides evidence that the transport properties are affected by some sort of lattice defects or impurities. We will not take up a detailed discussion on how to model these effects,or on the possibility that defects may lead to localized states in one-dimensional systems. Instead we will in an extremely simplified model assume that the effect of defects can be represented by a relaxation time on equal terms with the other scattering mechanisms.

In the model we assume that the defects can be represented by an effective average chainlength consisting of $\nu$ molecules, $\ell = \nu \cdot b$. The scattering is then given by the inverse relaxation-time, as

$$\tau_d = v/\nu b \tag{4.73}$$

where v is the velocity of the charge carriers. In a tight binding band model we thus have

$$\tau_d = \frac{[\varepsilon(W-\varepsilon)]^{\frac{1}{2}}}{\nu\hbar} \tag{4.74}$$

In Fig. 4.17 some calculations are shown in order to illustrate the influence of the defects. The example gives the TCNQ-band with 0.59 electrons per molecule and width equal to 0.50 eV. Besides the effect of an effective finite chain-length, the scattering is taken to occur via interaction with the LA-mode. The chain-length is assumed to be independent of temperature.

The effect of an additional scattering mechanism due to such chain-breaks is obviously a reduced conductivity, but also a

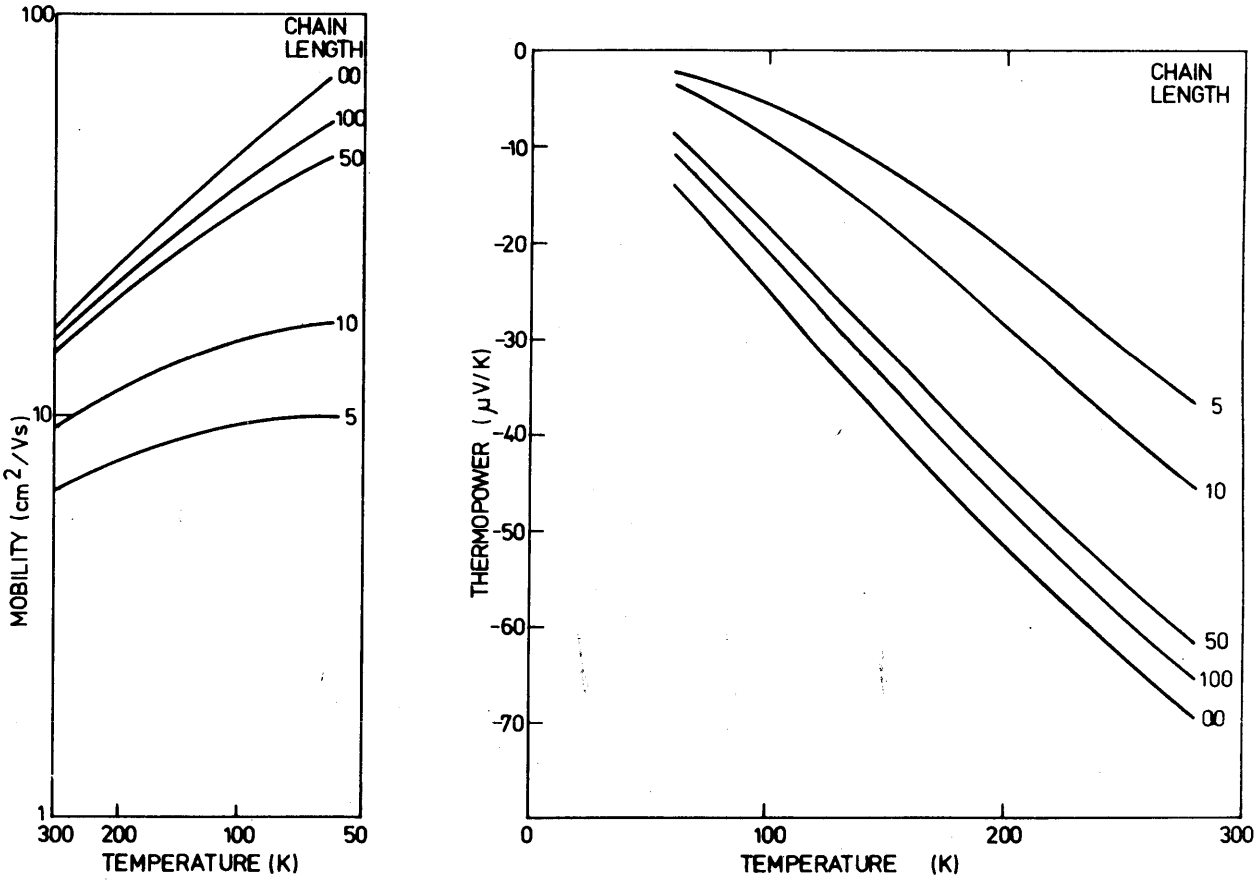


a b

Fig. 4.17 Numerical calculations of a mobility and b thermopower for scattering due to a finite chain legnth (=ν•b) and acoustic modes.

reduced thermopower. If we for a moment imagine $\tau_d^{-1}$ to be the dominating scattering term, we have from (4.73) and (3.66) a vanishing thermopower. That is to say that the intrinsic thermopower due to the effect of a finite chain-length is zero. This is a property of the 1D Fermi surfaces (In the case of a 3D-spherical FS, the pure impurity scattering would reduce the band-TEP with a factor of three).

From the Nordheim-Gorter rule (3.55), when more scattering mechanisms are prominent, the resulting thermopower is reduced in proportion to the intrinsic parts, as

$$S = \frac{\rho_o}{\rho_o + \rho_d} S_o \qquad (4.75)$$

as it was seen in Fig. 4.17b. The labels d and o marks the intrinsic values due to scattering by the defects and all other mechanisms, respectively.

The assumed impurity model of an effective chainlength independent of the electron energy is probably somewhat erroneous. Detailed calculations in 3D systems with isotropic scattering by ionized impurities lead on the contrary to a $\ell \propto v^4$, i.e. $\tau \propto v^3$ |96|. This kind of impurity scattering will result in an enhanced TEP rather than the reduced found above. The calculations are, however, based on isotropic scattering, and can therefore not in a simple way be transformed to the 1D situation. To our knowledge there are no impurity scattering models available for single-particle transport calculations.

Provided the characteristic chain-length is independent of the temperature, it is from (4.73) evident that the scattering term is as well. As T goes to zero, the common electron-phonon scattering vanishes. The impurity-term becomes therefore more important as T is lowered.

For impurities with magnetic moments, however, the spin-degeneracy lead to an impurity scattering which is intrinsically T-dependent. At low temperatures it is well known from 3D dilute alloys that such magnetic impurities are the origin of the peculiar resistivity minimum and the correlated strongly tem-

perature dependent susceptibility |97,98|.

In attempts to understand this effect of magnetic impurities, the scattering term must be calculated beyond the first Born approximation that usually is sufficient. To treat the interaction between a conduction electron with spin s and an impurity with spin S, we use the isotropic exchange Hamiltonian

$$H = -J/N \cdot S \cdot s \tag{4.76}$$

where J is the exchange coupling constant. In the first order Born approximation, we have the matrix-element

$$M_1(k+,k'+) = \langle k+|H|k'+\rangle \tag{4.77}$$

for an electron with spin (+) scattered from state k to k'. By using (4.76) we get

$$M_1(k+,k'+) = -J/2N\ S_z \tag{4.78}$$

This term will in principle act like the (unmagnetic) impurities discussed above. However, going to the second order Born approximation, Kondo has shown that a rather large temperature dependent scattering results. Scattering from the state (k+) to the state (k'+) via an intermediate state (k"σ) can appear in two kinds of processes. i The electron is first scattered to (k",σ) and then to the final state, and ii, an electron is first scattered from the (k",σ) into the final state and then the "initial" electron is accepted in (k",σ). The matrix element corresponding to these processes is |97|

$$M_2 = \sum_{k"\sigma} \frac{1}{\varepsilon_k - \varepsilon_{k"}} \left[ (1-f_{k"}) \langle k+|H|k"\sigma\rangle\langle k"\sigma|H|k'+\rangle + f_{k"} \langle k"\sigma|H|k'+\rangle\langle k+|H|k"\sigma\rangle \right] \tag{4.79}$$

Unlike normal scattering processes, the order of the terms in the bracket of (4.79) for spin correlation is significant. The Fermi-Dirac function $f_{k"}$ is therefore not canceled, but leads

to a strongly energy dependent scattering term, which approximately may be written in the form |97|

$$M_2 \simeq 2 \left(\frac{J}{2N}\right)^2 S_z N(\varepsilon_F) \ln \left(W/(\varepsilon_F-\varepsilon_k)\right) \qquad (4.80)$$

The singularity in this expression can be shown to lead to an impurity resistivity of logarithmic temperature dependence |97|

$$\rho(T) \sim \rho_o \left[1-2(J/N)N(\varepsilon_F) \ln (W/k_BT)\right] \qquad (4.81)$$

which combined with the common e-p scattering can explain the observed resistivity minimum.

From the thermopower expression (3.66) we notice that the strongly energy dependent scattering (4.80) will lead to a rather large thermopower, as the impurity scattering becomes dominating, i.e. at low temperatures. This is in agreement with experiments, e.g. Fe-impurities in Au, which characteristically show a well defined peak in S(T).

These effects of localized magnetic impurities, the Kondo effects, are in the derivation based on isotropic 3D scattering. To our knowledge corresponding calculations have never been done in strictly 1D models, but we believe that the results are qualitatively the same.

The arguments above, concerning lattice defects and (unmagnetic) impurities have assumed these to be evenly distributed, so that an effective chain length can be defined. Often, however, this is probably not the situation in the crystals of interest. In the example shown in Fig. 4.18b there are only a few, but violent defects. The electrical contacts between the domains are probably more or less destroyed, resulting in a large external resistance, although the intrinsic material may be highly conducting. The thermal contacts between the domains need not be affected in a corresponding manner. More likely the small region of defect is almost thermally shortened. From (3.58) we find the measured thermopower to be equal to the intrinsic value.

Thus, the TEP measurement is well-suited for the quasi-one-dimensional compounds.

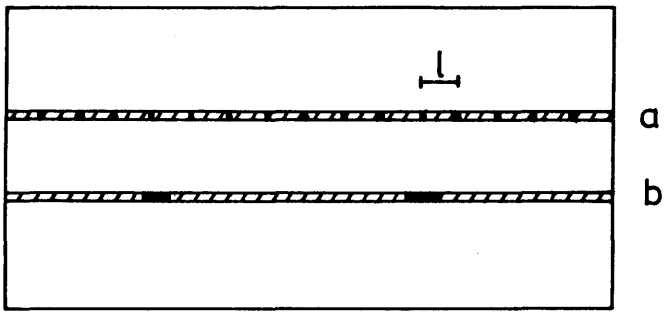


Fig. 4.18 Illustration of defects in the chain. a The defects lead to an additional scattering mechanism represented by the length l, and b, the defects separate the chain into independent domains.

# CHAPTER V

# PHONON DRAG

Until now all calculations of the transport properties have been made under the Bloch assumption, which take the phonon system to be in equilibrium. However, from the fact that electrical insulators do conduct heat, we know that a temperature gradient induces heat transport via lattice vibrations. Such a flow of phonons may interact with charge carriers, sweeping them along from the hot end to the cold end of the specimen. Generally in 3D conductors, the phonon scattering at high temperatures more frequently is due to interaction with other phonons than with electrons. The phonon flow is therefore mainly affecting the electrical transport properties at low temperatures.

Formally the transport properties including the phonon current can be described in terms of the Boltzmann transport theory (Ch. 3). In addition to the equation for the equilibrium of the electron system we must add a corresponding equation for the phonons. The treatment of the transport properties requires thus simultaneous solution of two Boltzmann kind of equations, and may be done by use of a variational method |99|. We will not expound these calculations, but only give some qualitative comments.

## 5.1 RESISTIVITY

The electrical resistivity is affected by the phonon flow only through the lattice resistance, $\rho_L$, i.e. the scattering by lattice vibrations. The resistance can be written in the form |99|.

$$\rho = \rho_o + \rho_L^N (1 - \gamma^N) + \rho_L^U (1 - \gamma^U) \qquad (5.1)$$

where N and U denotes normal and Umklapp processes respectively and the drag parameter $\gamma$ is a measure of the probability for the phonons to transfer their momentum to the electrons.

In ordinary 3D metals, the phonons are mainly scattered by impurities and other phonons, the latter especially at high temperatures. Thus the drag effect on the resistivity only occurs at low temperatures and only when the materials are very pure.

In 1D metals, on the contrary, Gutfreund and others |100-102| have proposed that phonon drag may play a major role in the conductivity, even at ambient temperature. Kaveh et al. |102| showed that the phonon drag only affects the Normal scattering processes. The Umklapp processes are unaffected apart from a multiplication with a nearly temperature-independent factor $(1-\gamma^U)$, whose magnitude is close to unity. On the other hand, since all electrons on the Fermi Surface of a 1D metal participate in the absorption of $2k_F$-phonons, the absorption rate of these $2k_F$ phonons by the electrons is far greater than in 3D systems. Thus the phonons with $q_{\parallel}=2k_F$ have no time to equilibrate with the lattice and are dragged along by the electrons |103|. In this model the phonon-drag therefore eliminates all normal electron-phonon scattering.

As remarked in chapter 4, there is no first order electron-phonon Umklapp processes in 1D systems with $4k_F < 2\pi/b$.

A consequence of the discussion above is therefore that the lattice resistivity is arising from second order electron-phonon (libron) Umklapp processes only. Evidence for this model has come from the experimental investigations of irradiated TTF-TCNQ samples, where the phonon-drag must be quenched by the phonon-impurity scattering |102|. The resistivity of these crystals can be given in the form

$$\rho = \rho_o + A \cdot T + B\, T^{2.3} \qquad (5.2)$$

where the linear term, AT, account for the scattering due to acoustic modes in the absence of phonon-drag, and the "quadractic" term, $BT^{2.3}$, approximately is doubled compared to pure samples because of the additional N-scattering processes.

The phonon-drag is a dc-effect. The enhanced conductivity will therefore only occur at low frequencies. This is in agreement with the observed very strong frequency dependent conductivity, which falls off considerably at $\omega \sim 10\ cm^{-1}$ |104,105|.

## 5.2 THERMOPOWER

In 3D metals the most striking consequence of phonon drag is usually seen in thermoelectric power |19-21|. As the phonon flow drags electrons with it, extra electrons tend to pile up at the cold end, creating a phonon-drag thermopower, $S_g$.

The size of this term must be proportional to the probability of a phonon-electron interaction process, relative to the probability of a phonon interacting with any particle. Thus

$$S_g \sim \frac{\tau_{pe}^{-1}}{\tau_{pe}^{-1} + \tau_{po}^{-1}} = \frac{\tau_{po}}{\tau_{po} + \tau_{pe}} \qquad (5.3)$$

where $\tau_{pe}$ and $\tau_{po}$ is the phonon relaxation time due to scattering by electrons and by any other particles, respectively. Actually the relationship (5.3) only takes into account a single phonon-state. In one-dimensional systems (5.3) may be sufficient for accurate treatment of the phonon-drag thermopower, whereas in 3D we must integrate over the phonon spectrum.

If $\tau_{pe} << \tau_{po}$, all the dissipated phonon momentum is transferred to the electrons. If we further restrict the processes to be of the N-type, we will get all the obtained momentum in the same direction, $p_e = \hbar q$, and thus the maximum attainable phonon-drag thermopower.

The force acting on the electron system from the flow of phonons |19| , is:

$$\frac{1}{3} \sum_q \frac{dn_q}{dt} \hbar q \qquad (5.4)$$

provided the phonon system behaves like an isotropic gas, $dn_q/dt$ is the rate at which phonons of wavevector q are destroyed by the N-process. (4) may be reorganized to the form

$$\frac{1}{3} \sum_q \frac{dn_q}{dT} \nabla_r T \frac{dr}{dt} \cdot \hbar q \qquad (5.5)$$

where $dr/dt = \nabla_q \omega_q$ is the phonon velocity.

But in the steady state situation, this must be equal to the electrostatic force appearing,

$$-eE_o NV \tag{5.6}$$

where NV is the number of conduction electrons in the volume V. The maximum phonon-drag thermopower, $S_g^{max} = E_o/\nabla_r T$, is thus from (5.5) and (5.6)

$$S_g^{max} = -\frac{1}{3Ne}\frac{1}{V}\sum_q \frac{dn_q}{dT} \cdot \nabla_q \omega_q \cdot \hbar\omega_q \tag{5.7}$$

Within the Debye approximation, $\omega_q \propto q$, we have

$$\nabla_q \omega_q \cdot \hbar q = \hbar\omega_q \tag{5.8}$$

Thus the phonon-drag thermopower is in the form

$$S_g^{max} = -\frac{1}{3Ne}\left(\frac{1}{V}\frac{d}{dT}\sum_q n_q \hbar\omega_q\right) \tag{5.9}$$

but the paranthesis is in fact just the lattice heat capacity, $C_v$, whereby [19]

$$S_g^{max} = -\frac{C_v}{3Ne} \tag{5.10}$$

At high temperatures, $C_v$ in the Debye approximation is constant and given by

$$C_v = 3N_o k_B \tag{5.11}$$

and so

$$S_g^{max} = -\frac{k_B}{e}\frac{N_o}{N} \tag{5.12}$$

where $N/N_o$ is the number of electrons per site.

In ordinary 3D metals, $N/N_o \sim 1$, and the maximum conceivable $S_g$ is thus of the order of $-86\mu V/K$. Umklapp-processes, however, may be as frequent as the Normal-process in this temperature regime. These processes reverse the electron velocity, resulting

in an electron flow to the hot end of the conductor, and thus contributing with a positive phonon-drag thermopower. The resulting $S_g$, which is a resistivity weighted sum of the two individual large terms, $S_g^N$ and $S_g^U$, is generally found to be very small at ambient temperatures. Whether it is positive or negative depends on the relative probability of N and U processes.

Furthermore, the phonon-drag thermopower is reduced relative to the scattering mechanism (5.3). In ordinary 3D metals the high-temperature phonon scattering is mainly due to phonon-phonon interactions. From (5.3) we therefore find

$$S_g \propto \tau_{pp}/\tau_{pe} \tag{5.13}$$

$\tau_{pp}^{-1}$ is proportional to the number of phonons, and thus approximately to the temperature, whereas $\tau_{pe}^{-1}$ is temperature-independent. We will therefore expect a phonon-drag thermopower

$$S_g \propto T^{-1} \tag{5.14}$$

a behaviour which actually is found in several metals, although deviations may be expected both from a different temperature dependence of the N and U processes, and from the influence of phonon dispersion.

At low temperatures, the phonon-electron scattering becomes dominant, and the U-processes will be frozen out. Thus the expression (5.10) should be valid. In simple 3D systems $C_v$ at low temperatures is in the form |67|

$$C_v \simeq \frac{12\pi^4}{S} N_o k_B \left(\frac{T}{\theta_D}\right)^3 \tag{5.15}$$

thus resulting in a

$$S_g \propto T^3 \tag{5.16}$$

behaviour, in accordance with several experimental results.

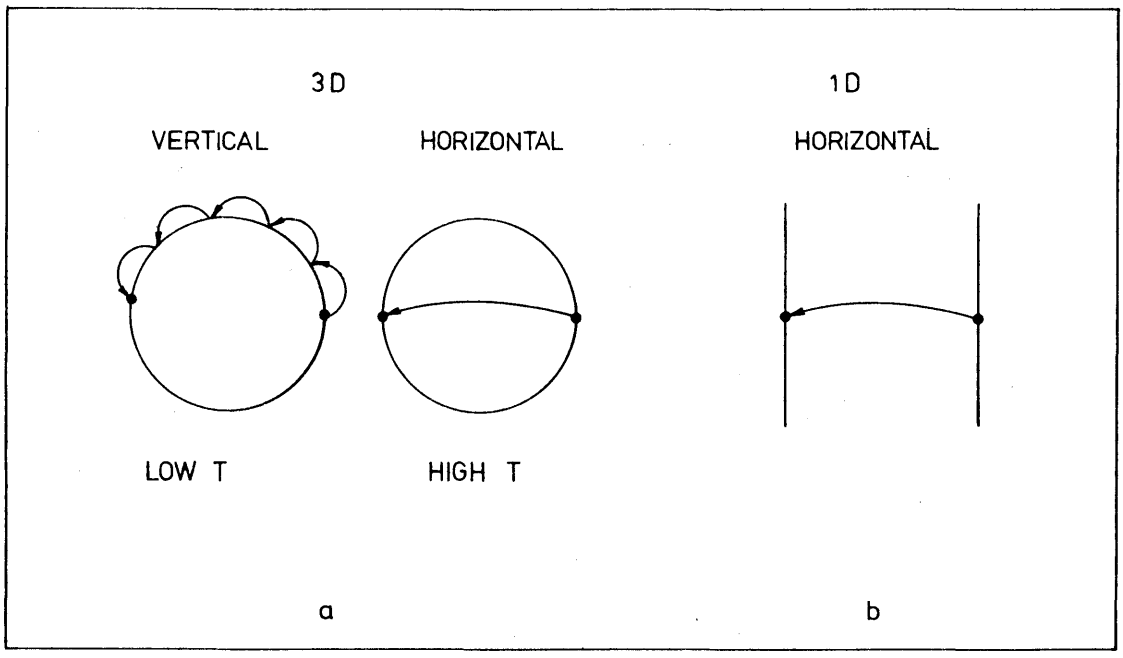


Fig. 5.1 Sketch of dominating scattering behaviour at high and low temperature in a 3D systems and in b 1D systems.

The transfer of momentum from phonons to electrons in a 3D metal is schematically outlined in Fig. 5.1a. At low temperatures there are only phonons with small energy. The main scattering is therefore "vertical", that is to say that electrons are scattered virtually at constant k |19|. At higher temperatures, on the other hand, these vertical transitions become less important. The more energetical phonons will dominate in "horizontal" processes.

In one-dimensional systems "horizontal" processes are the only possible. But the phonon softening still makes drag effects possible at all temperatures. Furthermore, we saw previously that U-processes are less frequent than momentum conserving ones in 1D systems. We would therefore from the discussion above, at first expect a rather large phonon-drag thermopower in 1D. However, from (5.7) we know that $S_g$ is proportional to the phonon group velocity. Both the librons and the intramolecular phonons are more or less dispersionless, giving only small intrinsic phonon-drag thermopowers. The dispersion of the acoustic modes is larger, but somewhat complicated by the Kohn effect, which may cause a reduced value near $q = -2k_F$. Further, the enhanced conductivity due to the acoustic phonon-drag makes the intrinsic $S_g$ less influential. The value of $S_g$ should thus be reduced appreciably compared to the Debye model.

However, much more theoretical investigations are necessary in order to understand the role of phonon-drag in one dimensional metallic systems.

CHAPTER VI

TRANSPORT PROPERTIES IN THE NON-METALLIC REGIME

In Chapter IV and V we have discussed the transport properties in one-dimensional systems based on metallic behaviour, i.e. a well defined conduction band of a width, which is large compared to the thermal energy, and an approximately temperature-independent number of uncorrelated charge carriers. However, all the known organic charge transfer compounds are at ambient pressure semiconducting below some finite temperature. The majority of charge transfer compounds are even insulating or semiconducting at ambient temperature.

The insulating, or semiconducting, state has many interesting properties of its own, but will not be discussed in detail in this thesis. However, it is appropriate to give some of the most important results. The present survey will be restricted to organic compounds of segregated stacks, which are the only candidates for metallic behaviour.

The origins of a prevalent insulating state are various.

The planar Fermi Surfaces, characteristic for 1D systems, give rise to a conduction band that is subject to the periodic lattice distortion (PLD) of wavevector $2k_F$. This formation of a superlattice causes a gap at the Fermi level producing an insulating material, the Peierls-semiconductor |18|. The dimerization of the alkali-TCNQ salts, has for example been suggested to be of the Peierls type |106|. In other materials the chains remain uniform down to reasonable low temperatures, e.g. TTF-TCNQ and $(TMTSF)_2-PF_6$ which undergo Peierls transitions at 53 K |107| and 19 K |31| respectively.

The effect of repulsive electron-electron interactions can also cause an insulating ground-state. The model Hamiltonian which is convenient to describe this situation, is the extended Hubbard-Hamiltonian |108|:

$$H = -t \sum_{\ell,\sigma} (c^{+}_{\ell,\sigma} c_{\ell+1,\sigma} + c^{+}_{\ell+1,\sigma} c_{\ell,\sigma})$$

$$+ U_o \sum_{\ell,\sigma} n_{\ell,\sigma} n_{\ell-\sigma} \qquad (6.1)$$

$$+ \sum_{\ell,j,\sigma,\sigma'} U_j \, n_{\ell,\sigma} n_{\ell+j,\sigma'}$$

where t is the ordinary nearest neighbor transfer integral, $U_o$ is the onsite Coulomb interaction and $U_j$ is the Coulomb interaction between electrons on sites j units apart.

If the Coulomb repulsion is large compared to the bandwidth, it is energetically favorable to localize the electrons |23|. In order to move an electron, double occupied sites must be created which cost the energy U, i.e. the uniform system is a semiconductor, the Mott-Hubbard insulator. For NMP-TCNQ, is has been suggested that the experimentally observed gap occurs because of onsite Coulomb repulsion |7-11|, i.e. the gap is a Mott-Hubbard gap at midband. For the quarter filled salts, e.g. $Qn(TCNQ)_2$, the nearest neighbor Coulomb interaction ($U_1$) is proposed to be responsible for the gap at the 1/4 band level |94,110-113|.

Localization of the electrons can also be a result of formation of small polarons, i.e. carriers followed by their induced polarization cloud of phonons. The organic compounds are particularly exposed to formation of small polarons, because of the appreciable electron-phonon interaction |114|. An important effect of the small polaron formation is a reduction in the effective Coulomb repulsion, but it also leads to severe band narrowing. This band narrowing tends to favor the insulating state |114|.

Also static disorder may cause an insulating behaviour. In one-dimensional systems, any disorder makes the electrons localized at least in the ground states, and electronic conduction can occur only by hopping |115|.

## 6.1 CONDUCTIVITY

The transport properties in the insulating 1D compounds are dependent of the origin of the insulating state.

Both the Peierls and the Mott-Hubbard semiconductors may, provided reasonable overlap integrals, be treated as conventional semiconductors with thermally activated conductivity

$$\sigma(T) = \sigma_o \exp(-E_a/k_BT) \tag{6.2}$$

where $E_a$ is the activation energy. The factor $\sigma_o$ may in general have a slight temperature dependence, but the dominating variation with temperature comes from the exponential function. Remembering that $\sigma$ involves both the mobility ($\mu$) and the carrier density (n),

$$\sigma = ne\mu \tag{6.3}$$

we may find the correct temperature dependence of the prefactor. The $\mu(T)$ behaviour is, in principle, the same as discussed under metallic conductivity. The density of carriers is given by

$$n = \frac{1}{L} \int_{\varepsilon_b}^{w+\varepsilon_b} f(\varepsilon)N(\varepsilon)d\varepsilon \tag{6.4}$$

which for a simple 1D tight binding band |15| in the limit: $(\varepsilon_b-\varepsilon_F) >> k_BT$, gives |16|

$$n \simeq \frac{2}{b}\left[\frac{k_BT}{\pi w}\right]^{\frac{1}{2}} \exp\left[\frac{\varepsilon_F-\varepsilon_b}{k_BT}\right] \tag{6.5}$$

Further deviation from the simple activated behaviour, (6.2), may arise from the presence of two conduction stacks in many of the compounds, as the carriers in these stacks contribute with different activation energies.

In case of disordered 1D systems, the electronic conductivity can occur only by phonon assisted hopping |115|. Following the

Mott-arguments |117| that an electron, instead of hopping to a nearest neighbor site, can hop to a distant but energetically more favorable state, Bloch et al. |115| from dimensional considerations proposed a temperature dependence of the form

$$\sigma \propto \exp\left[-(T_o/T)^{\frac{1}{2}}\right] \tag{6.6}$$

where $T_o$ is a constant. Shante has in a corresponding model based on anisotropic hopping |118|, i.e. including interchain hopping, found the form

$$\sigma \propto \exp\left[-(T_o/T)^{1/m}\right] \tag{6.7}$$

where m is weakly temperature dependent. For asymptotically low temperatures, m equals 4(3) for 3D (2D) anisotropic conductors, and decrease to a value between 2.7 and 2.9 for increasing temperatures. At still higher temperatures, the hopping model breaks down, as the chains becomes essentially decoupled |118|. The conductivity is then activated, and m=1.

## 6.2 THERMOPOWER

The thermoelectric power may for semiconductors, as well as for metals, in general be deduced from the Kubo-Greenwood formula (3.65) |53|,

$$S = -\frac{k_B}{e}\int \frac{\varepsilon-\varepsilon_F}{k_B T}\,\frac{\sigma(\varepsilon)}{\sigma}\,d\varepsilon \tag{6.8}$$

Since $\varepsilon_F$ is outside the conduction band(s), it is convenient to split $(\varepsilon-\varepsilon_F)$ into the two parts

$$(\varepsilon-\varepsilon_F) = (\varepsilon-\varepsilon_b) + (\varepsilon_b-\varepsilon_F) \tag{6.9}$$

where $\varepsilon_b$ denotes the band-edge. (Fig. 6.1).

For a single band, eq. (6.8) now lead to the expression for the intrinsic thermopower

$$S = -\frac{k_B}{e}\left[\frac{\varepsilon_b-\varepsilon_F}{k_B T} + A_1\right] \tag{6.10}$$

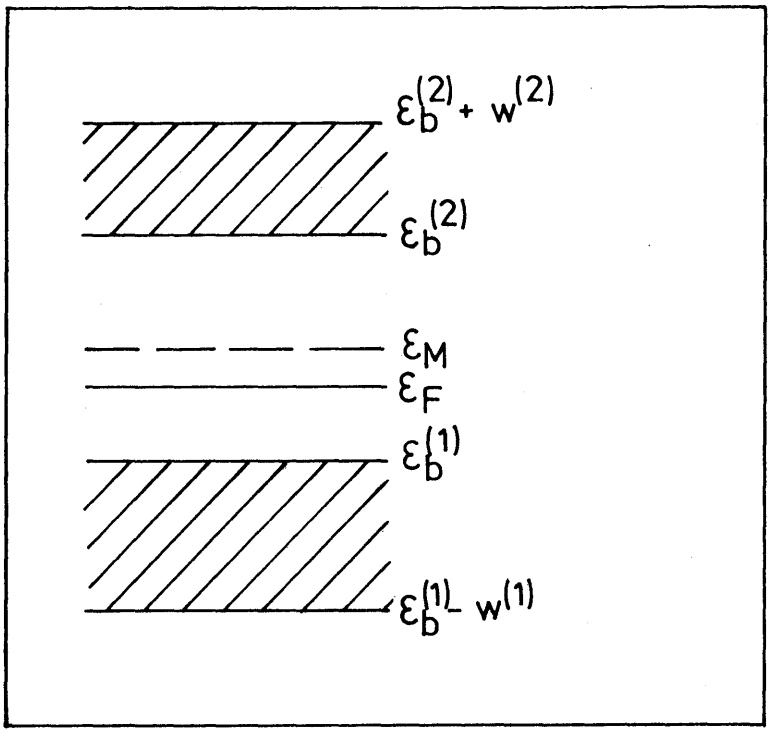


Fig. 6.1 Energy-level diagram of a two-band model.

where $A_1$, the "kinetic-energy term", accounts for the fact that the carriers are distributed beyond the band edge:

$$A_1 = \int_{\varepsilon_b}^{\varepsilon_b+w} \frac{\varepsilon-\varepsilon_b}{k_B T} \frac{\sigma(\varepsilon)}{\sigma} \, d\varepsilon \qquad (6.11)$$

Usually $A_1$ is fairly temperature independent compared to the $T^{-1}$ term.

For a two-band conduction mechanism, the upper and the lower bands in Fig. 6.1, the conductivity weighted sum rule, $S = \Sigma \, \sigma_i/\sigma \cdot S_i$, gives the total thermopower in the form

$$S = - \frac{k_B}{e} \left[ \frac{\sigma_e - \sigma_n}{\sigma_e + \sigma_n} \cdot \frac{\varepsilon_g}{2k_B T} - \frac{\varepsilon_F - \varepsilon_M}{k_B T} + A \right] \qquad (6.12)$$

where e and h denotes electrons in the upper band and holes in the lower band, $\varepsilon_g$ is the gap, $\varepsilon_g = \varepsilon_b^{(2)} - \varepsilon_b^{(1)}$, and $\varepsilon_M$ is the gap center, $\varepsilon_M = \frac{1}{2}(\varepsilon_b^{(2)} + \varepsilon_b^{(1)})$. A is the weighted sum of $A_1^{(1)}$ and $A_1^{(2)}$.

For an intrinsic semiconductor, the $(\varepsilon_F - \varepsilon_M)$ difference is given from the density of states ratio

$$\begin{aligned} \varepsilon_F - \varepsilon_M &= \tfrac{1}{2}k_B T \ln \left[N_e/N_h\right] \\ &= \tfrac{3}{4}k_B T \ln \left[m_e/m_h\right] \end{aligned} \tag{6.13}$$

where $m_e$ and $m_h$ are the masses of electrons and holes, respectively. Thus

$$S = -\frac{k_B}{e}\left[\frac{\sigma_e-\sigma_h}{\sigma_e+\sigma_h}\frac{\varepsilon_g}{2k_BT} + \frac{3}{4}\ln\frac{m_e}{m_h} + A\right] \tag{6.14}$$

From the slope of the $S(T^{-1})$ curve, one then can find an "effective" energy-gap, $\varepsilon_{g,eff} = (\sigma_e-\sigma_h)/(\sigma_e+\sigma_h)\times\varepsilon_g$. It should be smaller than the value, we can deduce from the activated conductivity. In fig. 6.2, a plot of the thermopower for TTF-TCNQ, is shown as function of $T^{-1}$. We notice the characteristically semiconducting behaviour below the 38K-transition.

In many of the organic salts, e.g. TTF-TCNQ, both the donor and the acceptor molecules form chains taking part in the conduction process. Then, we do not have two kinds of carriers, but rather four in the semiconducting state. Neglecting the two latter terms in (6.14), we still find a $T^{-1}$-behaviour:

$$S \simeq -\frac{K_B}{e}\left[\frac{\sigma_e^A - \sigma_h^A}{\sigma^A + \sigma^D}\varepsilon_g^A + \frac{\sigma_e^D - \sigma_h^D}{\sigma^A + \sigma^D}\varepsilon_g^D\right] /2k_BT \tag{6.15}$$

but the analysis of the prefactor is now rather complicated.

From eq. (6.12) we note that the thermopower is strongly impurity dependent, due to the dependence of the position of the Fermi-level. Also strong Coulomb correlations affect the location of

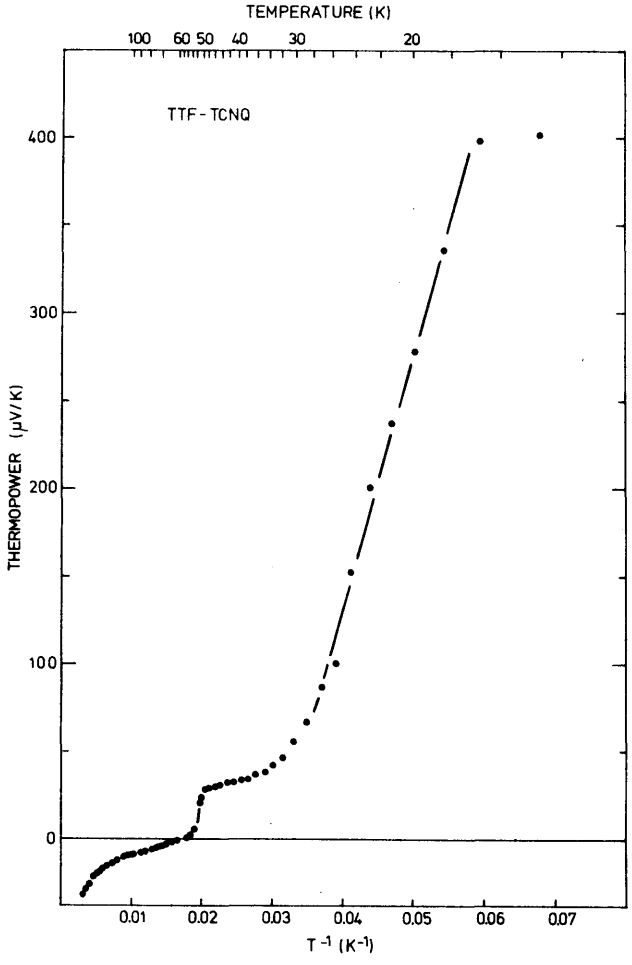


Fig. 6.2 Thermopower of TTF-TCNQ (batch IB7/MA 67).

the Fermi level, and thus the thermopower. For narrow-band semiconductors, the atomic limit, the kinetic term A in (6.12) vanish, and the asymptotical high-temperature thermopower is seen to be a matter of the Fermi-level location only.

The location of the Fermi energy can be deduced from the number of electrons, and from the form of the distribution function. Since the states for highly correlated carriers are only singly occupied, but spin degenerated, the distribution function is not the usual Fermi-Dirac function, but has the form |120|

$$f(\varepsilon) = \left[1 + \tfrac{1}{2}\exp\left(\frac{\varepsilon - \varepsilon_F}{k_B T}\right)\right]^{-1} \qquad (6.16)$$

for $\rho < 1$. The expression (6.16) can with advantage be rewritten in the form

$$f(\varepsilon) = \left[1 + \exp\left(\frac{\varepsilon - \varepsilon_F'}{k_B T}\right)\right]^{-1} \tag{6.17}$$

where $\varepsilon_F'$ is given by

$$\varepsilon_F = \varepsilon_F' - k_B T \ln 2 \tag{6.18}$$

Thus, the effect of the charge carrier correlation is to lower the Fermi-level by $k_B T \ln 2$. By use of the Kubo-Greenwood formula (6.8), the thermopower of strongly correlated charge carriers is then

$$S = -\frac{k_B}{e}\int \frac{\varepsilon - \varepsilon_F' + k_B T \ln 2}{k_B T} \frac{\sigma(\varepsilon)}{\sigma} \, d\varepsilon \tag{6.19}$$

$$= S_o - \frac{k_B}{e} \ln 2, \quad \rho < 1$$

where $S_o$ is the thermopower of the system of "uncorrelated" carriers. Eq. (6.19) is based on the assumption that $\rho < 1$. For $\rho > 1$, the distribution function is given by |119|

$$f(\varepsilon) = \left[1 + 2\exp\left(\frac{\varepsilon - \varepsilon_F}{k_B T}\right)\right]^{-1}$$

$$= \left[1 + \exp\left(\frac{\varepsilon - \varepsilon_F' + k_B T \ln 2}{k_B T}\right)\right]^{-1} \tag{6.20}$$

leading to the thermopower

$$S = S_o + \frac{k_b}{e} \ln 2 \ , \ \rho > 1 \tag{6.21}$$

Since generally the charge transfer in the organic salts is less than one, strong correlation effects will lead to an additional temperature independent thermopower of $k_B/e \cdot \ln 2 = 60$ μV/K for the donor chain, and $-k_B/e \cdot \ln 2 = -60$ μV/K for the acceptor chain. The expressions (6.19) and (6.21) are incidentally independent of the electrical transport behaviour, i.e. it may be metallic, semiconducting or hopping transport.

For an intrinsic semiconductor, for example, eq. (6.12), (6.13), (6.14) and (6.21) give the form

$$S = -\frac{k_B}{e}\left[\pm\ln 2 + \frac{\sigma_e - \sigma_h}{\sigma_e + \sigma_h}\frac{E_g}{2k_BT} + \frac{3}{4}\ln\frac{m_e}{m_h} + A\right] \qquad (6.22)$$

for correlated charge carriers. This is the same expression as that deduced by Conwell, using a simple two band model for $\rho < 1$. |113|.

In a number of 2:1 complex salts, e.g. $Qn(TCNQ)_2$, the thermopower shows a temperature dependence such as (6.22), saturating at a value close to -60μV/K |126|. This property has been explained in terms of the Hubbard model (6.1) with $U_o >> k_BT$ |120, 113, 124|. As these complex compounds have quarter filled bands, only the lower Mott-Hubbard (M-H) band is of interest. Further, as a nearest neighbor interaction, $U_1$, lead to a gap at the 1/4 band level, the compounds may be narrow band semiconductors with strong onsite Coulomb correlation, and as the gap is in the center of the lower M-H band, the two conducting bands must be rather symmetric with respect to bandwidths, scattering processes etc. Therefore, the latter three terms in (6.22) at reasonable high temperatures, vanish, in agreement with the experiments.

Also some simple salts, e.g. NMP-TCNQ, with incomplete charge transfer, shows an asymptotical high-temperature thermopower of the order of $-k_B/e$ ln2. Since the charge transfer of NMP-TCNQ is about 0.8 |120|, the gap leading to semiconducting behaviour can not be due to $U_1$. On the contrary, experimental doping results indicate a gap at the Fermi-level arising from electrostatic interchain interaction between charge density waves |127|. The deviation from the $-k_B/e$ ln2 value may be caused by unsymmetric properties of electrons and holes, i.e. it is a result of the magnitude of the charge transfer. In fig. 6.3 we show the experimental thermopower of $Qn(TCNQ)_2$ and NMP-TCNQ |126|, which distinctly exhibits the high-temperature saturation.

When the correlation effect becomes very strong, the Bloch-wave representation leading to the band-model is not valid anymore.

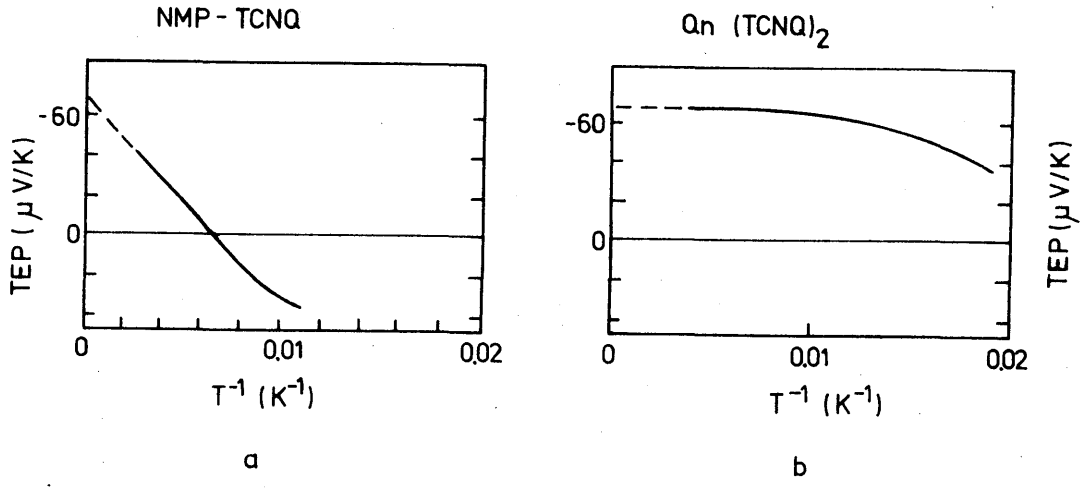


Fig. 6.3 Thermopower vs $T^{-1}$ for $Qn(TCNQ)_2$ and NMP-TCNQ.

The physics must then be described in a site representation. In a first approximation, however, we still can represent the strongly correlated M-H semiconductor by a band model, but with bands of zero width.

In the limit $k_BT << U$, only the lower M-H band is occupied, provided $\rho < 1$. And as there is no "kinetic" contribution to the thermopower in a band of zero width, eq. (6.12) gives

$$S(T \to \infty) = -\frac{k_B}{e} \frac{\varepsilon_b^{(1)} - \varepsilon_F}{k_BT} \qquad k_BT << U \tag{6.23}$$

where $\varepsilon_b^{(1)}$ is the energy in the lower M-H band. In the other extremum, $k_BT >> U$, both bands contribute to the conductivity. Provided the scattering mechanisms are the same, the thermopower then is

$$S(T \to \infty) = \frac{k_B}{e} \left[ \frac{\varepsilon_F - \varepsilon_b^{(1)}}{2k_BT} + \frac{\varepsilon_F - \varepsilon_b^{(2)}}{2k_BT} \right] \qquad k_BT >> E_g \tag{6.24}$$

Following the arguments of Lewis |119|, we will now derive the thermopower of correlated charge carriers in the Mott-Hubbard semiconductor (6.1) using simple thermodynamic arguments and neglecting terms of $U_j$, $j \geq 1$.

In a band of "zero" width, all states have an equal probability of occupation, and in the limit $U_o >> k_BT$ all carriers must be

in the lower band, provided $\rho < 1$. Thus, the charge transfer must be equal to the distribution function at $\varepsilon_b^{(1)}$:

$$f(\varepsilon_b^{(1)}) = \rho, \quad k_B T << U_o \tag{6.25}$$

Correspondingly, the distribution function in the limit $U_o << k_B T$, is equal half of the charge transfer, as the two band are equally occupied:

$$f(\varepsilon_b^{(1)}) = f(\varepsilon_b^{(2)}) = \tfrac{1}{2}\rho, \quad k_B T >> U_o \tag{6.26}$$

From the form of the distribution function we may thus deduce the Fermi energy as a function of charge transfer, and thus an expression for the thermopower.

i. Fermions in the $k_B T >> U_o >> t$ limit.

In this region, the electrons are localized, but distributed randomly, i.e. are essentially noninteracting Fermions. The distribution function is then the Fermi-Dirac function

$$f(\varepsilon) = \{1 + \exp(\frac{\varepsilon - \varepsilon_F}{k_B T})\}^{-1} \tag{6.27}$$

and from (6.26) this leads to

$$\frac{\varepsilon(1)_b - \varepsilon_F}{k_B T} \simeq \frac{\varepsilon(2)_b - \varepsilon_F}{k_B T} \simeq \ln \frac{2-\rho}{\rho} \tag{6.28}$$

The thermopower is consequently

$$S(T \to \infty) = - \frac{k_b}{e} \ln \frac{2-\rho}{\rho} \tag{6.29}$$

ii. Fermions without spin, in the $U_o >> k_B T >> t$ limit.

The distribution function for highly correlated spinless charge-carriers must be equal to the distribution function for uncorrelated carriers with spin, i.e. the ordinary Fermi-Dirac factor (6.27). From (6.25) we then have the position of the Fermi level:

$$\frac{\varepsilon_b^{(1)} - \varepsilon_F}{k_B T} = \ln \frac{1-\rho}{\rho} \tag{6.30}$$

and thus, from (6.23), the thermopower

$$S(T \to \infty) = - \frac{k_B}{e} \ln \frac{1-\rho}{\rho} \qquad (6.31)$$

Equation (6.26) represents the well known Heikes formula |11|. It should be noted, however, that it is only physical applicable to systems in enormous magnetic fields, or to electrons paired with strong binding energy |122|. More frequently, the spin degeneracy must be taken into account:

iii. Fermions with spin in the $U_o >> k_BT >> t$ limit.

The distribution function for strongly correlated carriers with spin is that already discussed (6.16). For $\rho < 1$, we therefore have

$$\varepsilon_b^{(1)} - \varepsilon_F = k_BT \ln(2 \frac{1-\rho}{\rho}) \qquad (6.32)$$

and then the thermopower

$$S(T \to \infty) = - \frac{k_B}{e} \left[ \ln 2 + \ln \frac{1-\rho}{\rho} \right] \qquad (6.33)$$

The thermopower of the 1D M-H semiconductor in the atomic limit ($t << U_o$), has been deduced by a number of authors beyond those already mentioned |94, 110-113, 119-124|, leading to results similar to the forms (6.29), (6.31) and (6.33). For example, Chaiking and Beni |122| used in the limit $T \to \infty$, that the thermopower is a measure of the entropy per carriers. Since the entropy in that limit is given by the degeneracy of the states, the calculation was reduced to simple combinatorial problems dependent only on the density of carriers and the interactions stronger than the thermal energy.

For more detailed calculations of the thermopower as a function of temperature, in the atomic limit, it is advantageous to use the Kubo-formalism |125|. Bari and Beni |121, 110| studied in that way the thermopower of the narrow-band M-H semiconductor, including only on-site Coulomb interactions, $U_o$, whereas Kwak and Beni |120| took into account arbitrary nearest neighbor

repulsion $U_1$. Ihle and Eifrig |124| calculated the thermopower in the 1D M-H model for $U_o >> t$, but included finite values of both $U_o$ and t.

## CHAPTER VII

## TECHNIQUE USED FOR THERMOPOWER MEASUREMENTS

The thermoelectric power of a compound is basically measured by constructing a thermocouple arrangement, which consists of the sample and a suitable material with a well known thermopower ($S_1$). The Seebeck emf. is then measured when one junction is raised $\Delta T$ in temperature relative to the other:

$$\Delta V = (S - S_1)\Delta T \qquad (7.1)$$

S is the unknown sample-thermopower. One of two procedures is commonly adopted to obtain the temperature dependence of S. In one, a constant temperature bath is used to hold one junction at a known temperature, the other junction is varied in temperature and the total emf. measured as a function of T. To obtain S, it is then necessary to differentiate the emf. versus T curve. Alternatively, the thermopower can be obtained directly by adjusting both junctions to the required temperature, and then heat one junction by a small amount $\Delta T$, measuring the small emf., $\Delta V$, so created. Both methods are capable of giving accurate thermopowers. The first, however, requires more data processing but the second requires at best three measurements, i.e. T, $\Delta T$, $\Delta V$, whereas only T and V are required in the former case.

In studies of the transport properties of highly conducting organic compounds, including phase changes, the latter, differential method is the only practical. Also the size of the crystals, typical 1-5 mm in the stacking direction, and 10-100 μm in the two transverse directions, favour the differential method.

In practice, the emf. as indicated by a precision potentiometer will include some stray steady thermo-emf.s generated in the leads to the measuring instrument. These can arise, for example, from inhomogeneityof the conductors and can lead to serious errors.

To eliminate these stray emf.s in the $\Delta V$ and $\Delta T$ measurements, $\Delta T$ measured by a thermocouple, it is common to use a slowly

alternating temperature gradient, and use the slope of the $\Delta V$-$\Delta T$ plot, for example displayed on an X-Y recorder |128, 129|.

Another problem encountered in making thermopower measurements, is to make certain that the temperature gradient measured, is entirely across the sample. To eliminate this problem, long and thin samples must be chosen, in order to get high thermal resistance.

Apparatus.

The apparatus used is a slightly modified form of that described by Chaikin and Kwak |129| , which is based on the slow ac-technique mentioned above. In Fig. 7.1 it is illustrated schematically. The heart of the device is a set of two 12x9x4 $mm^3$ single-crystal quartz blocks, which have high thermal conductivity ensuring a reasonable short measuring time. One of the plane surfaces of each of the blocks, is covered with a Nickel-Chromium (c. 80 Ni, 20 Cr) heating element of resistivity of the order of 1 k$\Omega$. The Ni/Cr is evaporated directly onto the quartz. The form of the element is of a suitable pattern to ensure that the quartz blocks is heated as uniformly as possible.

The two quartz-blocks are by phosphorus-bronze springs placed 1-3 mm apart on a PVC substrate 1.5 mm thick. As a result of different coefficients of thermal expansion, it is not appropriate to glue the blocks onto the substrate. The PVC material is fastened with screws to a copper block, 3 mm thick, which serves as a heat sink. Finally, the copper block is screwed in a cylinder of copper so that the heart of the apparatus effectively is enclosed in a region of well-known temperature.

The whole system is located, either in the inner can of a conventional variable temperature cryostat (I), on the cold finger of a variable temperature flow cryostat (II) or on the cold finger of a cooling machine (III). As the apparatus requires evacuated surroundings, the copper cylinder also serves as a vacuum shield in the cryostat I, whereas in the latter two the cold fingers are insulated by vacuum anyway. The temperature is electronically controlled by Oxford Instuments, DTC 2 in I and II and EA 2349 in III. The cryostat I is crudely controlled by taking a small flow of liquid helium from the main bath through

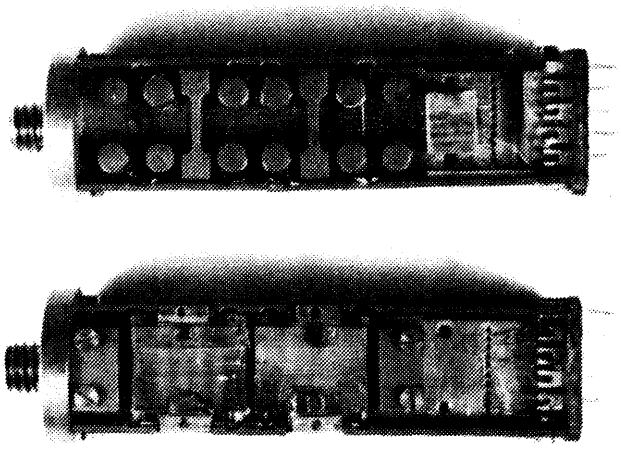

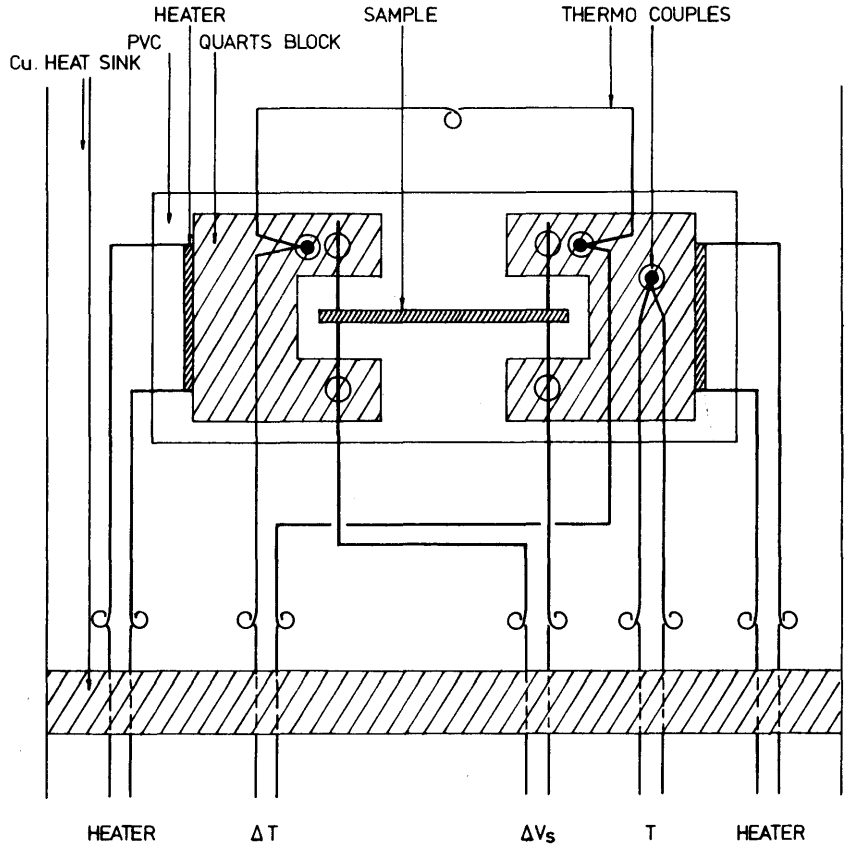


Fig. 7.1 Apparatus used for thermopower measurements.

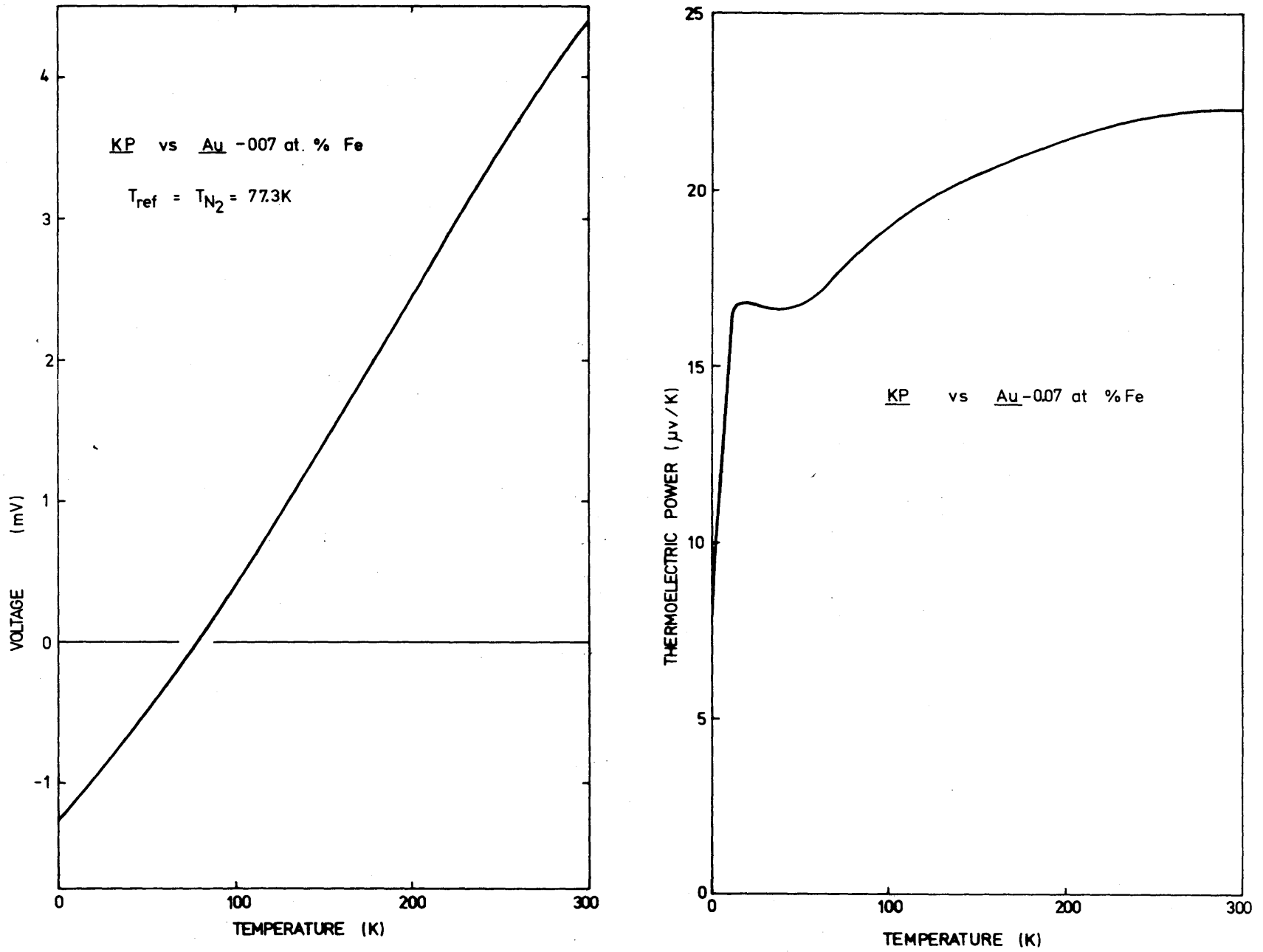


Fig. 7.2 Data for chromel vs Au-.07% Fe thermocouple. a Thermopower and b, thermoelectric voltage with reference temperature equal to that of liqued Nitrogen |130|.

a needle valve and capillary tube to the heat exchanger, or by introducing a small amount of exchange gas to the vacuum between the helium vessel and heat exchanger. The flow-cryostat is roughly controlled by the choice of helium flow through the system. The lowest tempeatures attainable at the quartz blocks is approximately 2K, 9K and 14K for the three cryostats I, II, and III, respectively.

For the thermopower measurement, a 0.15 mm or .025 mm 99.99% pure gold wire is placed across the gap on the quartz blocks, and glued to them with Ge 7031 low temperature varnish, which ensure good thermal anchoring. The organic crystal to be measured is then placed on these two wires so that the needle axis is perpendicular to the goldwires and the wires are at the end of the crystal. Electrical and thermal contact is subsequently made by applying silver paint (Dupont 7941) with a piece of the gold wire, or a 0.065 mm thick copper wire. In some cases, Au contacts were evaporated onto the crystal. Thus the gold leads serve both as electrodes and as thermal conductors to transmit the temperature drop across the quartz blocks to the sample. The size of the gold wires are a compromise between the requirements of large thermal conductance and flexible behaviour in order to allow the crystal to contract as the temperature is lowered. The leads are connected through a high impedance (maximum recommended source resistance 30KΩ) Keithley 140 Precision Nanovolt DC Amplifier to the Y-axis of an X-Y recorder.

The temperature of the sample is measured with a chromel (KP) versus Au-0.07 at. pct. Fe thermocouple, mounted on one of the quartz blocks. As reference temperature a bath of liquid Nitrogen (77.3K) is used. The thermoelectric emf. is measured with a Keithley 174 Digital Multimeter, and is converted to the absolute temperature by use of the data of Sparks and Powell |130| shown in Fig. 7.2.

The small temperature drop between the two quartz blocks is also measured using a chromel versus Au-0.07 at. % Fe thermocouple, which is particular suitable because of the quasi constant thermopower, shown in Fig. 7.2 a |130| . Such behaviour is obtained by exploiting the increased low-temperature thermo-

power of Gold following doping with a small amount of ferromagnetic impurities (Fe), i.e. the Kondo effect described in chapter 4.10. The induced thermoelectric voltage is measured with a Keithley 149 Milli-Micro Voltmeter, the analogue output from which is connected to the X-axis of the X-Y recorder.

Of particular importance in this type of apparatus, is the time constants for reaching thermal equilibrium. The heat sink must come into equilibrium quickly. The thermocouples responding to the temperatures of the quartz blocks must also be fast, as well as the transfer from the quartz to the sample. Slow relaxation should occur from the quartz to heat sink through the PVC substrate and the number of leads, and from the quartz to quartz block through the thermocouple, the PVC and the sample. A suitable length of the leads is 20 cm for the 0.075 mm teflon coated chromel wire and 30-40 cm for the 0.075 mm Au-0.07 at. % Fe and the 0.09 mm copper wires. |131, 132|. The thermal relaxation time of quartz to quartz and quartz to heat sink is then typical a few minutes.

All the leads are thermally connected to the heat sink at one end. Thus, although there are many contacts between different metals in the apparatus, and hence many sources of stray thermal emf.s, the only junctions where temperature vary appreciable during the heating cycles are the Gold-sample junctions and the thermocouple junctions. The leads between the heat sink and the measuring instruments are all, except the thermocouple for absolute temperature measurement, 0.09 mm Cu-wires. Outside the cryostat, the wires are screened individually in order to minimize pick-up.

For the thermopower measurement, a current is supplied to the heater of one quartz block so that the temperature over typically 30 seconds increases between 1/10 and 1/4 K depending on the S(T) behaviour. The current necessary for this heating is of the order of 1 mA, corresponding to power of 1 mW deposed in the heater, but it varies somewhat with the temperature. When the temperature increase has reached the desired value, the current is switched to the second quartz block, and finally the first block may be heated again to ensure that the two blocks

are at the same temperature. The maximum temperature drop across the sample is then less than 1/5-1/2 degree K.

In Fig. 7.3, typical X-Y recorder traces is shown. The traces come out as loops of variable hysteresis, dependent of the thermal time constant of the quartz to sample connection via varnish, gold wires and silver paint, and the time constant of the quartz to KP-Au thermocouple via varnish. If the trace is not a closed loop, there is probably poor thermal contact somewhere. At low temperatures, the loop usually degenerate into a stright line as the thermal conductivity grows large and heat capacities get small. However, also a large sample electrical resistance may cause a large hysteresis, as a result of the increased rise time of the nano-volt meter.

The slope of the linear regions of the curves is the thermopower of the sample minus the thermopower of gold, divided by the thermopower of the KP vs. Au-Fe thermocouple:

$$\text{Slope} = \frac{S_{\text{sample}} - S_{\text{Au}}}{S_{\text{KP vs Au-Fe}}} \qquad (7.2)$$

The thermopower of gold is taken from Huebener and Guenault and Hawksworth [133, 134], and is shown in Fig. 7.4.

Data for the sample must be taken only when slopes for both signs of the temperature gradient are the same. The measurement thus represents an average thermopower over less than one-half a degree temperature interval.

A major potential source of error in this type of apparatus is in determining whether the temperature gradient across the sample is equal to the temperature drop measured between the quartz blocks. There may be an appreciable temperature drop along the gold leads as well as over the varnish and silver paint contacts. Also, if the sample chamber is not effectively evacuated, the thermal shortening by the surrounding gas can be a problem. An easy, but not definitive, test of these difficulties is to vary the length of the sample, and the pressure of the sample chamber. By varying the length, we change the thermal resistance of the sample

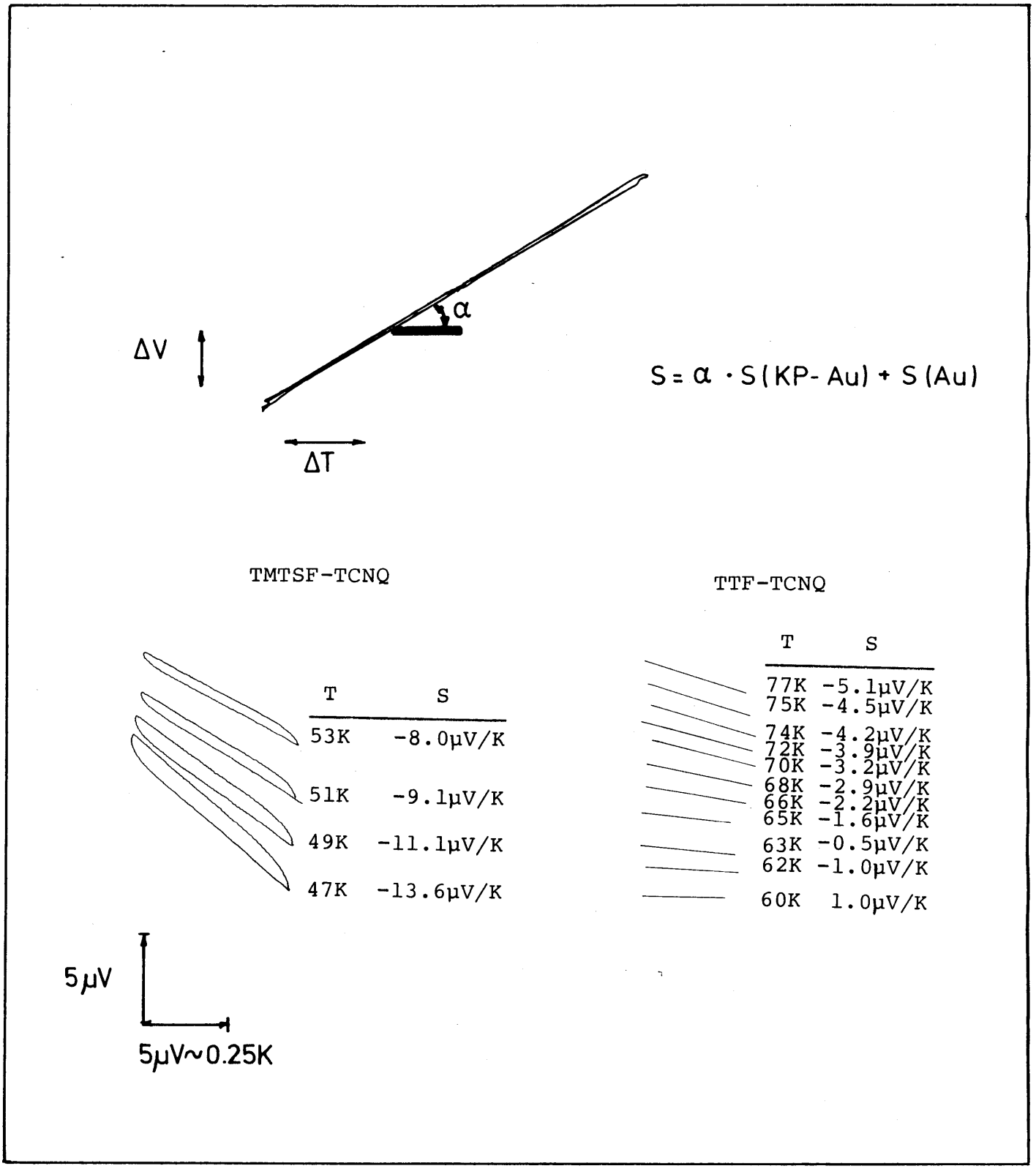


Fig. 7.3 Typical traces of thermocouple output versus thermopower differences between sample and gold leads.

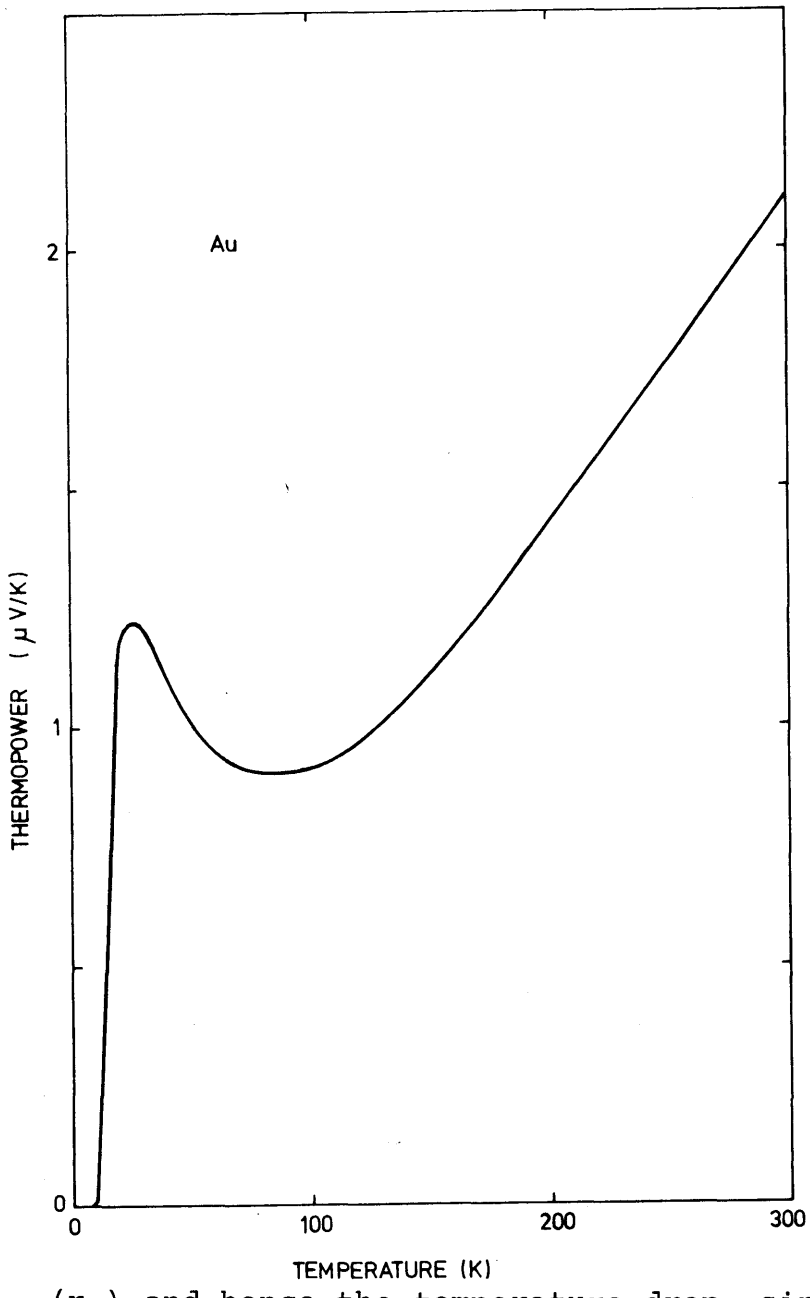


Fig. 7.4 Thermopower of Au, [133, 134].

($r_s$) and hence the temperature drop, since

$$\Delta T_{sample} = \frac{r_s}{r_s + r_o} \Delta T_{quartz} \qquad (7.3)$$

where $r_o$ is the thermal resistance of the gold wires, varnish and silver paint contacts. Only if $r_s >> r_o$, we can trust the measurements. The results shown in Fig. 7.5 shows a slight variation in a plot of S versus crystal length. Also there is some scatter, probably as a result of differences in the silver paint contacts. The experiment is conservative, however, as the cross section area is much larger than those used in the compounds investigated. The pressure dependence, Fig. 7.5, points out that the measurements should be done for $P < 10^{-2}$ torr.

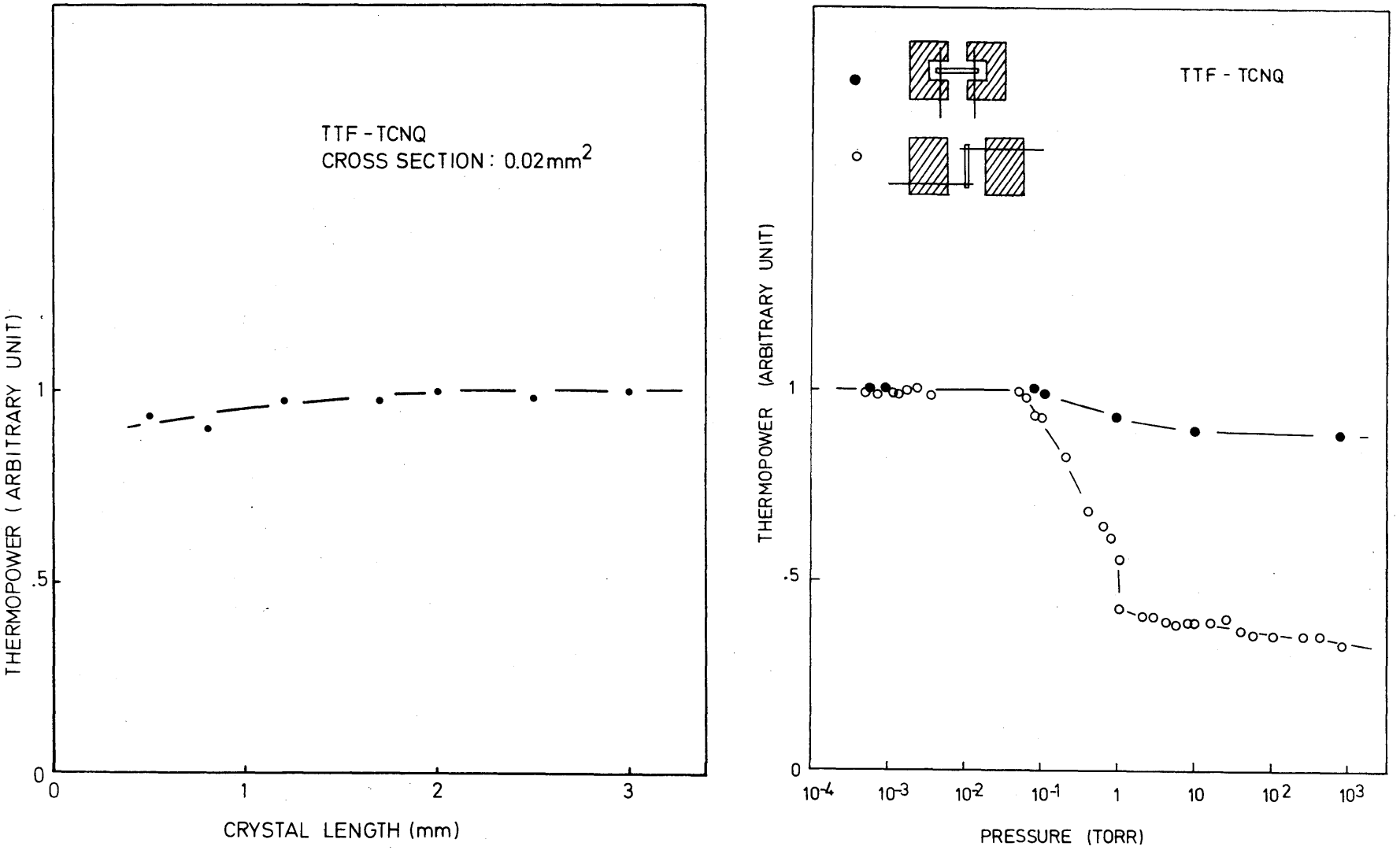


Fig. 7.5 Test of apparatus. a Dependence of crystal dimensions. b Dependence of surrounding gas density. In b, we show data of two sample configurations, o the one used by Chaikin and Kwak [129], o the one used by the author.

# CHAPTER VIII

## THERMOPOWER MEASUREMENTS ON ORGANIC CHARGE TRANSFER SALTS

In the present chapter we will present the thermoelectric power of a number of highly conducting organic salts. The discussions will be based on the theory already given, and the experimental values are measured as described in chapter VII. Along with the thermopower, the two probe sample resistance has been measured, as a control parameter.

## 8.1 THERMOPOWER OF TTF-TCNQ

The thermopower of TTF-TCNQ has already been discussed in detail in the sections concerning transport theory. However, it will be discussed once more, but now from the experimental point of view.

The samples used for thermopower studies were prepared at Phys. Lab. III, Tech. Univ. of Denmark. TTF-TCNQ single crystals were grown by diffusion in a solution of acetonitrile.

In Fig. 8.1 the S(T) behaviour is given for a typical sample of TTF-TCNQ |135|. The linear S(T) behaviour at high temperatures ($T > 140K$) should be noted. This result is one of the best pieces of evidence that TTF-TCNQ is metallic at high temperatures. From the theoretical discussions above, this behaviour may be somewhat surprising, since many sources lead to deviation from linearity, e.g. the limited bandwidth (Fig. 3.4) and the scattering term in equation (3.66). The negative sign indicate that the conduction mechanism is dominated by electrons, and since $\rho < 1$ that is the carriers on the acceptor chain (TCNQ).

It is clear from the data that there are phase transitions at about 38K and 54K, as also seen in the conductivity and magnitic behaviour. The thermopower indicates that the 54K-transition is sharp rather than gradual, and hence that we are not following a smooth transition from electron to hole domination. From the TEP we further should infer that the 54K-transition is driven by the TCNQ-chain, in agreement with the EPR analysis of Tomkiewicz et al. |136|.

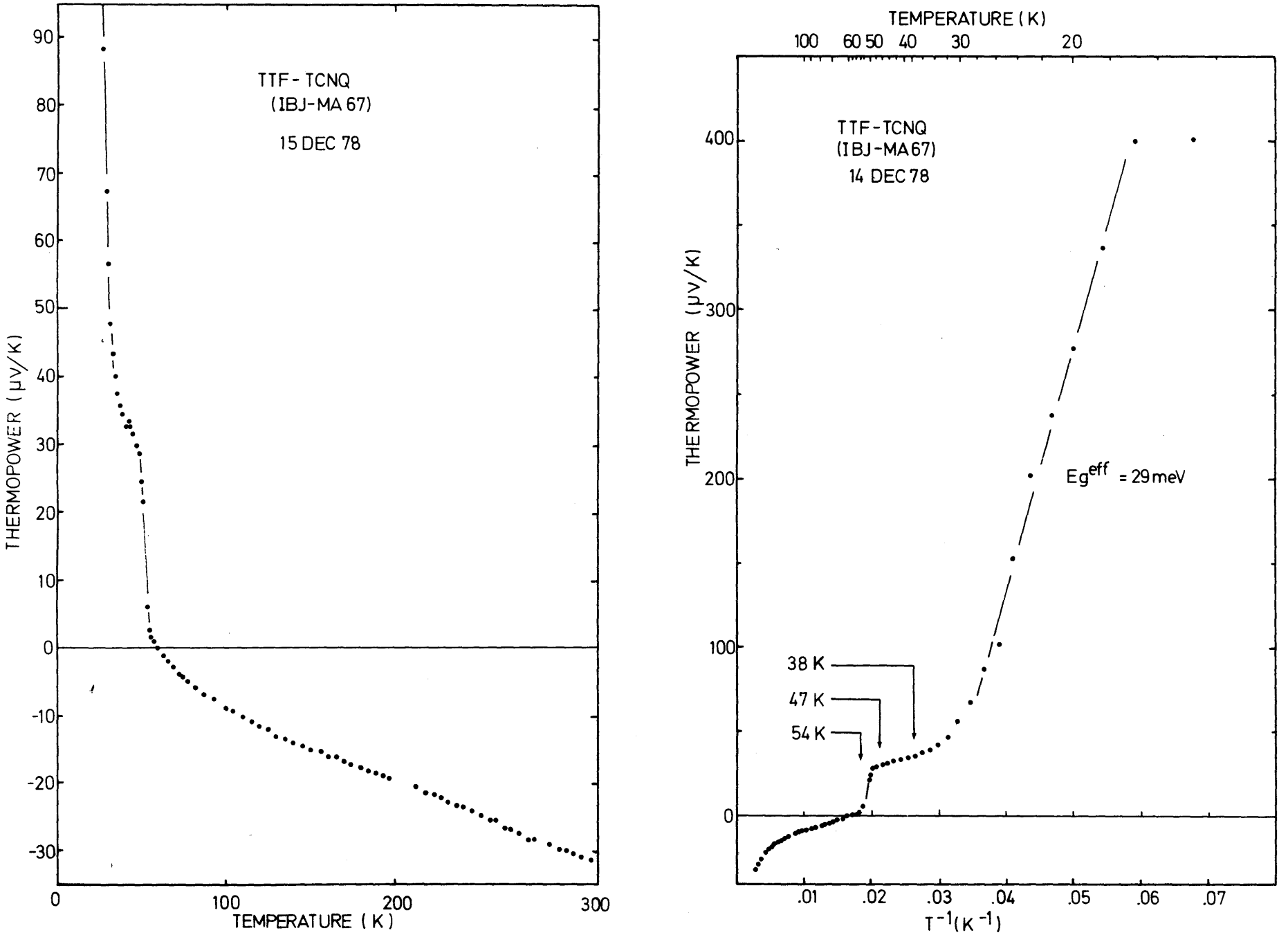


Fig. 8.1 Thermopower of TTF-TCNQ. a. S vs T. b S vs. 1/T.

In the region from 54K to 150K, there is a deviation from the linear T-dependence, with S increasing to a small positive value near the transition temperature. This is just the region, where diffuse X-ray scattering has shown that the coupled conduction-electron-lattice system fluctuates into an incommensurate CDW which increases in amplitude and coherence length as the temperature is lowered to $T_c$ |138|. The combination of these structural data, the large $\sigma_{max}/\sigma_{RT}$-ratio and strong frequency dependence |36, 105| has by a number of authors been proposed as evidence for superconducting fluctuations in TTF-TCNQ near $T_c$ |139|. The recent results of Andrieux et al. are probably the best "proof" of collective fluctuations, as they demonstrate that commensurability pinning cause a substantial drop in conductivity |137|.

It is well-known that the thermopower of a superconductor is zero. When fluctuations into a superconducting state are present, we also should expect a vanishing or stronly decreased numerical value. The thermopower of TTF-TCNQ therefore does not contradict the theory of collective fluctuations below 150K. On the other hand, since the TEP changes sign from the high temperature metallic state to the low temperature semiconducting, S must cross zero.

Below the 54K-transition the thermopower is positive and increases rapidly to approximately 30 μV/K (Fig. 8.1b). The sign implies that the conductivity is dominated by holes. Between the 38K and 54K transition temperatures, S is only weakly temperature dependent, whereas a $T^{-1}$-behaviour is observed below 38K, indicating semiconducting transport. The magnitude and sign of the S(1/T) slope, are strongly dependent on crystal purity |135|. A corresponding deviation in the activated conductivity behaviour never occur. The first TTF-TCNQ samples grown in our laboratory had a negative slope corresponding to $E_g^{eff}$ = 16 meV (6.12), and S became negative again below 28K |140|. On the contrary, the subsequent samples showed positive values to the lowest temperatures attainable. The sample shown in Fig. 8.1b has an effective energy gap equal to 29 meV, which must be compared with the gap found from conductivity

measurements, $E_g$ = 40 meV, setting Eg = $2E_A$. We believe that the latter samples are the single crystals of highest purity. Support for this is given by the rather general observation that S below $T_c$ has the opposite sign of S at high T. Detailed analysis, however, is rather complicated, as both chains represent a two-band semiconductor.

In order to find out whether the electrical transport is dominated by the TTF-band or by the TCNQ-band, we should know all four intrinsic conductivities in the compound (also see eq. 3.44). Since we do not expect the scattering mechanism to vary appreciably from holes to electrons in the same chain, a different mobility must result from the band term, usually represented by the effective mass

$$(m^*)^{-1} = \hbar^{-2} \frac{d^2\varepsilon_k}{dk^2} \tag{8.1}$$

giving

$$\mu = \frac{e\tau}{m^*} \tag{8.2}$$

To simplify such calculations for TTF-TCNQ, we will for a moment assume that $\rho = 2/3$ rather than .59, thus resulting in the trimerized semiconductor discussed in chapter 2. For that system, we found the dispersion relation

$$\varepsilon(K) = \omega\cos\left|\frac{1}{3}\,\mathrm{Arccos}(u\cos kb) + j\,\frac{2\pi}{3}\right| \tag{8.3}$$

where j = 1,2,3 and $\omega$ and u are given by the transfer integrals (2.11). From (8.1), this relation lead to the mass ratio

$$\frac{m_e}{m_h} = \left[\frac{\sin\left[\frac{1}{3}\,\mathrm{Arccos}(-u) + \frac{4\pi}{3}\right]}{\sin\left[\frac{1}{3}\,\mathrm{Arccos}(-u) + \frac{2\pi}{3}\right]}\right]^{\alpha} \tag{8.4}$$

where $\alpha$ = 1 for a TCNQ-like system, and $\alpha$ = -1 for a TTF system. In the tabel below, we show the calculations for bands with the right bandwidths, and band gaps corresponding to that observed in conductivity behaviour.

Table 8.1 Mass-ratio calculated by use of (8.4)

| | t eV | δ eV | εg meV | $m_e/m_h$ |
|---|---|---|---|---|
| TTF | .063 | .03 | 41 | 1.3 |
| TCNQ | .125 | .03 | 40 | .89 |

In an intrinsic semiconductor, the conductivity ratio is given by the masses

$$\sigma_e/\sigma_h = m_h/m_e \tag{8.5}$$

Thus, the effective gap (6.14) should be reduced to approximately 10% of the true gap in TTF-TCNQ. This is inconsistent with the experiments. We therefore conclude that the compounds are not intrinsic, but impurity dominated. This also accounts for the large sample-dependence observed.

An experimental study of these properties should be done by doping-experiments, which vary the physical parameters of one chain at a time. Chaikin et al. have investigated TTF-TCNQ compounds doped with i TSeF and ii MTCNQ |87,141|. In both cases they find a changed low-temperature behaviour, compared to their pure TTF-TCNQ sample. However, in all samples they find $dS/d(1/T)<0$. Based on the discussion above we therefore believe that the compounds used were of too poor quality to make a systematic low-temperature study. (It should be noted that all the conclusions of Chaikin et al. are based on the high temperature behaviour, which on the contrary is very little dependent on sample quality).

We have made some preliminary thermopower studies of TTF-TCNQ doped with tetrathiafulvalene S-oxid (TTF-ox) |142|. Since TTF-ox has a size similar to TTF, it is very useful as a "donor impurity", in order to investigate the physical properties. Further, as TTF-ox is always present in TTF that has been exposed to oxygen, a known (TTF-ox)/(TTF) ratio may help in identifying the role the oxydization plays as impurity centers.

Four-probe conductivity measurements showed almost no effects, and it was concluded then by Carlsen et al. that the S-oxid is not of major importance for electric conductivity |142|. Contrary to that we find a significant change in the low-temperature thermopower, whereas the high-temperature value and transition temperatures are almost unaffected (Fig.8.2). Thus the different thermoelectric behaviour found in TTF-TCNQ samples may well be a result of the oxidation.

In Table 8.2 we show the effective energy-gap found from the S(1/T) slope below 30K. The results are based on only one sample from each batch, and as the gap varies somewhat from sample to sample in the same batch, it should be taken with some caution. However, the tendency is evident: As the impurity concentration is enhanced, the effective energy-gap, $E_{g,eff} = (\sigma_e - \sigma_h)/(\sigma_e + \sigma_h)E_g$, indicates that the electron conductivity rises compared to the hole conductivity.

Table 8.2 Effective energy-gap as a function of impurity content.

| $(TTF)_{1-x}$ $(TTF\text{-}ox)_x$ - (TCNQ) | | | | |
|---|---|---|---|---|
| x | 0 | .0003 | .010 | |
| $E_{g,eff}$ | 29 | 22 | 5 | meV |

Several explanations are possible for this behaviour.

i. The impurities enhance the scattering rate of carriers on the TTF-chain, resulting in a decreased conductivity, i.e.

$\sigma \simeq \sigma_h$ (TTF) for pure material
$\sigma \simeq \sigma_e$ (TCNQ) for doped material

ii. The impurities enhance the number of free electrons in the TTF-band, by introducing an impurity band:

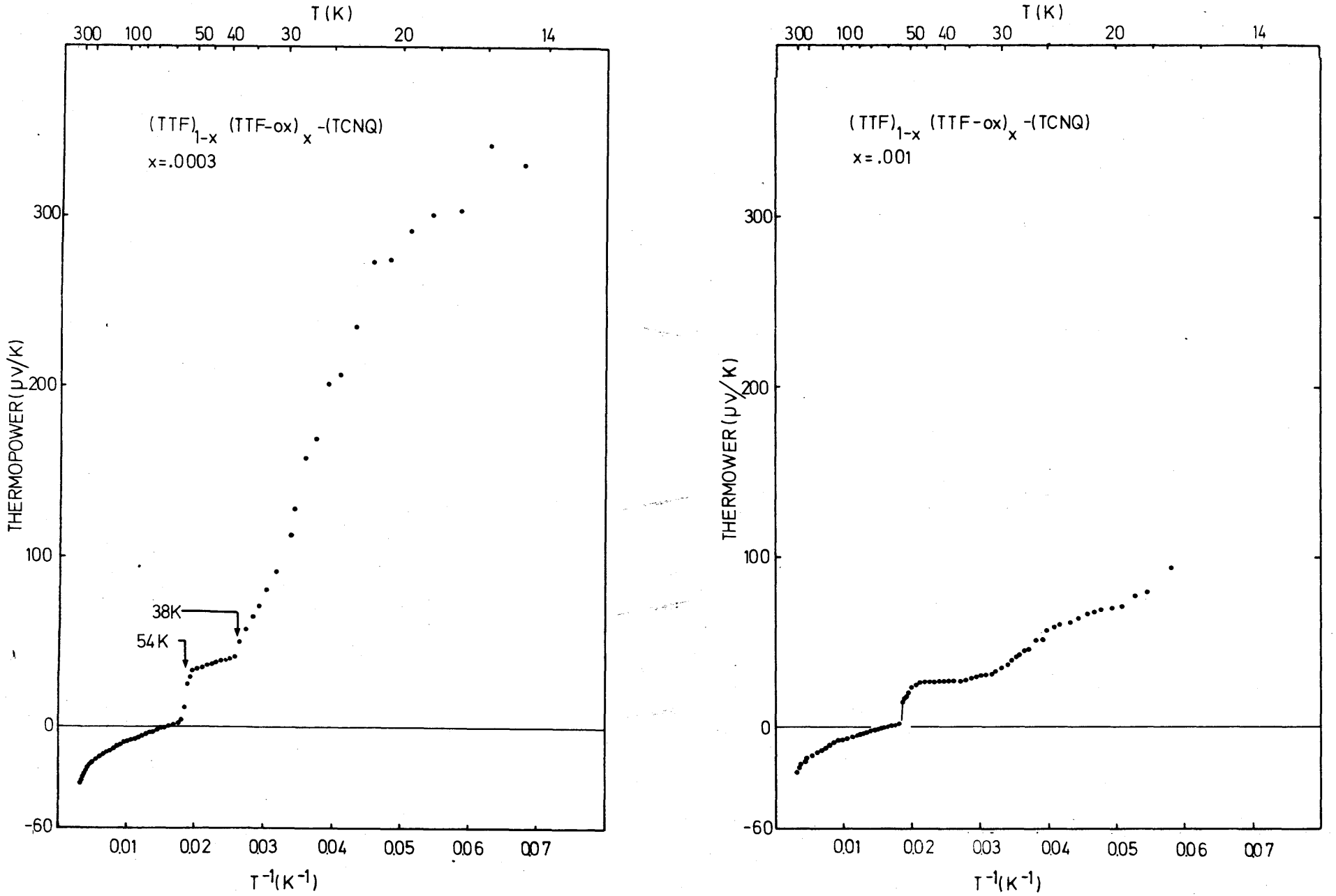


Fig. 8.2 Thermopower versus reciprocal temperature for $(TTF)_{1-x}$ $(TTF\text{-}ox)_x$-TCNQ, where x = .003 in a and x = .001 in b.

$\sigma \simeq \sigma_h$ (TTF) or $\sigma_h$ (TCNQ) for pure material

$\sigma \simeq \sigma_e$ (TTF) for doped material

The first of these explanations is perhaps the most plausible, since there is no effect on the activation energy seen in the conductivity plot |142, 135|. It should be noted, however, that the .03%-sample has a very sharp 38K phase transition. The $\sigma_{max}/\sigma_{RT}$ ratio was found to be rather large, 25, in samples from that batch |11|. Both of these facts indicate a very small amount of impurity. We therefore apparently should exclude the presence of TTF-ox in the TTF-TCNQ lattice, and suggest that only the very outer parts of the crystals are oxidized. The very drastic effect on the 0.1%-crystal could be an effect of poor crystal quality. This quality is probably not a specific effect of the S-oxid, but rather reflects a tendency for crystals to be of poor quality when grown in impure media.

Additional support for the first explanation that holes on TTF dominate in pure crystals, is found in the opposite signs of S above and below $T_c$. Since the TCNQ chain is dominating at high T the interactions will tend to be stronger here, and a bigger energy-gap will appear in this band. At low temperature the TTF-band with the smaller gap will dominate the conductivity and therefore the thermopower.

## 8.2 THERMOPOWER OF SOME ALKYLATED DERIVATIVES OF TTF-TCNQ AND TSF-TCNQ:

### TMTSF-TCNQ, DEDMTSF-TCNQ, TMTTF-DMTCNQ, TMTSF-DMTCNQ and TMTSF-$DMTCNQ_{1-x}$-$MTCNQ_x$

In order to learn more about the quasi one-dimensional metallic state, a number of derivatives of TTF-TCNQ have been synthesized, with a range of crystal structure parameters. The substitution of sulphur with selenium, giving TSF-TCNQ, leads to increased orbital overlap in the donor stacks and results in comparable conductivities in the two subsystems |61|. Alkylation in available positions on donors and acceptors, on the other hand, may serve as insulating steric

spacers, and in that way decrease the interchain Coulomb coupling and orbital overlap |143|. However, it will also create minor changes in the amount of charge transferred from donor to acceptor in the solid, and in the intrastack overlap. Moreover, it ppears that the distance between the atoms on the two sets of stacks do not always increase by the alkylation. For example, HMTSF-TCNQ, has a 2% smaller interchain distance than TSF-TCNQ |48|. In fact, the interchain interactions in HMTSF-TCNQ are so strong that the material approaches a 3D semimetallic state at low temperatures |144|.

In the present part, we will discuss the transport properties of some alkylated derivatives of both TTF- and TSF-TCNQ salts based mainly on the thermopower results. All the crystals are prepared at Risø Nat. Lab. and the H.C. Ørsted Inst., by slow evaporation of solvent from saturated solutions |29|. The molecular structure and names of constituent molecules are shown in Fig. 8.3.

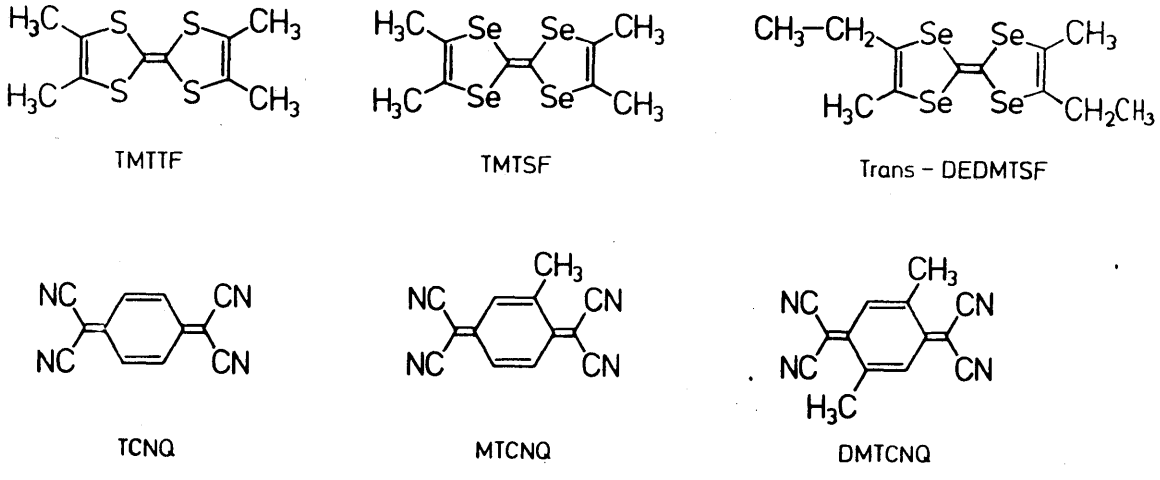


Fig. 8.3 Molecular design

All the crystals are black shiny needles, but of different qualities and mechanical properties. The selenium salts are clearly of higher quality than the sulphur analogous. The TMTSF-TCNQ samples are prismatic, about $2\times0.2\times0.05$ mm$^3$. They are quite brittle, but easily cut to desired dimensions.

TMTTF-DMTCNQ, TMTSF-DMTCNQ and DEDMTSF-TCNQ tend to grow in assemblies and are severely damaged when cut. They do not break, but are deformed just like a bunch of fibers. DEDMTSF-TCNQ is only available as very thin crystals with cross sections typical $20\times30\ \mu m^2$, whereas the DMTCNQ salts are about $0.1\times0.1\ mm^2$.

In Figures 8.4-8.8 and in Table 8.3, the conductivity and thermopower are shown for typical samples of the four alkyl substituted compounds.

The overall conductivity behaviour is very similar to what is found in other members of this class of compounds: Increasing conductivity with decreasing temperature and a relatively sharp maximum followed by a Metal-Insulator (M-I) transition below 100K. The conductivity of the selenium compounds is somewhat enhanced compared to the sulphur salts. A comparison is especially relevant for the two isostructural S-Se analogous TMTTF- and TMTSF-DMTCNQ |29|, where the difference in room temperature values is a factor of four. This feature is a result of the larger size of Se compared to S, and hence a larger intrastack overlap between donor molecules. From the positive sign of the high temperature thermopower for all the Se-compounds, we can conclude that the donor stacks have even become electrically dominating, in contrast to the acceptor being dominating in S-compounds. This is a general behaviour for all the investigated organic two-chain systems, until now.

The thermopower for the three Se containing salts are somewhat similar with small positive room-temperature values and linear S(T) segments above 150K, indicating bandlike metallic conductivity. Below approximately 150K, nonlinear behaviour is observed, and in the region of M-I transition, sudden change in slope are found. Below the transition temperature, the compounds are semiconducting. In contrast S(T) for TMTTF-DMTCNQ has a high, nearly constant negative value from 100-300K. Together with the low absolute conductivity at ambient temperature, this is an indication that this salt must be placed in a non-bandlike transport regime.

The transition temperatures ($T_c$) are easily identified from TEP measurements, and are equal to the value obtained by the

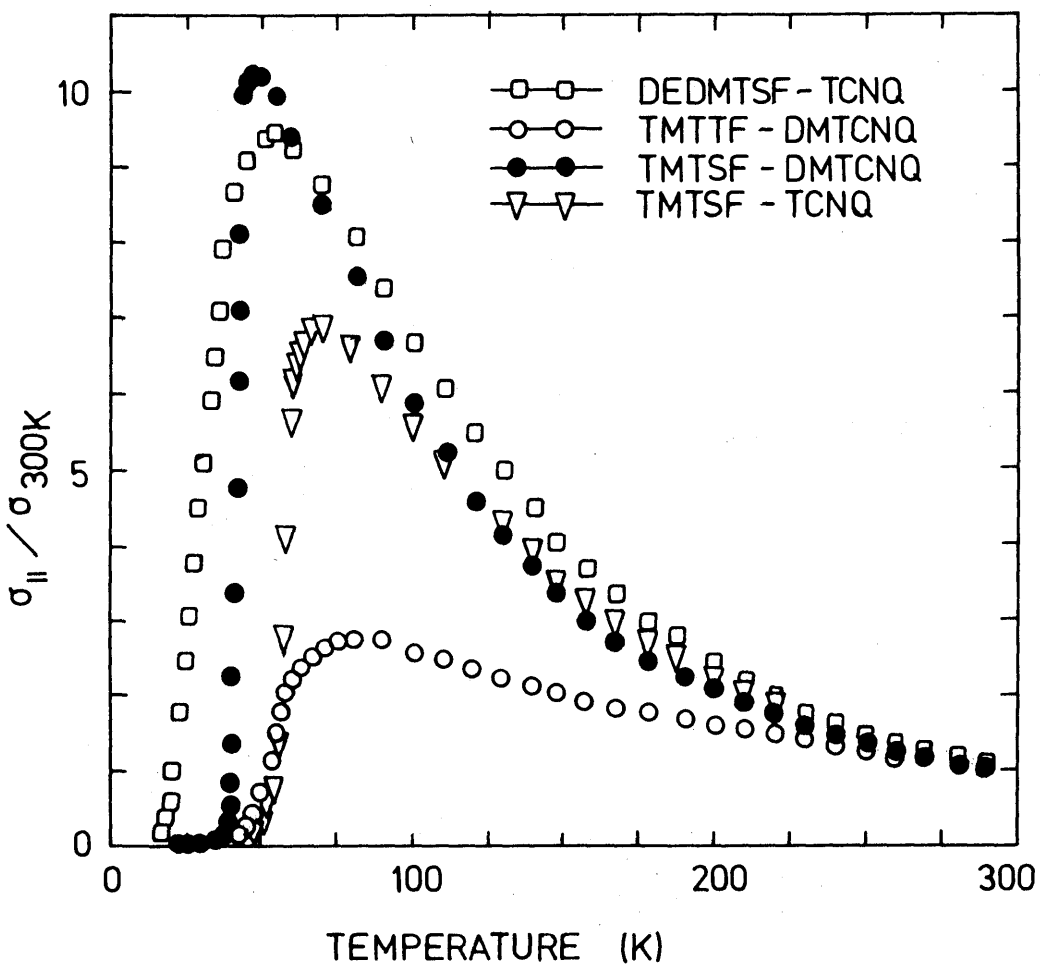


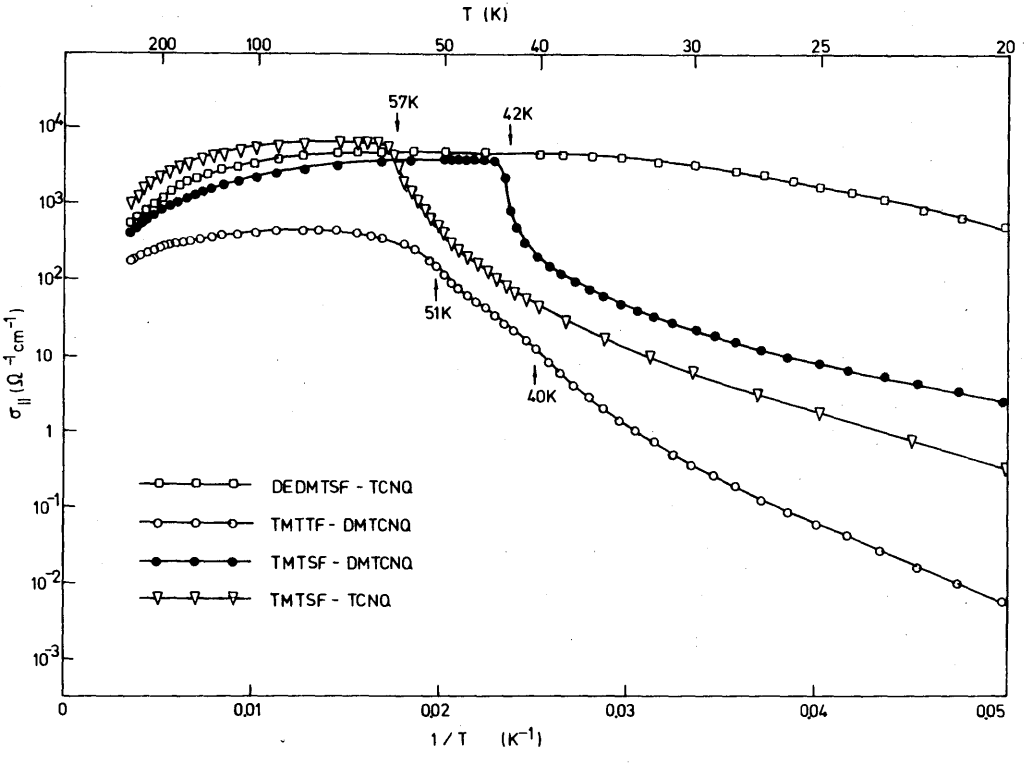


Fig. 8.4 Conductivity of some alkyl substituted organic compounds [29, 145].

Table 8.3 Transport properties of some alkylated derivatives of TTF-TCNQ

| | TMTSF-TCNQ | DEDMTSF-TCNQ | TMTSF-DMTCNQ | TMTTF-DMTCNQ |
|---|---|---|---|---|
| $\sigma_a$(300K) $\lvert(\Omega\ cm)^{-1}\rvert$ | 1000 | 500 | 400-600 | 120 |
| $\sigma_a/\sigma_b$ (300K) | 100 | ? | 200-300 | ? |
| $\sigma_a/\sigma_c$ (300K) | 250 | ? | 200-300 | ? |
| $\sigma_{max}/\sigma$ (300K) | 7 | 9 | 10 | 3 |
| $T(\sigma_{max})$ $\lvert K\rvert$ | 65 | 55 | 47 | 80 |
| $E_a$* $\lvert meV\rvert$ | 14.7 | ? | 12.5 | 19.8 |
| S (300K) $\lvert\mu V/K\rvert$ | 8 | 18 | 11 | -32 |
| $\Delta$** $\lvert meV\rvert$ | 3.2<br>7.8 | <0.2 | 3.4<br>10.00 | <11.5 |
| $T_c$ $\lvert K\rvert$ | 57 | 28 | 42 | 39.51 |
| Dominating chain at 300K | Donor | Donor | Donor | Acceptor |
| $\Lambda/a$ *** | 1.1 | ? | 0.7 | 0.15 |

* Activation energy defined from conductivity, eq. 6.2

** Activation energy defined from thermopower, eq. 6.12

***Relative mean free path, given as $\Lambda/a = \pi\hbar bc\sigma/4e^2a$ |29|

normal definition of the temperature of maximum $d(\log\sigma)/d(1/T)$. All the Se-salts show one phase transition only, whereas TMTTF-DMTCNQ shows two transitions.

We will now discuss the four compounds one by one.

TMTSF-TCNQ

The thermopower of TMTSF-TCNQ is small and positive (S(300K) = 8 μV/K), and approximately linear in temperature. The sign suggests donor stack dominance in the conductivity, but the TCNQ stack may contribute with a non negligible term. The linear segment of S extrapolates to negative values at low T:

$$S \simeq S_o + AT, \tag{8.6}$$

$S_o \simeq -5$ μV/K and $A = 0.043$ μV/K$^2$.
Such a behaviour, as well as the deviation from linearity just above $T_c$, can be qualitatively understood as resulting from different temperature dependences of donor and acceptor stack conductivities, even when the intrinsic S(TMTSF) and S(TCNQ) are both proportional to T. To explain the data, the TCNQ stack conductivity must be assumed to rise faster as the temperature is lowered than the donor stack conductivity, according to the sum rule, eq. 3.44. Support for such an interpretation has previously been suggestes by us [29] to come from the fact that the normalized conductivity in TMTTF-TCNQ rises more rapidly ($\sigma_{max}/\sigma_{RT} = 15$) [147] than in TMTSF-TCNQ. However, at low temperatures (T < 80K), the TEP data of Cowan et al. [146] show that the low temperature conductivity of the S-salt is dominated by the donor stack and not by the acceptor stack as proposed in ref. 29. Further, the comparison between TMTTF-TCNQ and TMTSF-TCNQ is somewhat doubtful, since the S and Se analogues are not isostructural [148, 149].

Another explanation for the negative $S_o$-value could be the theoretical deviation from linear S(T) behaviour in tight binding bands of very small bandwidth (see Fig. 3.4), or the additional constant thermoelectric power term arising from correlation effects, provided strong onsite Coulomb repulsion (see chapter 6). We expect such characteristics to be mainly a property of the acceptor chain.

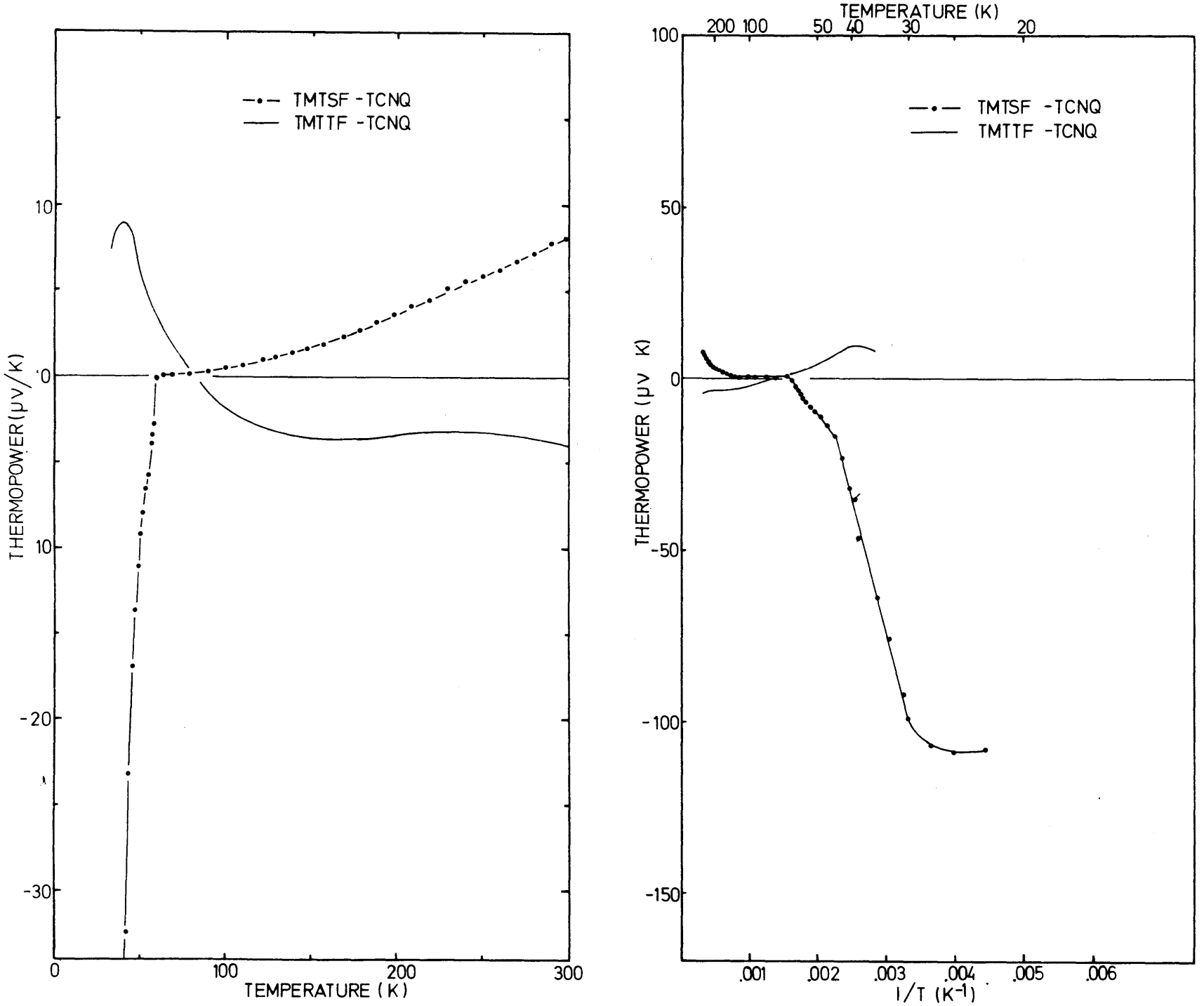


Fig. 8.5 Thermopower of TMTSF-TCNQ and TMTTF-TCNQ |18|.

The deviation from linearity below 150K could be due to collective fluctuations, corresponding to the discussion for TTF-TCNQ, but can as well be explained by the temperature dependent $\sigma_A/\sigma_D$. Moreover, the increasing TEP by lowered temperature can be a result of single particle phonon-drag.

At $T_c$ = 57K, a sharp change in the S(T) slope indicate the M-I transition. Below $T_c$, S is negative and two linear segments are found in the 1/T plot (Fig. 8.5b): Down to 45K the corresponding activation energy

$$\Delta = \left|\frac{\sigma_e - \sigma_h}{\sigma_e + \sigma_h}\right| \frac{E_g}{2} \qquad (8.7)$$

is 3.2 meV, and below 45K $\Delta$ = 7.8 meV. Both energies are smaller than $E_a$ = 14.7 meV derived from conductivity, in agreement with our expectation from (6.2) and (6.12). The change into higher activation energy at about 45K may be due to a transition from being an intrinsic semiconductor to an extrinsic, as the number of impurity-introduced carriers exceeds the number of intrinsic carriers.

DEDMTSF-TCNQ

The thermopower of DEDMTSF-TCNQ is small and positive, 18 μV/K at 300K, and linear in temperature down to 180K. Hence the salt is metallic at high T, and dominated by the donor stacks. The somewhat larger absolute TEP of DEDMTSF-TCNQ compared to TMTSF-TCNQ is attributed to a smaller bandwidth in the former, caused by the substitution of rather bulky ethyl groups. The chain-axis lattice constant in the latter salt is 3.88 Å |148| as compared to 4.0 Å in the first |150|. A difference in charge transfer could also give rise to enhanced thermopower, but the important role of bandwidths is supported by the conductivity data, as $\sigma_{RT}$ (DEDMTSF-TCNQ) is only half the value of $\sigma_{RT}$(TMTSF-TCNQ).

The linear high temperature segment of S extrapolates to negative values at low T,

$$S = -7\ \mu V/K + 0.083\ \mu V/K^2 \times T\ , \quad T > 180K \qquad (8.8)$$

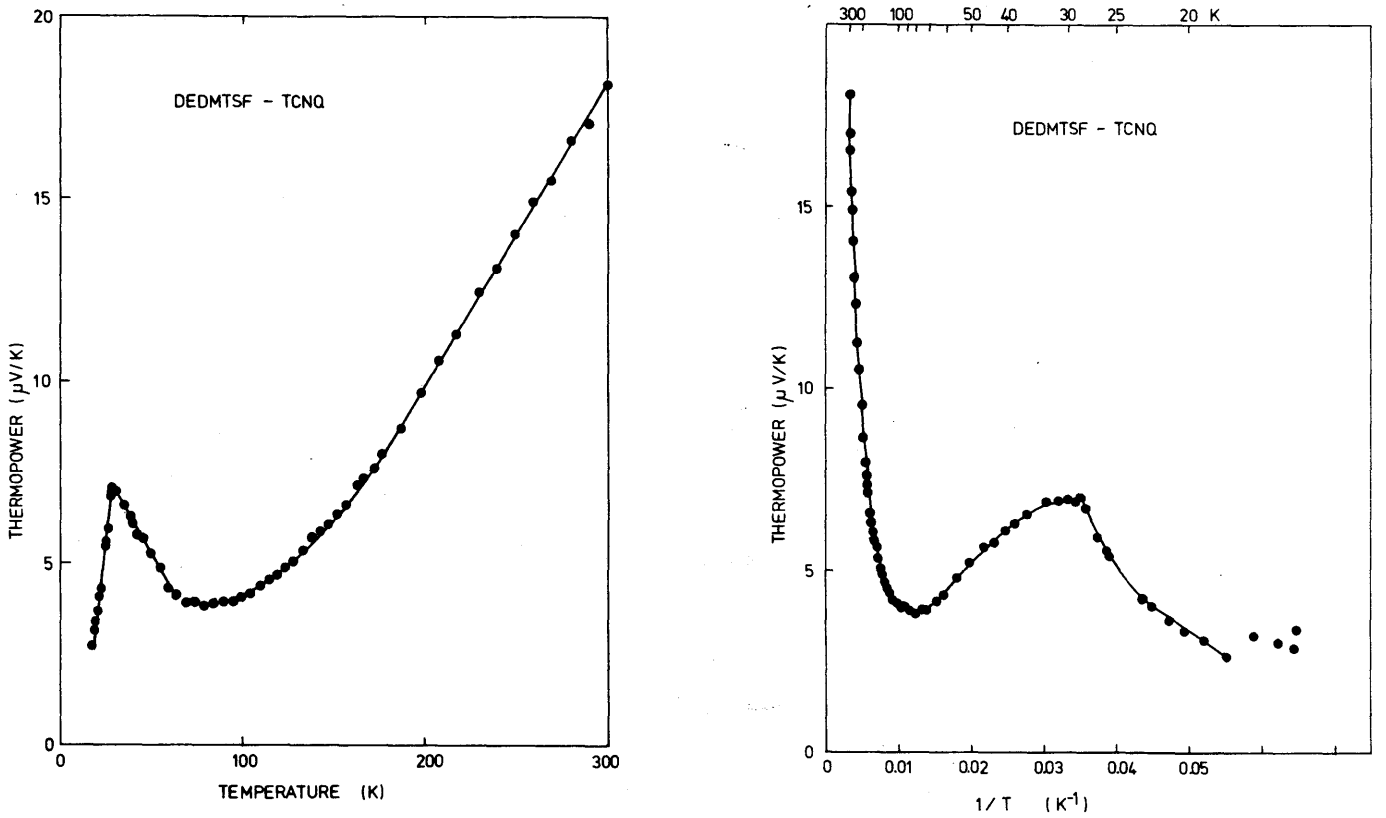


Fig. 8.6 Thermopower of DEDMTSF-TCNQ.

This behaviour must qualitatively be understood on the basis of the discussion concerning TMTSF-TCNQ, as a result of temperature dependence of $\sigma_A/\sigma_D$ or possible Coulomb correlations on the TCNQ stack. Below 180K, a deviation from the linear S(T) behaviour is seen, resulting in an increasing thermopower with decreasing temperature below 80K.

The donor stack consists of both the cis and trans forms of DEDMTSF molecules. The random stacking of these molecules cause static disorder in the donor subsystem, and probably affects the acceptor stacks too. This disorder has been proposed to give rise to the total smearing of $\sigma(T)$ in the transition region |29|, and might as well be the origin of the anomalous S(T) behaviour. The sign of the thermopower, $\Delta s$, additional to the linear term is positive. If S is only diffusive and bandlike, this should indicate that the donor stack dominance has been enhanced by the disorder. But this is in disagreement with our expectation of the disorder being of greatest importance on the donor stack itself. It seems more reasonable that $\Delta S$ is a matter of the scattering term in eq. (3.66). As discussed in chapter 4.10, impurity scattering should enhance the TEP, provided $\tau(\varepsilon)$ increase with a power of $\varepsilon$ larger than zero.

Another origin for the enhanced thermopower below 180K, could be the properties of the intra and inter chain coupling. The disorder may give rise to changed effective overlap, probably resulting in a decreased $t_{\parallel}/t_{\perp}$-ratio. The system has thus become more three dimensional, and in view of the discussions in in chapter 2, we will expect opening of gaps at the Fermi surface, somewhat like the state known from HMTSF-TCNQ |43|. Thus, the material tend to be semimetallic, with the ensuing large thermopower.

At 28K, there is a break in the S(T) slope, best seen in the 1/T plot shown in Fig. 6b. The break takes place where there is a maximum slope in ln $\sigma$ versus 1/T, and we identify it as a Peierls transition. Below the transition temperature, we find semiconducting behaviour, but the activation energy is not well defined.

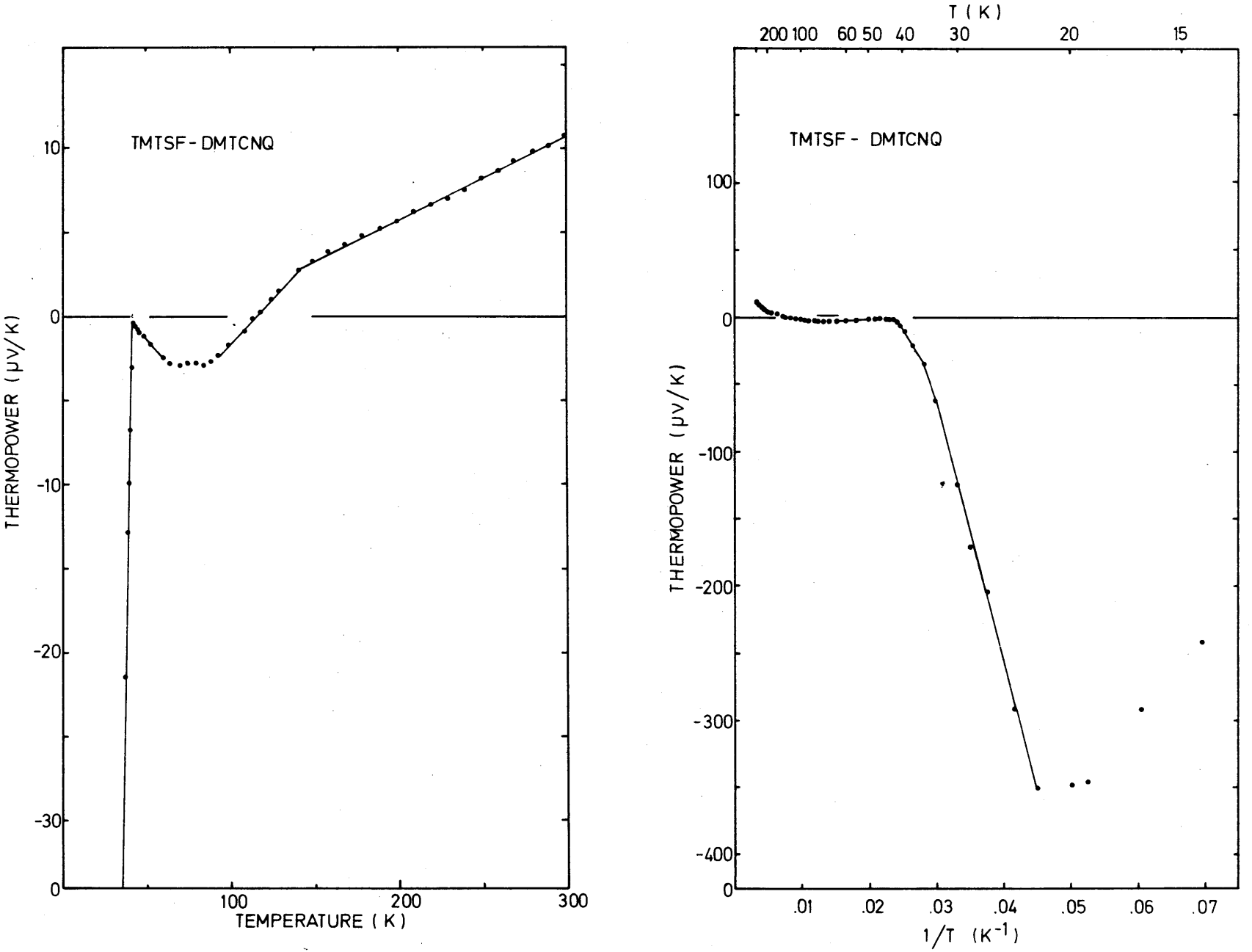


Fig. 8.7 Thermopower of TMTSF-DMTCNQ.

The high-temperature thermopower of TMTSF-DMTCNQ is very similar to the two other Se-compounds, with a small, positive room-temperature value, indicating donor dominance, and with a linear segment down to 140K, extrapolating to negative values at low T. Roughly, S(T) can be written

$$S \simeq -4\ \mu V/K + 0.05\ \mu V/K^2 \cdot T, \quad T > 140K \qquad (8.9)$$

At 140K, a sudden drop in the slope of S versus T takes place. This is just at the temperature region, where recent diffuse X-ray scattering experiments have indicated a phase transition as related to 3D ordering of the $4k_F$ charge density waves |151|. A corresponding anomaly is not seen in the conductivity behaviour (Fig. 4), nor in the magnetic data |152|. The origin and possible connection between the TEP and X-ray experimental facts are still unknown. It should be noted, however, that it is also around 140K that short range transverse order builds up significantly for the $2k_F$ modulation waves |151|.

The diffuse X-ray data moreover give the magnitude of charge transfer. For TMTSF-DMTCNQ it appears to be 0.5 |151|.

Andrieux et al. have by recent experiments on TMTSF-DMTCNQ under pressure found anomalies which by first sight look very similar to that at 140K at ambient pressure |153|. However, they find a corresponding S-shape anomaly in the conductivity data, and further, this anomaly is seen only above approximately 7 kbar, where the CDW probably has been effectively depinned. The data were in |153 |attributed to a structural phase transition between two metallic states, without any significant modification of the 1D character.

Below 80K a new deviation in the TEP is seen. Since a corresponding behaviour is found in the S-analogous compound, this property is attributed to poorly conducting acceptor stacks (see the decomposition below). At $T_c$ = 42K, a Peierls transition take place, primarily driven by the donor stacks. This is in agreement with the magnetic analysis |152|. Below $T_c$, the material is semiconducting. Down to 35K, there is a linear S(1/T) segment corresponding to $\Delta$ = 3.4 meV, and

between 22K and 35K S is again linear in 1/T, but with $\Delta$ = 10 meV. Both $\Delta$'s are smaller than $E_a$ = 12.5 meV derived from conductivity. Below 22K, the conduction is presumably dominated by impurities.

TMTTF-DMTCNQ

The transport properties in TMTTF-DMTCNQ are drastically different from those in the selenium analogues discussed above. The conductivity is rather low, corresponding to a mean free path small compared to the intrachain lattice constant |29|, and the thermopower shown in Fig. 8.8 does not have the characteristic S ~ T behaviour. These features place TMTTF-DMTCNQ in a regime of localized electrons, where transport takes place by diffusion |29|. Such localization can be a result of small polaron formation (see chapter 6), which has the effect of exponential band narrowing.

The TEP of this low-mobility compound is approximately constant, S ≃ -30 μV/K, down to 100K. Qualitatively, such a behaviour is known from systems of highly correlated electrons, where one finds an asymptotical constant high temperature TEP dependent only on the interactions stronger than $k_BT$ and on the charge transfer (see chapter 6). The slight, but reproducible curvature seen above 100K is attributed to the temperature dependence of $\sigma_A/\sigma_D$. As $\rho < 1$, the negative sign of S suggests that the acceptor chain dominates the electric conductivity. In previous papers |29, 86| we assumed that $\sigma_A/\sigma_D >> 1$, so that our experimental findings were equal to the intrinsic DMTCNQ values. From the magnitude of the thermopower, we hence derived the charge transfer by use of the equations (6.29) - (6.33) for TEP of correlated carriers. Dependent of the $U_o/k_BT$ ratio. $U_o$ being the onsite Coulomb repulsion, we found $\rho$ between 0.59 and 0.83.

Until now, there has not been any experimental data for TMTTF-DMTCNQ, which refute these estimations. On the other hand, we know from several S-Se analogous compounds that the charge transfers are nearly equal in pairs, e.g. for TTF-TCNQ and TSF-TCNQ $\rho$ is 0.59 |107| and 0.63 |154| respectively, and for HMTTF-TCNQ and HMTSF-TCNQ $\rho$ is 0.72 |155| and 0.74 |154|. Especially in the region of one half the charge transfer tends

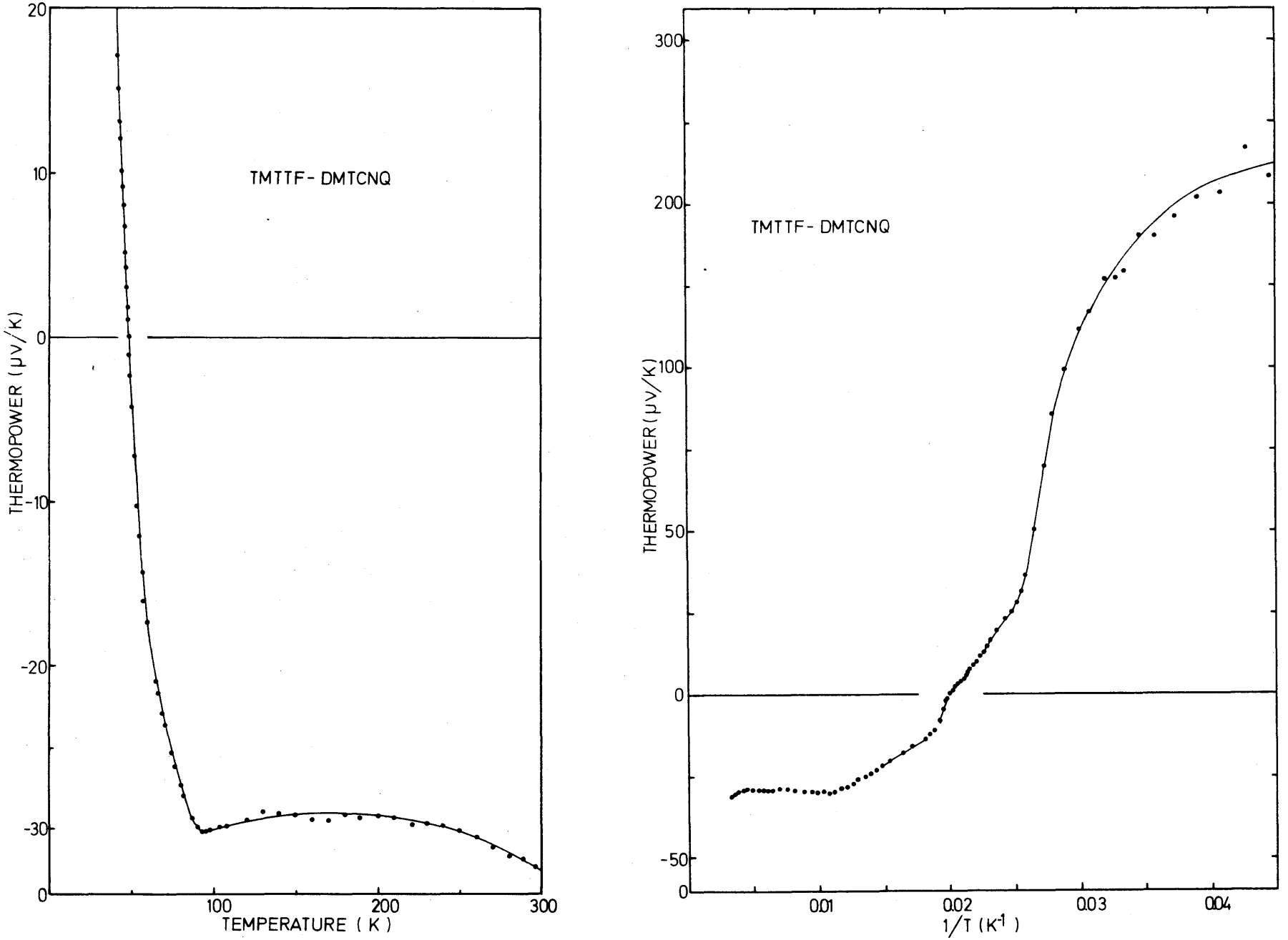


Fig. 8.8 Thermopower of TMTTF-DMTCNQ.

to be exactly 0.5 |156|. Thus, we now believe that

$$\rho(\text{TMTTF-DMTCNQ}) \simeq \rho(\text{TMTSF-DMTCNQ}) = 0.5 \qquad (8.10)$$

But a charge transfer of 0.5 gives in the large U limit a thermopower of 60 μV/K. Assuming strong Coulomb correlation in each of the two types of stacks, we can then derive the $\sigma_A/\sigma_D$ ratio, and thus the absolute intrinsic conductivity:

$$S = \sigma_A/(\sigma_A+\sigma_D) \cdot S_A + \sigma_D/(\sigma_A+\sigma_D) \cdot S_D \qquad (8.11)$$

Taken $S = -30$ μV/K and $S_A = -S_D = -60$ μV/K, we get

$$\sigma_A/\sigma_D = 3 \qquad (8.12)$$

provided $U_o >> k_BT >> t$ for each band.

Below 100K, |S| decreases rapidly reaching zero at 50K, where an anomaly is seen in S as well as in σ. The rather narrow temperature regime, where S goes to zero is consistent with the interpretation developed for transport. The thermal disorder given the diffuse character of the conduction process does not allow development of any order until at a fairly low temperature. But as band behaviour is approached the $2k_F$ instability develops. Presumably the order is primarily developing on the acceptor stacks like in TTF-TCNQ, so that the ordering is not complete until around 40K, where the second anomaly is seen. This behaviour is very similar to that found in TTF-TCNQ.

Below $T_c$, the compound is semiconducting, but without a well defined activation energy, Δ. This is probably caused by poor crystal quality.

## 8.3 DECOMPOSITION OF TRANSPORT PARAMETERS IN TMTSF-DMTCNQ AND TMTTF-DMTCNQ

Both the TTF-TCNQ salt and the four alkylated derivatives discussed above contain the two subsystems, donor and acceptor stacks, which are more or less independent. We have already given some qualitative interpretations concerning the role of

the individual subsystem. e.g. the high temperature and phase-transition driving dominans of acceptor stacks in the sulphur salts and of donor stacks in the selenium salts. But in order to test the different transport models given in chapter 4, for example, detailed knowledge of the intrinsic transport parameters is necessary |86|. An essential basis for a decomposition is that the two chains are effectively decoupled. Then we have (see chapter 3.4)

$$\sigma = \sigma_A + \sigma_D \tag{8.13}$$

$$S = \sigma_A/\sigma \cdot S_A + \sigma_D/\sigma \cdot S_D \tag{8.14}$$

where A and D indicate intrinsic values for acceptor- and donor-stacks respectively.

Before attempting a decomposition, one may raise the question whether a specific kind of stack will have the same intrinsic parameters, $\sigma$ and S, in different materials, provided the intrastack overlap and charge transfer are unchanged. This clearly depends on what scattering mechanisms are dominant. If the scattering is mainly due to intramolecular vibrations, then the behaviour of a specific donor stack should only depend on the charge transfer, and if movements of the molecules as a whole are involved in the electron scattering, the stack arrangement may be quite important. Considering isostructural compounds, however, we do expect the intrinsic parameters to behave approximately in the same way.

The two S-Se analogous DMTCNQ salts fulfil these conditions. Thus we claim

$$\sigma_A(\text{TMTSF-DMTCNQ}) \simeq \sigma_A(\text{TMTTF-DMTCNQ}) \tag{8.15}$$

and

$$S_A(\text{TMTSF-DMTCNQ}) \simeq S_A(\text{TMTTF-DMTCNQ}) \tag{8.16}$$

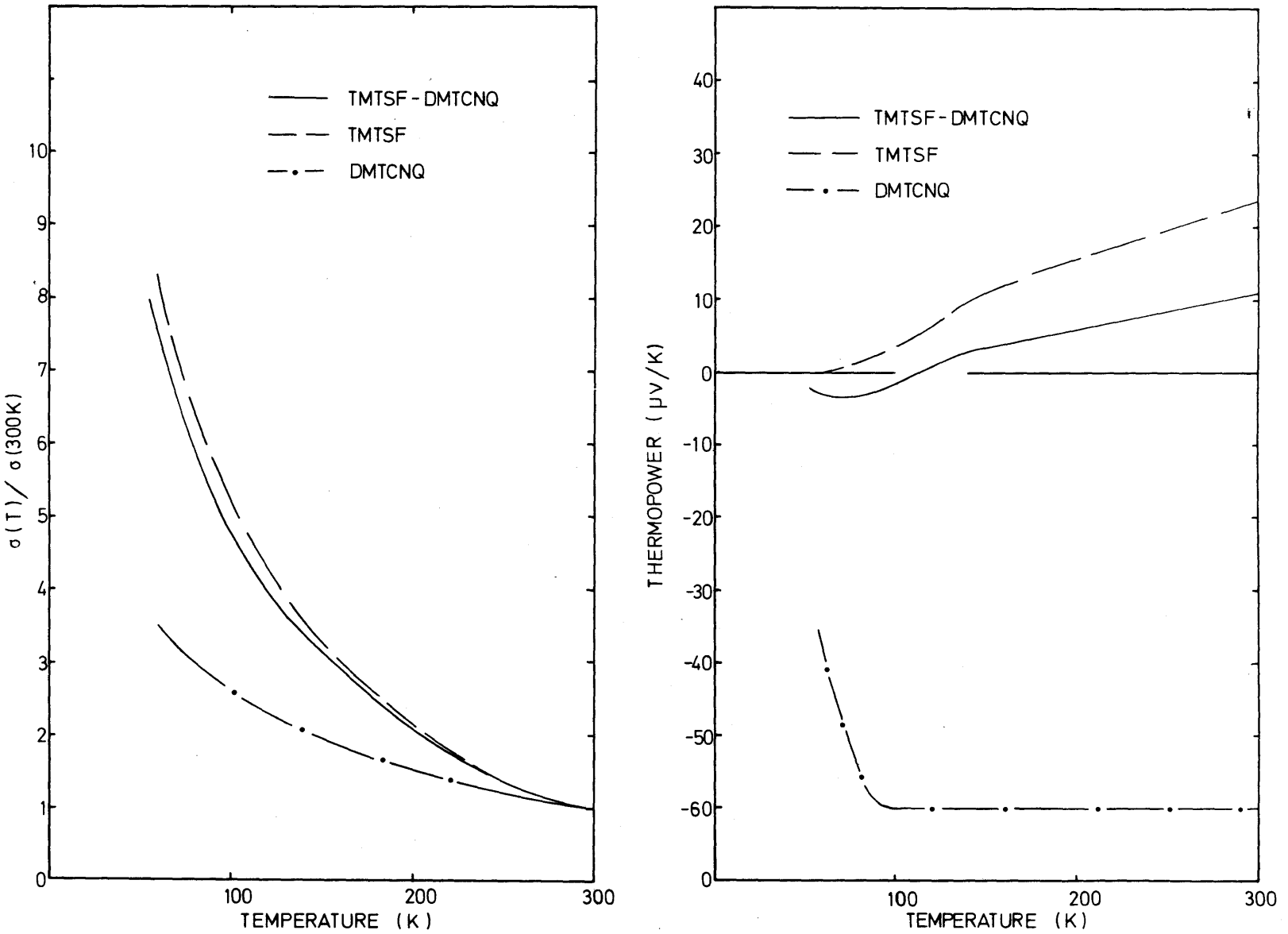


Fig. 8.9 Intrinsic conductivity (a) and thermopower (b) for the stacks of TMTSF-DMTCNQ.

Based on the indication of strong Coulomb correlations in TMTTF-DMTCNQ, we already have made the high temperature decomposition:

$$S_A(\text{TMTTF-DMTCNQ}) \simeq -S_D(\text{TMTTF-DMTCNQ}) \simeq -60\ \mu V/K \qquad (8.17)$$

The nearly constant extrinsic thermopower above 100K indicate that $\sigma_A$ and $\sigma_D$ have approximately the same temperature dependence, equal to that of the total conductivity, $\sigma \sim T^{-1.3}$. Thus, since $S = -30\ \mu V/K$ and $\sigma = 120\ \Omega^{-1}\ cm^{-1}$:

$$\sigma_A(\text{TMTTF-DMTCNQ}) \simeq \frac{3}{4}\sigma(\text{TMTTF-DMTCNQ}) \simeq 90\ \Omega^{-1}cm^{-1}\cdot\left(\frac{T}{300K}\right)^{-1.3} \qquad (8.18)$$

$$\sigma_D(\text{TMTTF-DMTCNQ}) \simeq \frac{1}{4}\sigma(\text{TMTTF-DMTCNQ}) \simeq 30\ \Omega^{-1}cm^{-1}\cdot\left(\frac{T}{300K}\right)^{-1.3} \qquad (8.19)$$

As the phase transition was supposed to be driven mainly by the acceptor stack, we believe that the thermopower in the region $T_c$-100K reflects the intrinsic DMTCNQ behaviour, but a decomposition in this regime is probably not allowed.

Now, let us look at the selenium salt, TMTSF-DMTCNQ. According to the discussion above, we know the intrinsic transport parameters of the DMTCNQ stack, and by use of (3.47a) and (3.47b) it is simple to calculate the values for the TMTSF stack too. The results are shown in Fig. 8.9.

At high temperatures (T > 140 K), the intrinsic thermopower for the TMTSF-stack is seen to be given by

$$S(\text{TMTSF}) \simeq 0.78\ \mu V/K^2 \times T \qquad (8.20)$$

Such a linear behaviour is just what we would expect for a metallic band, using the tight binding formula (see chapter 3.6).

$$S = -\frac{2\pi^2}{3}\frac{k_B}{e}\frac{k_B T}{W}\left[\frac{\cos(\pi\rho/2)}{\sin^2(\pi\rho/2)} + \frac{W}{2}\frac{\tau'}{\tau}\right]_{\varepsilon_F} \qquad (8.21)$$

For all the theories of mobility given in chapter 4, we found the sign of the scattering term in (8.21) equal to the sign of the band term. Thus (8.20) and (8.21) give a lower limit for the bandwidth

$$W(\text{TMTSF}) \geq 0.86 \text{ eV} \qquad (8.22)$$

as $\rho = 0.5$. The discussions given in chapter 4 suggest, however, that the $\tau'/\tau$ term is of the same magnitude as the band term, thus giving a bandwidth twice as large as the one in (8.22). This is in good agreement with the value estimated from optical data |29|. Using a tight-binding approximation one gets from the plasma frequency, $\omega_p = 9030 \text{ cm}^{-1}$, the bandwidth

$$W(\text{TMTSF}) \simeq 1.2 \text{ eV} \qquad (8.23)$$

provided of the acceptor band is totally disregarded.

Below 150K the decoupling seems to show that the 140K-anomaly is connected to the TMTSF stack, whereas the increasing TEP below 80K is due to the DMTCNQ stack. However, the decoupling in this region may be upset by fluctuations.

A justification of the decomposition above 140K is given by the analysis of TMTSF-DMTCNQ salt doped with MTCNQ. The doping is not expected to change the structure, charge-transfer or transfer integrals appreciably. But the introduced disorder may reduce the conductivity on the doped DMTCNQ stack. Thus the doped compound should behave approximately as the intrinsic TMTSF stack. This is just what is found.

TMTSF-DMTCNQ$_{0.75}$MTCNQ$_{0.25}$

The room-temperature conductivity of TMTSF-DMTCNQ$_{0.75}$-MTCNQ$_{0.25}$ is only reduced 10-20% compared to the pure salt TMTSF-DMTCNQ. MTCNQ is known to have important effects on the electronic properties |157|, and the introduction into the DMTCNQ stack is expected to severely limit the intrinsic mobility of the acceptor band, whereas the donor band is only slightly affected. Thus, the measured conductivity of the doped compound should approach

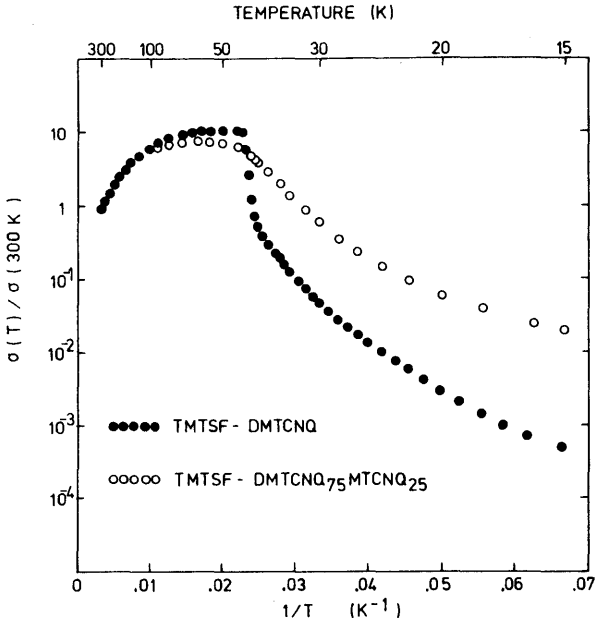


Fig. 8.10 Conductivity of TMTSF-DMTCNQ and TMTSF-$DMTCNQ_{0.75}MTCNQ_{0.25}$.

the intrinsic donor conductivity. This is confirmed as the measured $\sigma$ is equal to $\sigma_D$ found by decomposition.

In Fig. 12 we show the influence on the thermopower of doping. S is shifted to higher values at high temperatures and is approximately linear in T, $S = A \cdot T$, in accordance with the metallic behaviour of $S_D$ found by decomposition. The absolute value of S is somewhat smaller than the decomposed value, probably a result of the rather large intrinsic $S_A$ which still may have an influence on S, although $\sigma_A/\sigma_D << 1$.

S(T) deviates from the simple linear temperature behaviour below 200K, exactly where the normalized conductivity starts falling below that of the undoped system (Fig. 8.10). This is obviously an effect of the introduced disorder, which via randomly oriented dipole fields also may affect the donor stack. The qualitative S(T) behaviour is very similar to that found in DEDMTSF-TCNQ (Fig. 8.6), which also was attributed to disorder. For more detailed discussions, we will refer to the treatment of the latter compound.

At temperatures below $T_c$, the effect of doping is to enhance the normalized conductivity by approximately one order of mag-

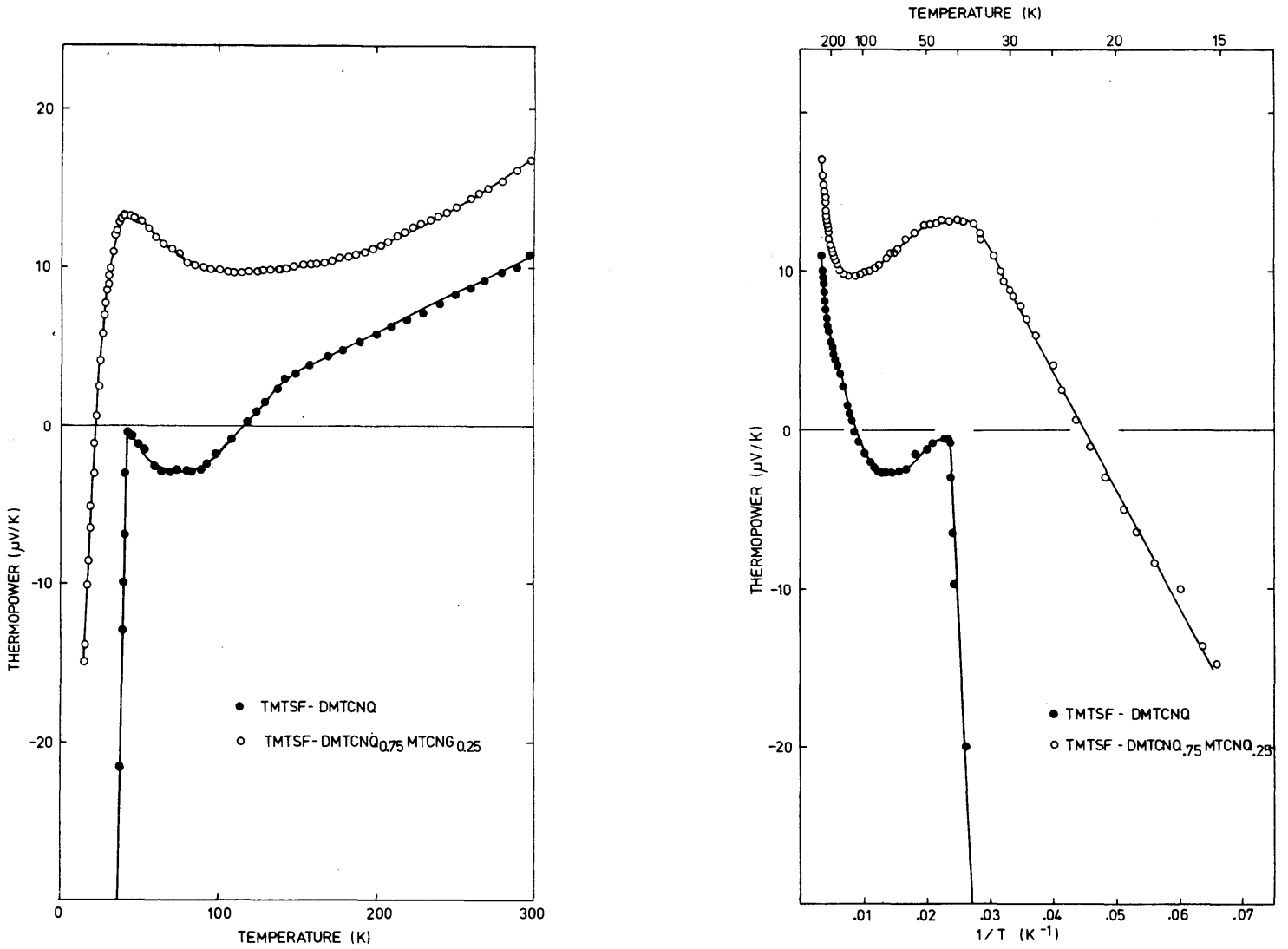


Fig. 8.11 Thermopower of TMTSF-DMTCNQ and TMTSF-$DMTCNQ_{0.75}MTCNQ_{0.25}$.

nitude compared to the undoped compound. In the conductivity plot, Fig. 8.10, the phase transition seems to be somewhat smeared out, but from the thermopower data, Fig. 8.11, it is still possible to obtain a well defined transition temperature,

$$T_c(\text{TMTSF-DMTCNQ}_{0.75}\text{MTCNQ}_{0.25}) = 37\text{K}$$

which is somewhat lowered compared to $T_c$ of TMTSF-DMTCNQ. Below $T_c$ we find a small gap semiconductor with an effective energy gap

$$\sigma(\text{TMTSF-DMTCNQ}_{0.75}\text{MTCNQ}_{0.25}) = 0.4 \text{ meV}$$

Apparently the disorder has created impurity levels in the band gap.

## 8.4 THERMOPOWER OF THE SALTS $(TMTSF)_2$-X, X = $PF_6^-$, $AsF_6^-$, $SbF_6^-$, $NO_3^-$ and $BF_4^-$, DERIVED FROM TETRAMETHYLTETRASELENAFULVALENE (TMTSF).

Single crystals of the solids, $(TMTSF)_2$-X, were prepared at the Ørsted Institute by electrochemical oxidation of neutral TMTSF in $CH_2Cl_2$ at constant current |31|. These systems should be attractive in testing the various transport theories as they have only one conducting chain. Detailed analysis has been obtained for each salt, resulting in perfect 2:1 stoichiometry |31|. Thus the charge transfer is 0.5, and the CDW set up are commensurable with respect to the lattice. The structure is characterized by uniform donor stacks in sheets, separated by anion sheets. The donor molecules repeat by a pseudotranslation of period a/2 along a, and are nearly perpendicular to a. They seem to be overlapping symmetrically, thus giving rise to 3/4 filled bands, in contrast to the very similar sulphur compound $(TMTTF)_2$-Br |158|, which is dimerized.

In Table 8.4 and Fig. 8.12 and 8.13 the transport properties of the compounds are summarized. Room-temperature conductivities range from 500-800 $(\Omega\text{cm})^{-1}$. At high temperature (T>100K)

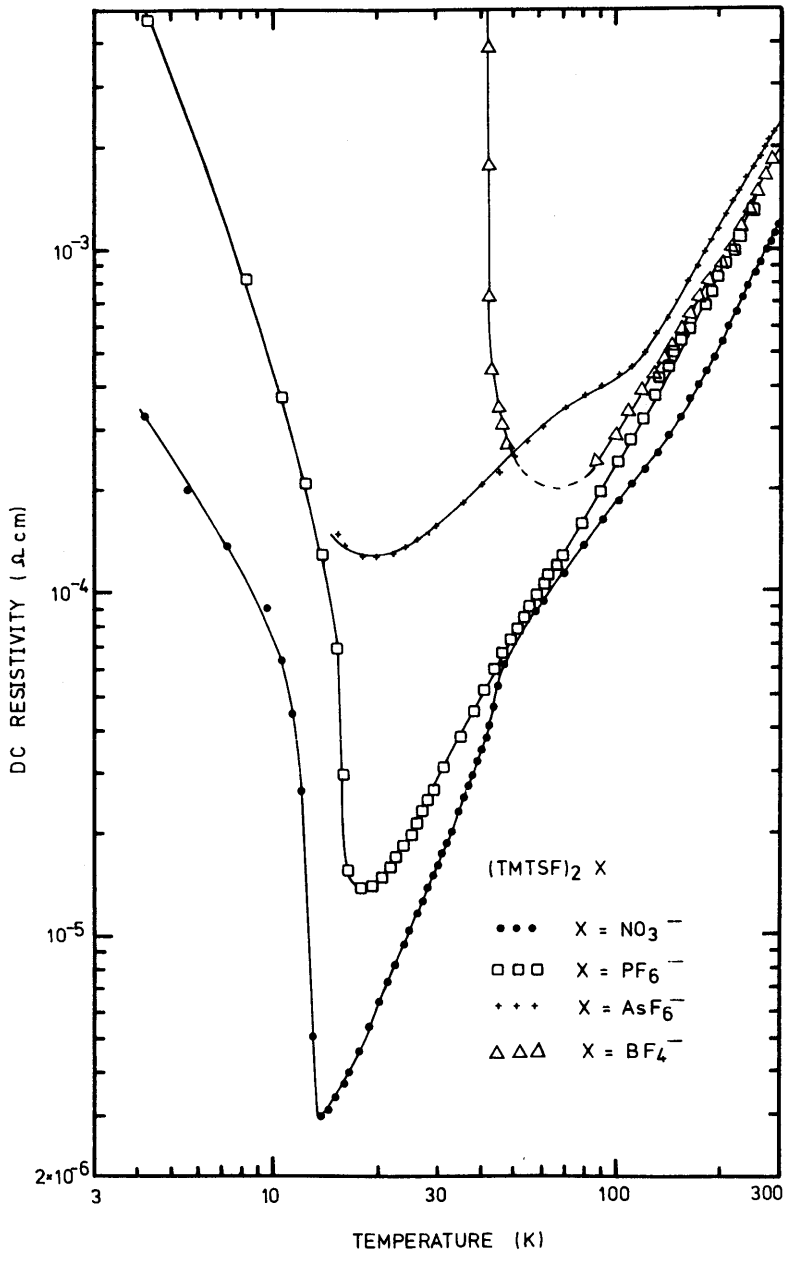


Fig. 8.12 Conductivity of $(TMTSF)_2$-X, X=$PF_6^-$, $AsF_6^-$, $SbF_6^-$, $NO_3^-$ and $BF_4^-$.

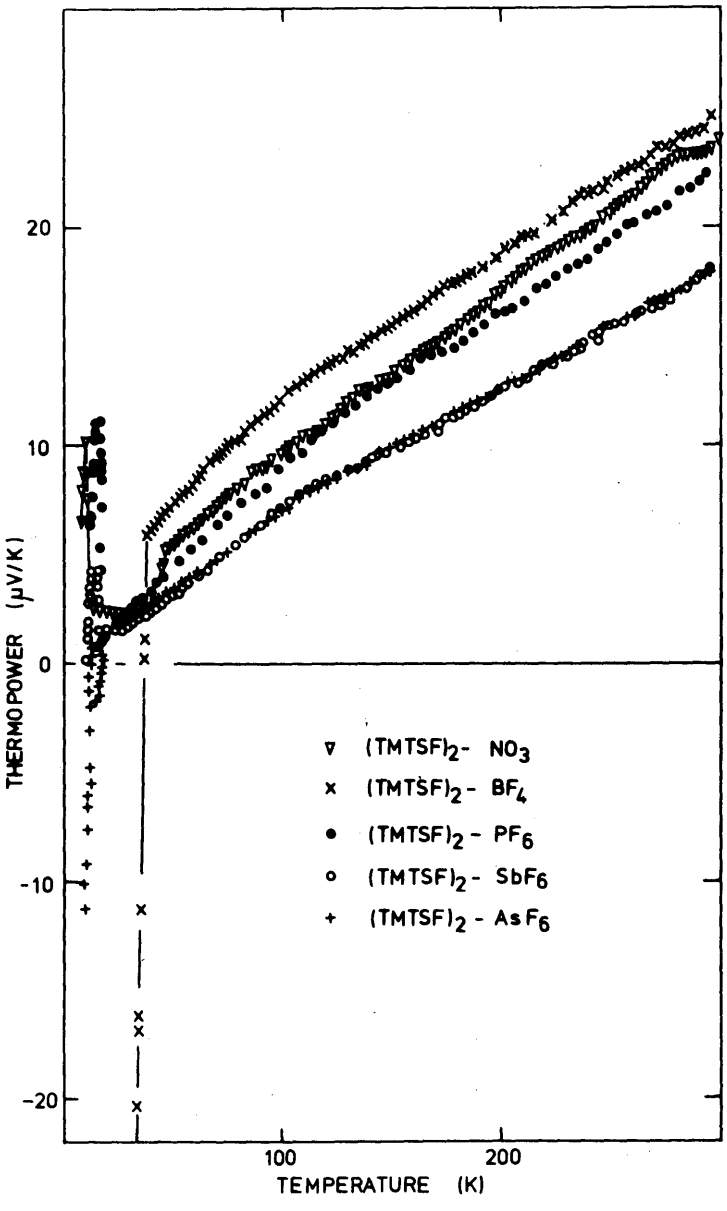


Fig. 8.13 Thermopower of $(TMTSF)_2$-X, X=$PF_6^-$, $AsF_6^-$, $SbF_6^-$, $NO_3^-$ and $BF_4^-$.

Table 4 Transport properties of $(TMTSF)_2X$, $X = PF_6^-$, $AsF_6^-$, $SbF_6^-$, $NO_3^-$, $BF_4^-$.

| x | $PF_6^-$ | $AsF_6^-$ | $SbF_6^-$ | $NO_3^-$ | $BF_4^-$ |
|---|---|---|---|---|---|
| $\sigma_a$(300K) $\|(\Omega cm)^{-1}\|$ | 540 | 430 | 500 | 780 | 540 |
| $\sigma_{\perp 1}$(300K) $\|(\Omega cm)^{-1}\|$ | 1.5 | - | - | - | - |
| $\sigma_{\perp 2}$(300K) $\|(\Omega cm)^{-1}\|$ | 0.015 | - | - | - | - |
| S(300K) $\|\mu V/K\|$ | 23 | 19 | 19 | 25 | 25 |
| $T_c$ $\|K\|$ | 19 | 15 | 17 | 12 | 39 |
| $W^*$ $\|eV\|$ | 0.9 | 1.1 | 1.1 | 0.8 | 0.8 |

*) The bandwidth W is derived from the high-temperature thermopower, neglecting the scattering term.

the resistivity can be fitted to $\rho = \rho_o + bT^2$, with $\rho_o$ close to zero, indicating good crystal quality. The anisotropy is 300 and 30.000 at 300K for the two transverse directions respectively, and increases rapidly with decreasing temperature |159, 31|, thus confirming the one-dimensional nature in accordance with the structural features.

In Fig. 8.14 we show the thermopower of the five compounds. The small room-temperature values, ranging from 19 to 25 μV/K, and the linear S(T) behaviour extrapolating to a value near zero at $0^oK$, reveal simple band conductors. One should notice the extremely regular S(T) curve down to only a few degrees above the transition temperature. Only a slight curvature against smaller S is seen, similar in all the materials. This could be indicative of enhanced influence of collective phenomena, but may as well be due to the $\tau'/\tau$-term in (8.24), or to the non-vanishing $k_BT/W$-quantity (see Fig. 3.3). Although there is no detailed theory for phonon-drag effects in 1D systems (see chapter 5 ), we see in the TEP data no features reminiscent of appreciable single particle drag effects.

By use of the 1D tight binding formula, eq. 3.67, which for $\rho = 3/4$ becomes

$$S(T) = \frac{2\pi^2}{3} \frac{k_B}{e} \frac{k_B T}{W} \left[\sqrt{2} + \frac{W}{2} \left(-\frac{\tau'}{\tau}\right)_{\varepsilon_F}\right] \qquad (8.24)$$

we can estimate the magnitude of the bandwidth. Since $(-\tau'/\tau)$ for $\rho > 1$ is expected to be positive (see chapter IV ), we get the lower limit of the bandwidth, W, between 0.8 eV and 1.1 eV. The correct bandwidths are probably between this value and a value twice as large. For $(TMTSF)_2-PF_6$, optical measurements show a plasma frequency of 10050 $cm^{-1}$, corresponding to the bandwidth, $W \sim 1$ eV, in good agreement with the value derived from TEP.

The low-temperature transport properties of the $(TMTSF)_2-BF_4$ compound differ distinctly from the other four materials. At 39K, $(TMTSF)_2-BF_4$ exhibits an extremely sharp phase transition into an insulating state. The thermopower below this transition becomes large and negative, but the very strong temperature dependence and the high sample resistance make detailed analysis impossible.

The remaining four compounds behave very similar, best seen in the S versus 1/T plot (Fig. 8.14). All exhibit phase transitions well below 20K, showing up in the TEP plot as very sharp anomalies to larger S-values. A few degrees above $T_c$ a slight lowering in S is observed in the $PF_6^-$, $AsF_6^-$ and $SbF_6^-$ compounds. Below $T_c$, all compounds are seen to be semiconducting, as they follow the form (6.12)

$$S = S_o - \frac{k_B}{e} \frac{\Delta}{k_B T} \qquad (8.25)$$

The constant $S_o$ is in all four materials of the order of 30 μV/K, and the effective activation energy, $\Delta$, range from 0.1 meV for $(TMTSF)_2-NO_3$ to 0.2 meV for $AsF_6$. In $(TMTSF)_2-NO_3$ an additional anomaly appears at 45K. It gives rise to a decrease in TEP with lowered temperature, and an S-shape curve in the conductivity. This anomaly could arise from freezing of the $NO_3^-$ ions, but it is not clear what effect dynamic disorder of the anions may have on the transport properties.

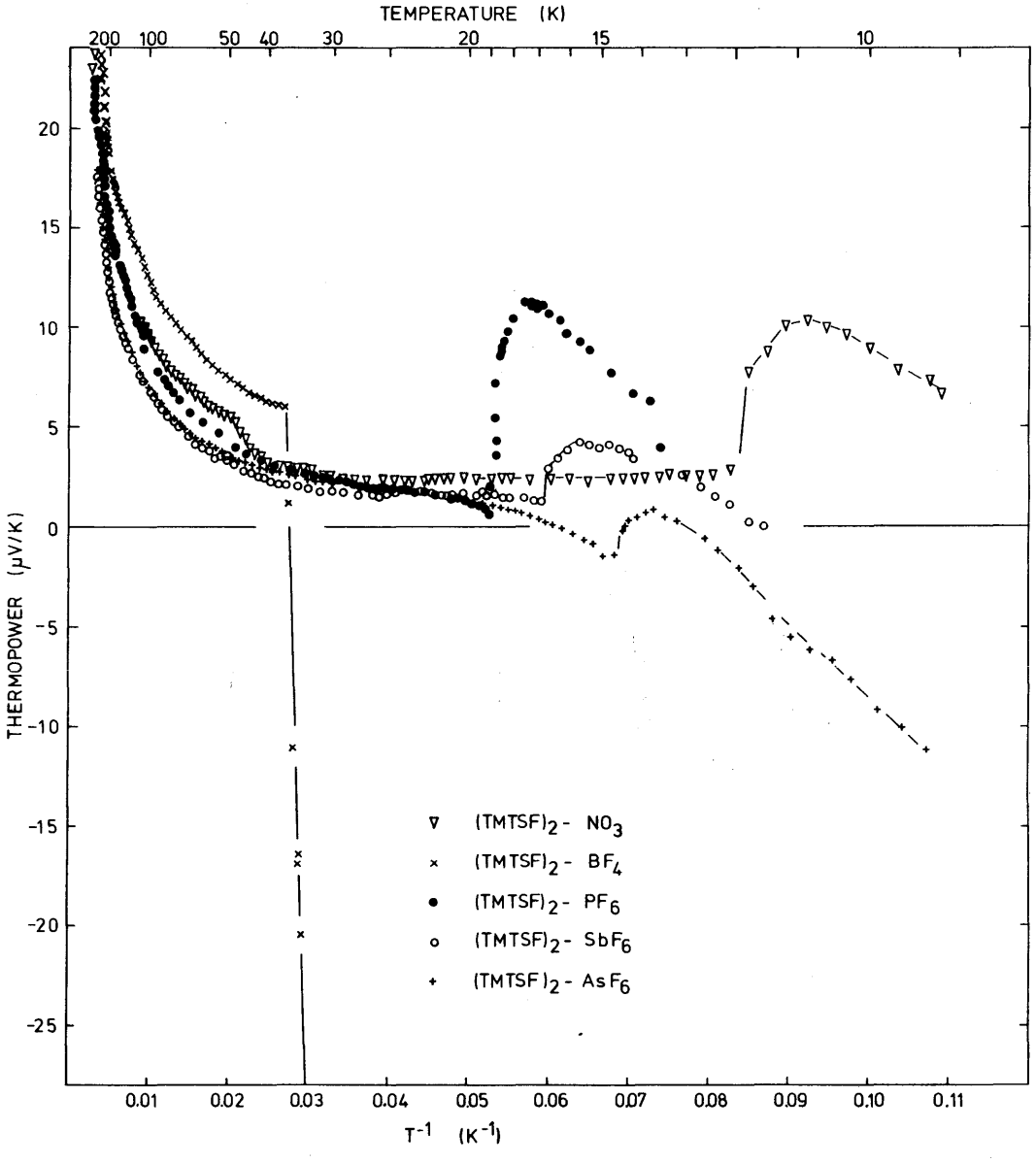


Fig. 8.14 Thermopower of $(TMTSF)_2$-X, X = $NO_3^-$, $BF_4^-$, $PF_6^-$, $SbF_6^-$ and $AsF_6^-$, versus 1/T.

## 8.5 THERMOPOWER OF $(TMTTF)_2$-$PF_6$

Crystals of $(TMTTF)_2$-$PF_6$ were prepared like those of the selenium analogues, discussed above. The crystals are brittle and of typical size $2\times0.2\times0.1$ $mm^3$. Our transport studies are only preliminary, and much more work is needed to fylly characterize this compound. The French group in Talence, Delhaes et al. |158| has done some studies on $(TMTTF)_2$-$PF_6$, but their transport work were only concerning conductivity in the region 180K-300K. More detailed studies were done on the compounds $(TMTTF)_2$-X, X = $ClO_4^-$, $BF_4^-$ and $Br^-$.

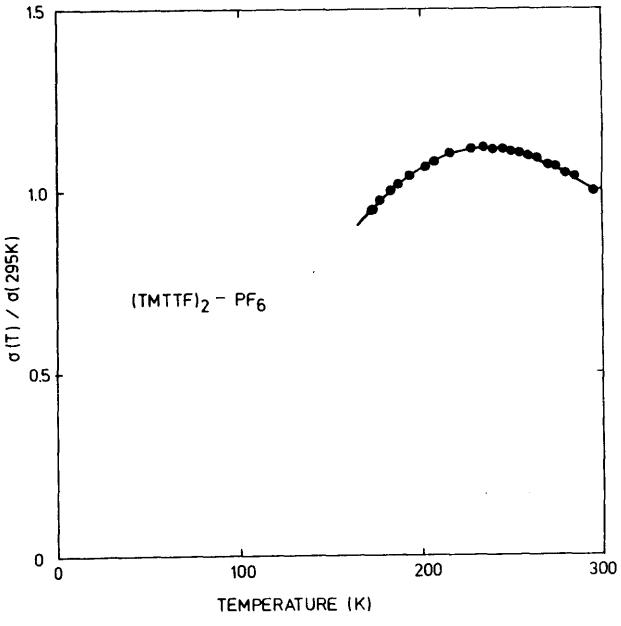


Fig. 8.15 Normalized conductivity versus temperature for $(TMTTF)_2$-$PF_6$ |150|

Delhaes et al. |158| found by chemical analysis a stoichiometry of 2:1. X-ray studies of the $Br^-$ salt showed a triclinic structure, but the TMTTF units are not symmetrically equivalent. The $PF_6^-$ salt is probably similar, i.e. with dimerized TMTTF stacks. Thus the electronic bands are 1/2 filled, rather than the 3/4 filled bands in the symmetric case. We do, however, wish to point out that such a weak dimerization is only expected to influence the transport properties at very low temperature, where thermal motion is less important.

The conductivity of $(TMTTF)_2$-$PF_6$ is shown in Fig. 8.15 |158|. The room-temperature value is typically 20 $(\Omega cm)^{-1}$, which places the system in a transport region of diffusion or activated hopping, rather than the band like conductivity observed in the

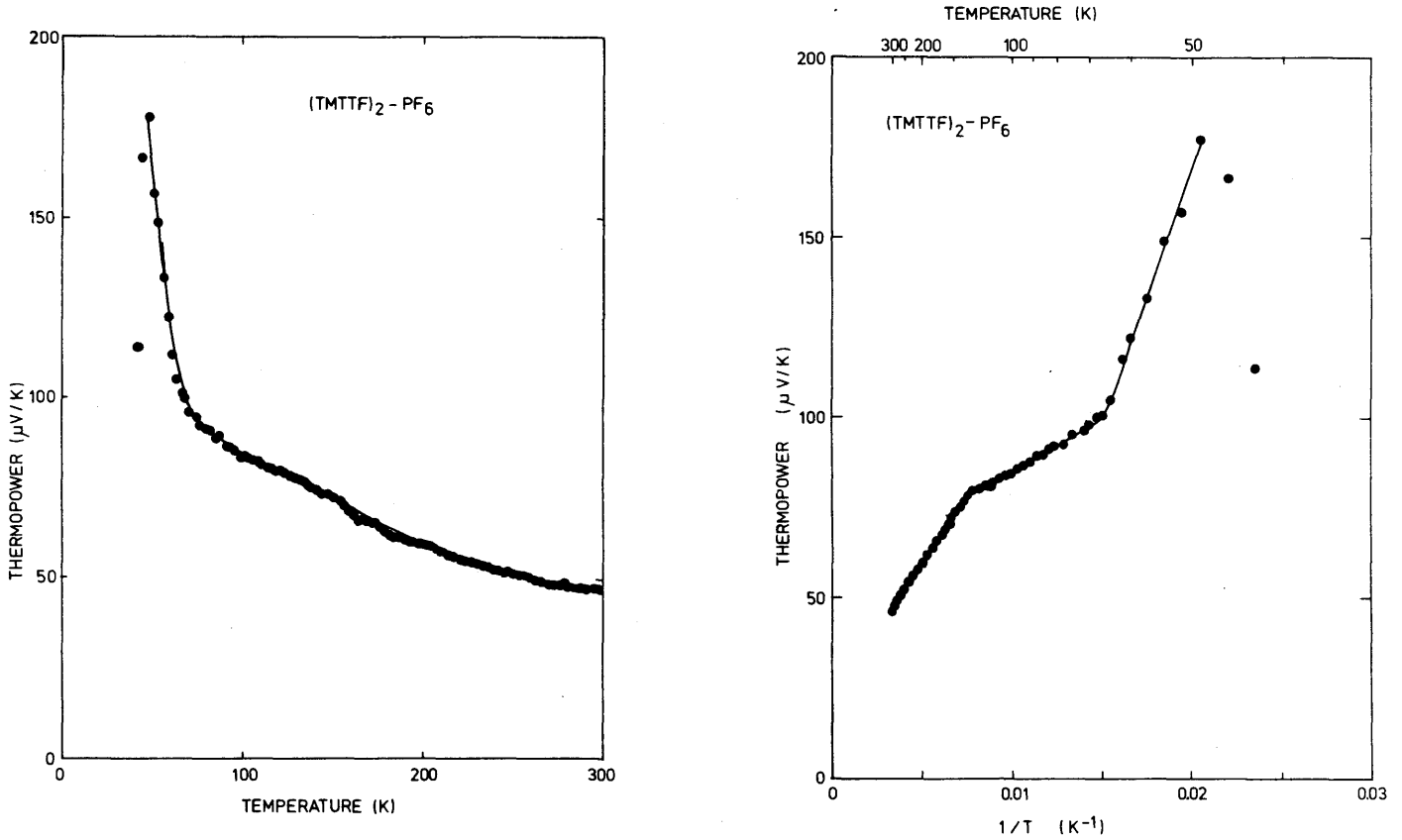


Fig. 8.16 Thermopower of $(TMTTF)_2PF_6$.

selenium analogue. At T = 245K, $\sigma(T)$ reaches a maximum value of $1.1\times\sigma(300K)$, and below 245K $\sigma(T)$ decreases moderately. The two $(TMTTF)_2$-x salts formed with $BF_4^-$ and $ClO_4^-$ exhibit MI phasetransitions at 41K and 70K respectively. In ref. 3 they were identified as Peierls transitions. The $PF_6$ salt will probably also show a transition, when going to sufficiently low temperatures.

Based on optical and paramagnetic susceptibility data, Delhaes et al. remarked that electron-electron interactions are not negligible in the $(TMTTF)_2$-x compounds.

In Fig. 8.16 we show the thermopower of $(TMTTF)_2$-$PF_6$. The positive TEP is in agreement with our expectation for conduction by a donor chain. The temperature dependence clearly corroborate the non band-like transport mechanism, and the possibility of strong intrasite Coulomb correlation. As best seen in the 1/T-plot, the S(T) falls into three regions: a T > 125K, b, 125K > T > 66K and c, T < 66K. In all three regions, S exhibits more or less semiconducting properties

$$S = S_o + \frac{k_B}{e}\frac{\Delta}{k_B T} \quad ,$$

but more independent experimental data are necessary for a detailed analysis. However, we wish to point out that the intermediate region has exactly the properties expected for a highly correlated semiconductor. The asymptotical high temperature thermopower is just $S_o = k_B/e \cdot \ln 2$ (see chapter 6). The properties above 125K are not yet understood, but the transition could be from essentially no dimerization to effectively dimerized donor stacks. The transition at 66K is attributed to the Peierls instability, but X-ray experiments have not been done to confirm this.

## 8.6 THERMOPOWER OF HMTSF-TNAP

The HMTSF-TNAP crystals (see Fig. 8.17) were prepared by slow cooling of a nitrobenzene solution of the purified constituents |160|. Typical samples had dimensions of $2\times0.2\times0.4$ mm$^3$, and exhibited a green shine in reflected light. The TNAP molecule differs from TCNQ in several aspects from its size and symmetry. This should change the intra-stack overlap and the possible

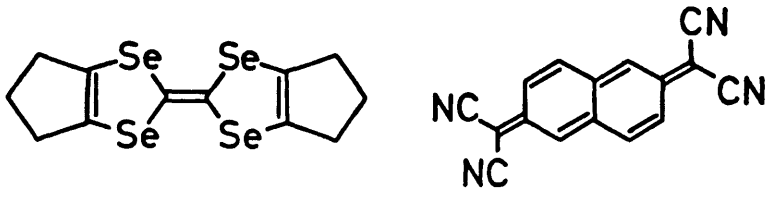


HMTSF TNAP

Fig. 8.17 Molecular constituents.

first order coupling between electrons and molecular vibrations. The donor and acceptor stacks are arranged in alternating rows [161].

In Fig. 8.18 we show the temperature dependence of the normalized conductivity [160]. Room temperature conductivity is in the range 1800-3000 $(\Omega cm)^{-1}$. A well defined maximum occur near $T_{max}$=47K with $\sigma_{max}/\sigma(300K)$ = 6. Below approximately 35K, a pronounced sample dependent $\sigma(T)/\sigma(300K)$-ratio is found. In Fig. 8.18 we also show the conductivities of HMTSF-TCNQ [49] and TMTSF-TCNQ [29], the first because the low temperature behaviour is similar and TMTSF-TCNQ because its crystal structure [148] is qualitative similar to that of HMTSF-TNAP. The anisotropy of HMTSF-TNAP is for both directions perpendicular to the highly conducting direction of order 100, at 300K.

In Fig. 8.19 the thermopower is shown versus temperature. Above 200K, S is approximately linear in T, and reaches at room temperature a small, positive value of 7 μV/K. Qualitatively this behaviour is similar to all other selenium derivatives of TTF-TCNQ, e.g. HMTSF-TCNQ [49] and TMTSF-TCNQ [29], and indicative of simple band conduction, dominated by the donor stack.

Below 200K we observe a residual TEP, increasing as the temperature is decreased. This could be due to phonon drag, which in

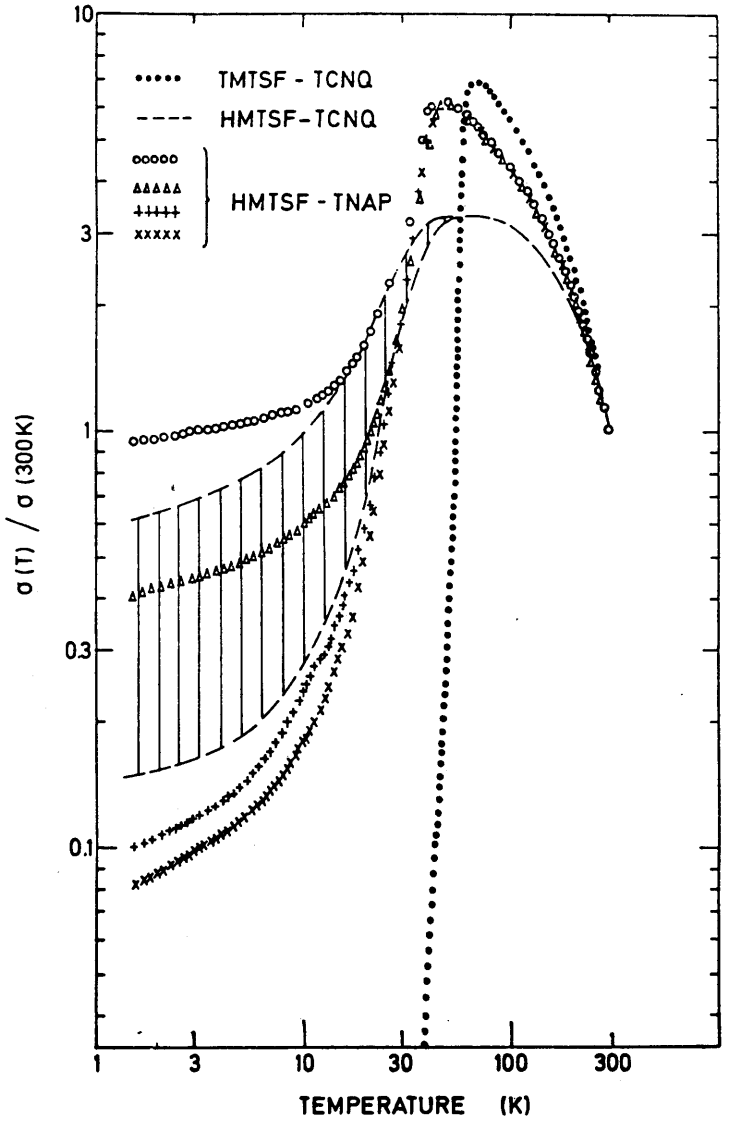


Fig. 8.18 Conductivity versus temperature of HMTSF-TNAP |160|, HMTSF-TCNQ 49 and TMTSF-TCNQ |29|.

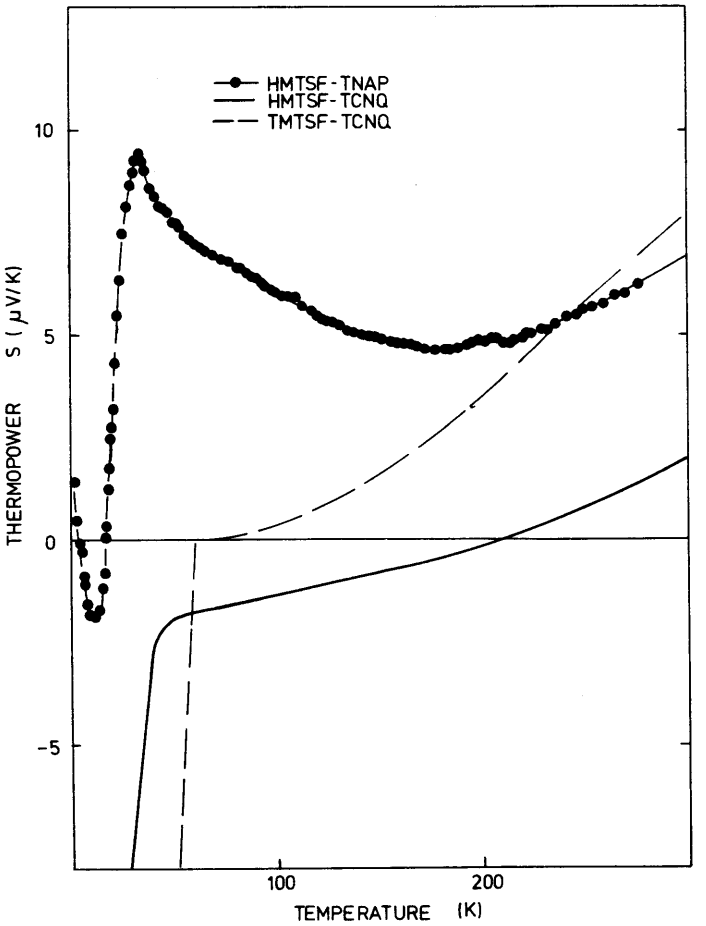


Fig. 8.19 Thermopower versus temperature of HMTSF-TNAP, HMTSF-TCNQ |49| and TMTSF-TCNQ |29|.

3D systems is known to give a $\Delta S$ proportional to 1/T (see chapter 5 ). However, a similar S(T) behaviour was seen in the compounds DEDMTSF-TCNQ and TMTSF-$DMTCNQ_{0.75}^{MTCNQ}{}_{0.25}$. In these systems, the $\Delta S$ was attributed to disorder effects. This could mean that HMTSF-TNAP is influenced by disorder below 200K. The large sample dependent low-temperature conductivity support this view. However, the large $\Delta S$ can also be a result of the relative large interstack interaction, due to the samll Se-N distance |161|. This interaction may give rise to opening of gaps on parts of the Fermi surface, resulting in a semimetallic state, as known from HMTSF-TCNQ |43|.

At 33K, a sharp change in the S(T) slope suggests a Metal-Insulator transition. This is just the temperature where the conductivity shows strong sample dependence, so a gap at the Fermi-surface may open here. The MI transition is presumably a Peierls transition |86|. Below $T_c$ the TEP decreases rapidly, but S remains small down to at least 2K. This may suggest that the Peierls gap destroys only part of the Fermi surface, hence the material becomes semimetallic.

The thermopower becomes negative below 17K, and reach a maximum in magnitude around 10K (Fig. 8.20b). The values of S below T = 4K are somewhat uncertain, as S is of the same magnitude as that of the reference material, Au, which on the other hand is extremely impurity dependent in this region. The TEP behaviour could suggest that HMTSF-TNAP is under influence of magnetic impurities, giving rise to a Kondo effect, showing up as a peak in the S(T) curve (see chapter 4.10). Support for this interpretation of the low-temperature TEP is the measurements of static magnetic susceptibility which indicate a certain amount of paramagnetic impurities |160|. Also the conductivity can be shown to follow a logarithmic temperature behaviour, characteristic for the Kondo effect. Such a fit to $\sigma(T)$ has been done for HMTSF-TNCQ |162|, which behaves very similar to HMTSF-TNAP below $T_c$.

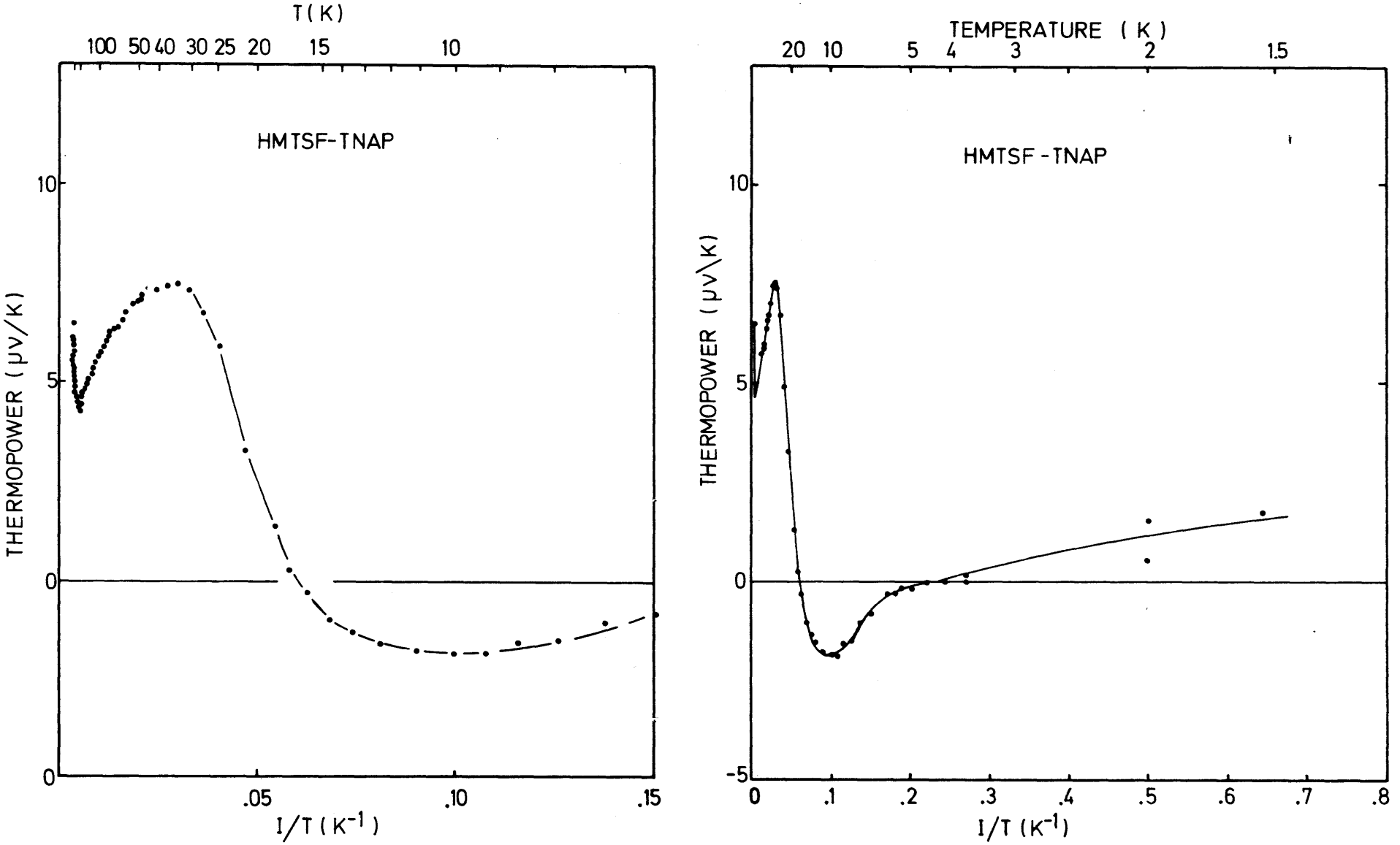


Fig. 8.20 Thermopower versus 1/T for HMTSF-TNAP.

## 8.7 THERMOPOWER OF TTTF-TCNQ and METTTF-TCNQ

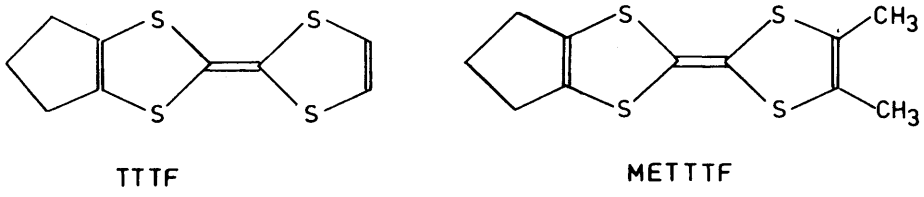


Fig. 8.21 Molecular design.

Crystals of TTTF-TCNQ and METTTF-TCNQ were prepared by the Montpellier group |163|. Both crystal structures are known |164|. The symmetry is monoclinic with regular segregated stacks of donors and acceptors. TCNQ-ions and cations of two adjacent chains are either nearly parallel (TTTF) or strongly tilted (METTTF). Thus the molecular orbital overlapping between donor and acceptor is expected to be more important for the first than for the second one.

Table 5

Transport properties of TTTF-TCNQ and METTTF-TCNQ

| | $\sigma$(300K) $(\Omega cm)^{-1}$ | $\sigma_{max}/\sigma_{RT}$ | $T_{max}$ (K) | S(300K) ($\mu$V/K) | $T_c$ (K) | $\Delta$ meV |
|---|---|---|---|---|---|---|
| TTTF | 400 | 2.7 | 120 | -7 | 81 | 5.1 |
| METTTF | 80 | 1.8 | 165 | -5.5 | 95 | 0.7 |

In Fig. 8.22 we show the normalized conductivities. Room-temperature values are for METTTF-TCNQ about 90 $(\Omega cm)^{-1}$ and for TTTF-TCNQ in the range 200-400 $(\Omega cm)^{-1}$. A broad maximum of $\sigma$ is observed at about 165K and 120K, respectively, and the maximum in slope of log $\sigma$ versus 1/T indicates phase transitions at 95K for the former and 81K for the latter compound.

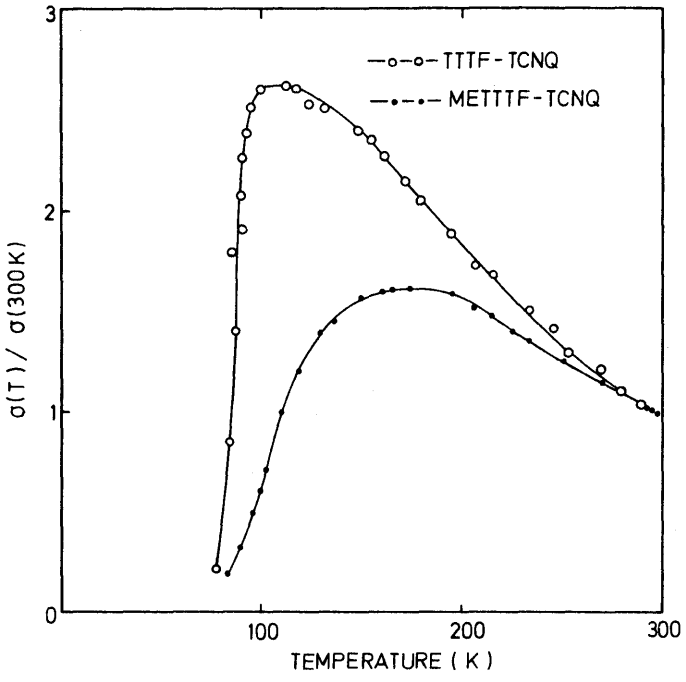


Fig. 8.22 Normalized conductivity of TTTF-TCNQ and METTTF-TCNQ |163|.

In Fig. 8.23 the thermopower of the two compounds is shown. Both materials show small negative values at room temperature, $S_{RT}$(TTTF-TCNQ) = -7 μV/K and $S_{RT}$ (METTTF-TCNQ) = -5.5 μV/K. The rather small magnitude of S suggests that both kind of stacks contribute comparably to the electrical transport. This also explains the high T temperature dependence: Since the magnitude of the intrinsic TEP corresponding to the individual stacks probably is large compared to the resulting one, only a small change in the $\sigma_A/\sigma_D$-ratio may give rise to relatively large changes in S. A similar S(T) behaviour is found in TMTTF-TCNQ, shown in Fig. 8.5.

Both of the compounds exhibit a change in slope of S(T) near the transition temperature ($T_c$). Below $T_c$ the materials are semiconducting, with the effective activation energies: Δ(TTTF-TCNQ) = 5.1 meV and Δ(METTTF-TCNQ) = 0.7 meV. Below 60K the materials indicate strong impurity dependence in S.

## 8.8 THERMOPOWER OF DBTTF-TCNQCl$_2$

Dibenzo-TTF-dichloro-TCNQ (DBTTF-TCNQCl$_2$) crystals were prepared at the Ørsted Institute by diffusive crystallization in an inverted U-tube |165|. The samples obtained were black needles of good quality and of typical size 2×0.2×0.02 mm$^2$. Chemically, DBTTF-TCNQCl$_2$ is analogous to TTF-TCNQ, namely a 1:1 donor-acceptor compound, and also the triclinic crystal structure consisting of uniform stacks is qualitatively similar |166|. The molecular design is shown in Fig. 8.24.

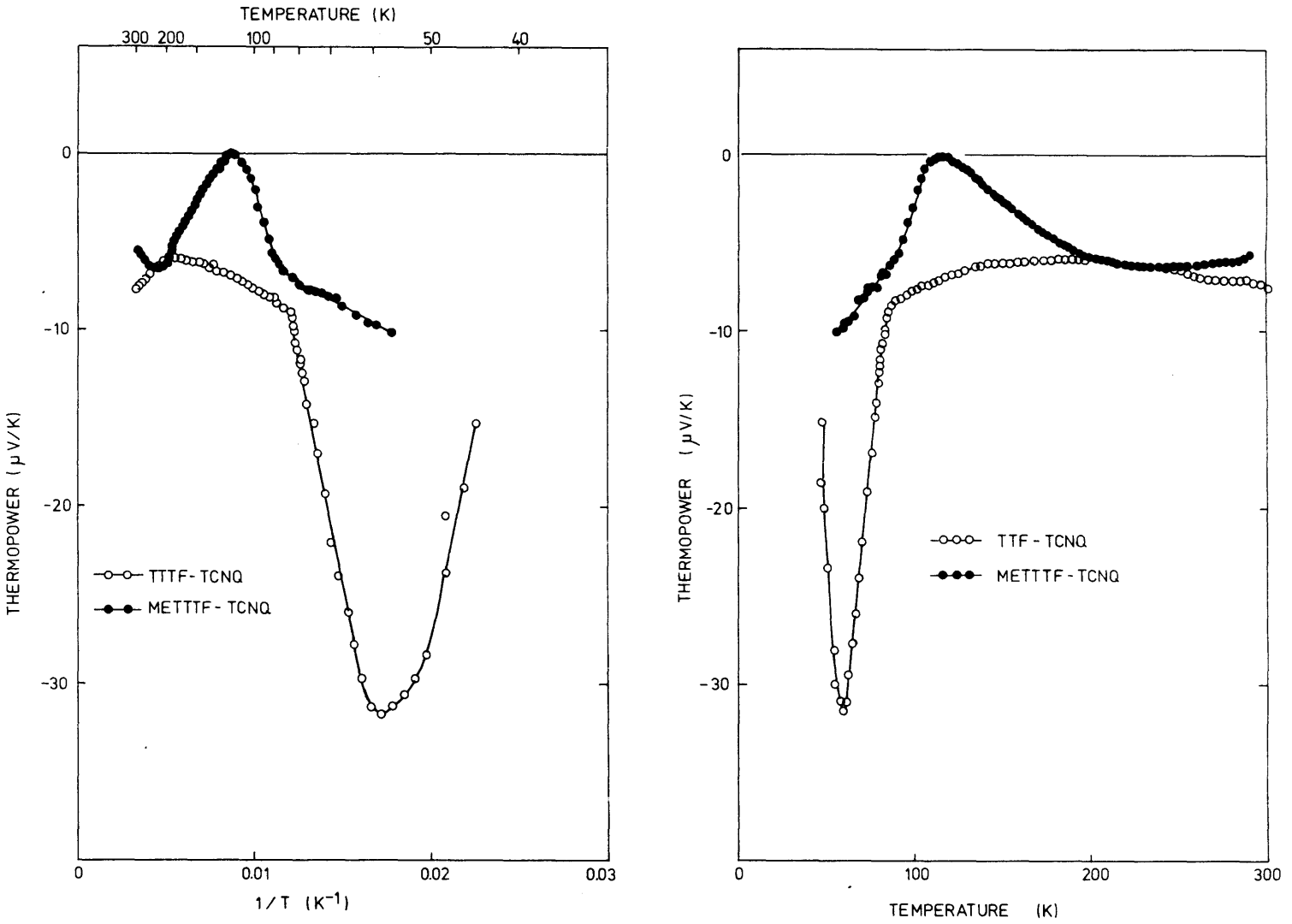


Fig. 8.23 Thermopower of TTTF-TCNQ and METTTF-TCNQ.

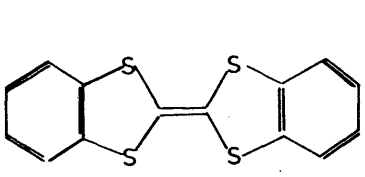

DBTTF

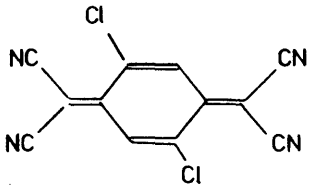


$TCNQCl_2$

Fig. 8.24 Constituent molecules

The substitution of chlorines for hydrogens in the acceptor stack gives rise to both steric and electronic changes |11|. The transport data given below indicate an essential reduction of the bandwidth. The overlap of the DBTTF molecules are, on the other hand, very similar to that in TTF-TCNQ.

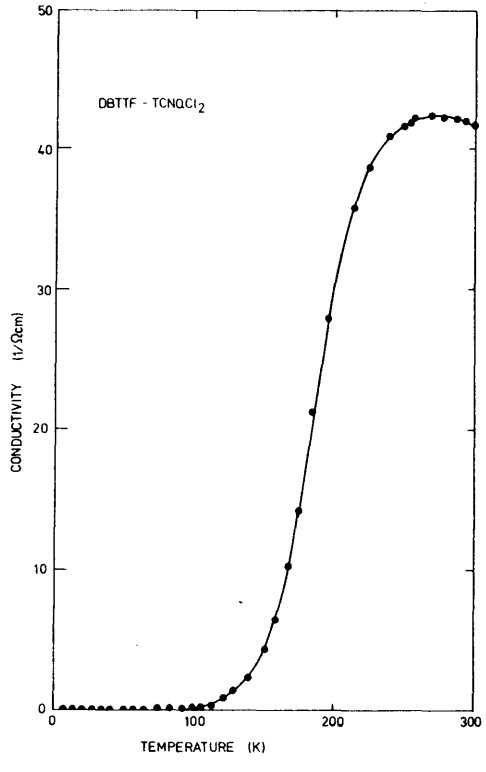


Fig. 8.25 Conductivity

The temperature dependent conductivity is shown in Fig. 8.25. The room-temperature value is approximately 40 $(\Omega cm)^{-1}$, and $\sigma$ rises by cooling a few percent to a broad maximum around 260K. Below 260K $\sigma$ falls off, and a maximum in the slope of $\ln\sigma$ versus $1/T$ indicates a phase transition at $T_c$ = 180K. Below $T_c$ a simple activated conductivity is observed with $E_a$ = 64 meV. The anisotropy is large, about 400 (35 GHz) at room temperature, and increases with decreasing temperature.

The thermopower of DBTTF-$TCNQCl_2$ is shown in Fig. 8.26. At 400K the TEP is 9μV/K, and S increases with decreasing temperature. Thus, DBTTF-$TCNQCl_2$ is not described simple by metallic bandpicture, which should show a TEP linear in T. This is further corroborated by the absolute value of the conductivity, which corresponds to a mean free path of order 1/10-1/20 lattice constant. In the plot of S versus 1/T in Fig. 8.26, two regimes can be identified, above and below 180K. Both regimes exhibit the semiconducting property, given in the form

$$S = S_o + \frac{k_B}{e} \frac{\Delta}{k_B T}$$

with the effective activation energies $\Delta(T > 180K) \simeq 14$ meV and $\Delta(T < 180K) \simeq 40$ meV. Both $\Delta$'s are smaller than the activation energy $E_a$ determined from conductivity. Below 100K, deviations from 1/T behaviour are found. The curvature is somewhat sample dependent, suggesting extrinsic domination. Also the conductivity is somewhat sample dependent below 100K.

The high-temperature variation of S could in principle arise from a metallic band behaviour. The $S \sim 1/T$ property should then result from the individual stack conductivities being of different temperature dependence. The positive sign of S thus suggests that the donor stacks become more dominating in transport as the temperature is lowered.

In order to confirm this simple metallic model, investigations on doped compounds of DBTTF-$TCNQCl_2$ should be done. By reasonable doping, the conductivity of a single type of stacks may be severely limited, thus leaving the macroscopic transport behaviour close to the intrinsic of the undoped stacks.

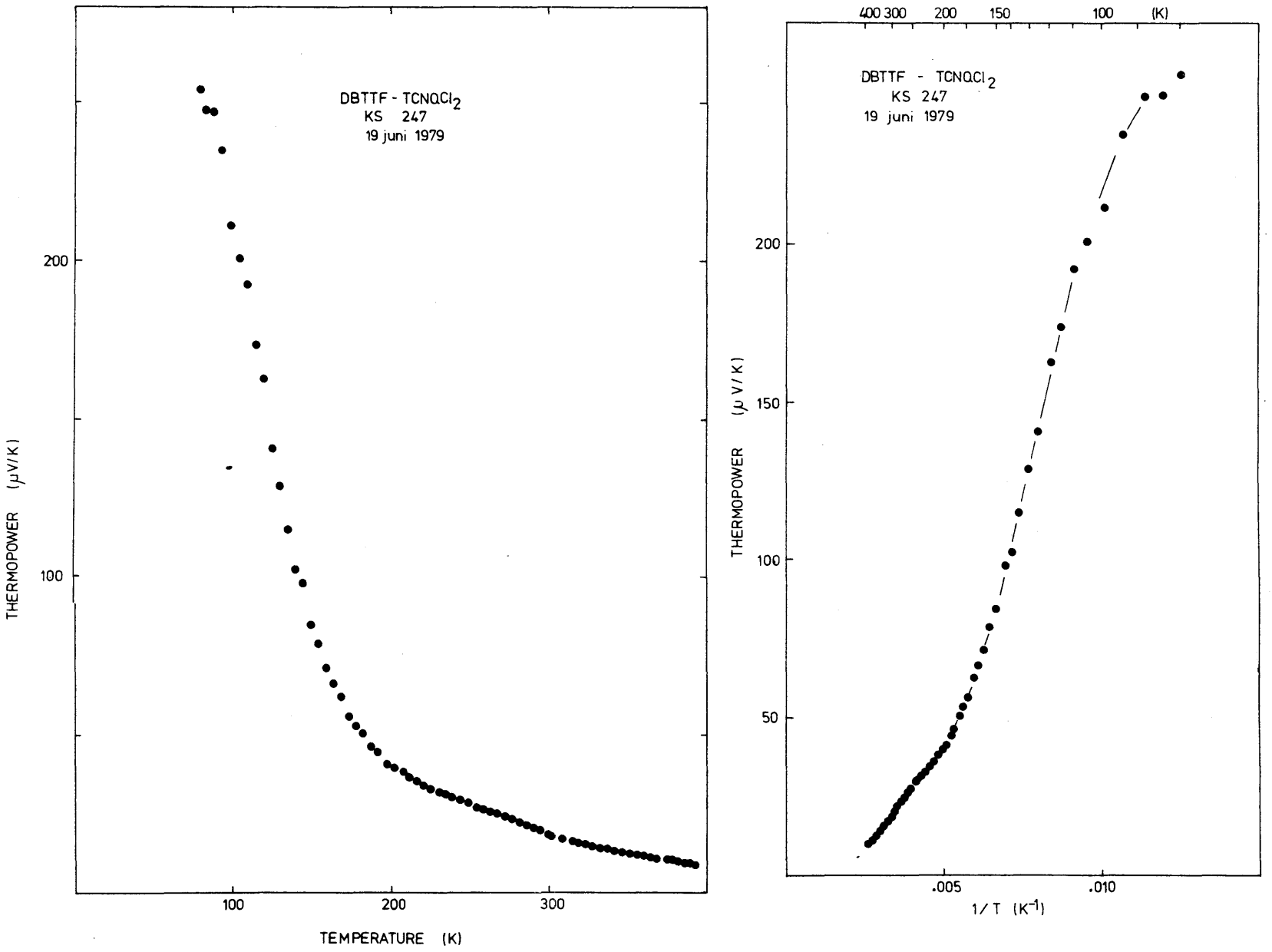


Fig. 8.26 Thermopower of DBTTF-$TCNQCl_2$

Another and more likely explanation for the high temperature $S \sim 1/T$ behaviour is given in a semiconducting picture. The electronic band gap need not be real, but could arise from fluctuations into the low temperature non-conducting state. The conductivity should in this picture be understood in view of an activated carrier density plus the strongly temperature dependent mobility known from the discussions in chapter 4 (see also ref. 116).

At 180K a phase transition into a semiconducting low temperature state is found in both the $\sigma$ and S behaviour. The paramagnetic susceptibility, however, does not exhibit any changes |165|. Thus the transition is not due to the Peierls mechanism. Instead we suggest that the carriers become localized because of strong on-site Coulomb repulsion, corresponding to a $4k_F$ transition.

## CHAPTER IX

## SUMMARY AND CONCLUSIONS

The experimental thermoelectric data shown in chapter VIII show several common properties. Generally the coherent conducting compounds have a linear S versus T dependence above the phase transition. It should be noticed, though, that many of these highly conducting compounds has a change in the S versus T slope around 100-150K. This change is especially abrupt in TMTSF-DMTCNQ, but is also clearly marked in the other TMTSF-compounds investigated. In 8.2 it was discussed whether the S(T) behaviour at 140K in TMTSF-DMTCNQ is related to a $4k_F$-anomaly. However, no $4k_F$-scattering is seen in the other TMTSF-compounds, and other explanations should therefore be investigated. Since several TMTSF-salts have shown superconductivity |167,168|, an attractive explanation would be based on superconducting fluctuations. Fluctuations into superconducting behaviour will result in a reduced thermopower, just as it is seen. However, more detailed studies of independent parameters must be done to clarify this. In compounds which are known to be influenced by impurities or disorder, a non-linear S(T) behaviour appears in the same temperature region. Another explanation of the 100-150K anomalies in the thermopower would therefore be a change in the scattering mechanism involved. In TTF-TCNQ the change in the S(T) slope is very smooth, and is most probably resulting from fluctuations into the insulating Peierls state.

The materials of low conductivity show a thermoelectric power that is either activated, $S \sim 1/T$, or large and temperature-independent. The former behaviour is due to semiconducting band-carriers, whereas the latter is for carriers in localized states.

Thus, the thermopower is a very good indicator of the properties of the charge-carriers and the related conduction mechanism, namely whether the conduction is coherent, activated or due to hopping between localized states. The conductivity in its own is less informative, since the carrier concentration, if activated as well as the mobility (see chapter IV) may be distinctly

temperature dependent. Furthermore the conductivity is very sensitive to breaks in the chains as opposed to the thermopower.

From the discussions in chapter IV concerning the scattering mechanism in highly conducting organic compounds, it is still not clear which mechanism, if any particular, dominates. It appears from the discussion that the problem is even more complicated as a result of the relatively large compressibility of organic materials. None of the analysis in chapter IV, however, refute scattering due to interaction with acoustic modes to be the most important one, as it is in classical metals.

Assuming this to be the case, measurements of the thermopower gives valuable information of the bandwidth, charge transfer and Fermi-energy. Typical bandwidths for the highly conducting compounds are between 0.5 eV and 1.5 eV. For the low-temperature semiconducting state, the thermopower indicates that the conduction is mainly due to impurities.

Finally it has been shown that from systematic studies of thermopower and conductivity, it is possible to deduce intrinsic transport parameters above $T_c$ of a single stack.

REFERENCES AND NOTES

1. Organic Conductors and Semiconductors Siofok 1976, Lecture Notes in Physics 65, Springer N.Y. 1977.
2. Quasi one-dimensional conductors I Dubrovnik 1978, Lecture Notes in Physics 95, Springer N.Y. 1979.
3. Quasi one-dimensional conductors II Dubrovnik 1978, Lecture Notes in Physics 96, Springer N.Y. 1979.
4. Synthesis and Properties of Low-Dimensional Materials, Ed. J.S. Miller, A.J. Epstein, Ann. New York Academy of Science 313, (1978).
5. Molecular Metals, Ed. W.E. Hatfield, Plenum Press 1979.
6. Low Dimensional Cooperative Phenomena, ASI, Summer School, Starnberg 1974, Ed. H.J. Keller, Plenum Press B7, N.Y. 1975.
7. One Dimensional Conductors, GPS Summer School, Lecture Notes in Physics 34, Springer N.Y. 1975.
8. Chemistry and Physics of One-Dimensional Metals, ASI Summer School, Bolzano 1976, Ed. H.J. Keller, Plenum Press B25, N.Y. 1977.
9. Physics and Chemistry of Low-Dimensional Solids, ASI Summer School, Tomar 1979, Ed. L. Alcacer, Plenum Press.
10. Highly Conducting One-Dimensional Solids, Ed. J.T. Devreese, R.P. Evrard, V.E. van Doren, Plenum Press, N.Y. 1979.
11. I.F. Shchegolev, Phys. Stat. Sol. a12, 9 (1972).
12. A.J. Berlinsky, Contemp. Phys. 17, 331 (1976).
13. G.A. Tombs, Physics Reports 40, 181 (1978).
14. R.H. Friend, D. Jerome, J. Phys. C: Solid State Phys. 12. 1441 (1979).
15. A.J. Heeger, Comments Solid State Phys. 9, 65 (1979).
16. J.M. Ziman, Principles of the Theory of Solids, Cambridge 1972.
17. J.M. Ziman, Electrons and Phonons, Oxford Press 1960.
18. R.E. Peierls, Quamtum Theory of Solids, Oxford Press 1955.
19. R.D. Barnard, Thermoelectricity in Metals and Alloys, Taylor and Francis 1972.
20. D.K.C. MacDonald, Thermoelectricity: An introduction to the principles, Wiley 1962.
21. R.P. Heubener, Thermoelectricity in Metals and Alloys, Solid State Phys. 27, 64 (1972).

22. H. Fröhlich, Proc. R. Soc. A233, 296 (1955).
23. Ziman, Chapter 5 in ref. 16.
24. M.J. Rice, S. Strässler, Solid State Comm. 13, 125 (1973).
25. S.K. Chan, V. Heine, Jou. Phys. F: Metal Phys. 3, 795 (1973).
26. P.A. Lee, T.M. Rice, P.W. Anderson, Phys. Rev. Lett. 31, 462 (1973) and Solid State Comm. 14, 703 (1974).
27. R. Comes, G. Shirane, p. 17-67 in ref. 10.
28. A.J. Berlinsky, J.F. Carolan, L. Weiler, Solid State Comm. 15, 795 (1974).
29. C.S. Jacobsen, Kell Mortensen, K. Bechgaard, J.R. Andersen, Phys. Rev. B18, 905 (1978).
30. A.J. Epstein, S. Etemad, A.F. Garito, A.J. Heeger, Phys. Rev. B5, 952 (1972).
31. K. Bechgaard, C.S. Jacobsen, Kell Mortensen, H.J. Pedersen, N. Thorup, Solid State Comm.,
32. L.B. Coleman, M.J. Cohen, D.J. Sandman, F.G. Yamagishi, A.F. Garito, A.J. Heeger, Solid State Comm. 12, 1125 (1973).
33. J. Bardeen, Solid State Comm. 13, 357 (1973).
34. D. Allender, J.W. Bray, J. Bardeen, Phys. Rev. B9, 119 (1974).
35. P.W. Anderson, P.A. Lee, M. Saitoh, Solid State Comm. 13, 595 (1973).
36. D.B. Tanner, C.S. Jacobsen, A.F. Garito, A.J. Heeger, Phys. Rev. Lett. 32, 1301 (1974) and
C.S. Jacobsen, D.B. Tanner, A.F. Garito, A.J. Heeger, Phys. Rev. Lett. 33, 1559 (1974).
37. M.B. Salamon, J.W. Bray, G. DePasquali, R.A. Graven, G. Stucky, A. Schultz, Phys. Ref. B11, 619 (1975).
38. R.P. Groff, A. Suna, R.E. Merrifield, Phys. Rev. Lett. 33, 418 (1974).
39. P.M. Chaikin, J.F. Kwak, T.E. Jones, A.F. Garito, A.J. Heeger, Phys. Rev. Lett. 31, 601 (1973).
40. J.R. Cooper, M. Miljak, G. Delplanque, D. Jerome, M. Weger, J.M. Fabre, L. Giral, Jou. Physique 38, 1097 (1977).
41. M.J. Cohen, L.B. Coleman, A.F. Garito, A.J. Heeger, Phys. Rev. B10, 1298 (1974).
42. U. Bernstein, P.M. Chaikin, P. Pincus, Phys. Rev. Lett. 34, 271 (1975).
43. M. Weger, Solid State Comm. 19, 1149 (1976).

44. S. Shitzkovsky, M. Weger, H. Gutfreund, Jou. Phys. 39, 711 (1978).
45. See f.ex. Ziman, Chapter 3.4 in ref. 16.
46. B.I. Bennett, F. Herman, Chem. Phys. Lett. 32, 334 (1975).
47. F. Herman, A.R. Williams, K.H. Johnson, J. Chem. Phys. 61, 3508 (1974).
48. T.E. Philips, T.J. Kistenmacher, A.N. Bloch, D.U. Cowan, J.C.S. Chem. Comm. 1976, 334 (1976).
49. A.N. Bloch, D.O. Cowan, K. Bechgaard, R.E. Pyle, R.H. Bands, T.O. Poehler, Phys. Rev. Lett. 34, 1561 (1975).
50. T.J. Kistenmacher, T.E. Philips, D.O. Cowan, Acta Cryst. B30, 763 (1974).
51. DC-Conductivity measurements were made by C.S. Jacobsen, except that regards to $(TMTTF)_2$-$PF_6$ |158| and TTTF-TCNQ and METTTF-TCNQ |163|.
52. See f.ex. Ziman, chapt. 7 in ref. 16 and chapter 7+9 in ref. 17.
53. H. Fritzsche, Solid State Comm. 9, 1813 (1971).
54. See f.ex. Ziman, p. 104 in ref. 17.
55. N.F. Mott, H. Jones, Theory of the Properties of Metals and Alloys 1936, p. 308.
56. See f.ex. E.H. Sondheimer, Proc. Roy. Soc. A193, 484 (1948).
57. A.V. Gold. D.K. C. MacDonald, W.B. Pearson, I.M. Templedon, Phil. Magazine 5, 765 (1960).
58. M. Kohler, H. Neckar, Zeit. Phys. 126, 495 (1949).
59. L. Nordheim, C.J. Borter, Physica 2, 383 (1935).
60. M. Kohler, Zeit. Phys. 126, 481 (1949).
61. P.M. Chaikin, R.L. Green, S. Etemad, E. Engler, Phys. Rev. B13, 1627 (1976).
62. M. Weger, Tomar 1979, p. 77 in ref. 9.
63. J.R. Cooper, Phys. Rev. B19, 2404 (1979).
64. M. Weger, J. Friedel, Jou. Physique 38, 241 (1977).
65. N.O. Lipari, M.J. Rice, C.B. Duke, R. Bozio, A. Girlando, C. Pecile, Int. Jou. Quant. Chem., Quant. Chem. Symp. 11, 583 (1977).
66. M.J. Rice, C.B. Duke, N.O. Lipari, Solid St. Comm.: 17, 1089 (1975).
67. See f.ex. Ziman, chapter 1 in ref. 17.

68. H. Morawitz, Phys. Rev. Lett. 34, 1096 (1975).
69. R.E. Merrifield, A. Suna, Phys. Rev. Lett. 36, 826 (1976).
70. G. Shirane, S.M. Shapiro, R. Comes, A.F. Garito, A.J. Heeger, Phys. Rev. B14, 2325 (1976).
71. S.M. Shapiro, G. Shirane, A.F. Garito, A.J. Heeger, Phys. Rev. B15, 2413 (1977).
72. E.M. Conwell, Dubrovnik - conference, p. 270 in ref. 2.
73. This mobility is twice the value given by Conwell |72|, who used a wrong density of states. Furthermore, Conwell used $\rho=0.55$.
74. J.R. Cooper, D. Jerome, M. Weger, S. Etemad, Jou. Physique Lett. 26, L-219 (1975).
75. H. Gutfreund, M. Weger, Phys. Rev. B16, 1753 (1977).
76. E. Conwell, private communication.
77. H.A. Mook, C.R. Watson, Phys. Rev. Lett. 801 (1976).
78. A. Girlando, C. Pecile, Spect. Acta 29A, 1859 (1973).
79. R. Bozio, A. Girlando, C. Pecile, Chem. Phys. 21, 257 (1977).
80. M.J. Rice, N.O. Lipari, Phys. Rev. Lett. 38, 437 (1977).
81. E.M. Conwell, Phys. Rev. Lett. 39, 777 (1977).
82. N.O. Lipari, C.B. Duke, L. Pietronero, Jou. Chem. Phys. 65, 1165 (1976).
83. See f.ex. ref. 65 and the references cited therein.
84. The expression (4.69) was first published by E. Conwell |81|. It should be notized, however, that there in |81| are some misleading printors errors.
85. R. Comes, S.M. Shapiro, G. Shirane, A.F. Garito, A.J. Heeger, Phys. Rev. Lett. 35, 1518 (1975).
86. Kell Mortensen, C.S. Jacobsen, K. Bechgaard, J.R. Andersen, Dubrovnik-conference, p. 159 in ref. 2.
87. P.M. Chaikin, J.F. Kwak, R.L. Green, S. Etemad, E.M. Engler, Solid State Comm. 19, 1201 (1976).
88. See f.ex. J.R. Torrance, Bolzano 1976, p.137 in ref. 8.
89. S. Etemad, T. Pennye, E.M. Engler, B.A. Scott, P.E. Seiden, Phys. Rev. Lett. 34, 741 (1975).
90. P.E. Seiden, D. Cabib, Phys. Rev. B13, 1846 (1976).
91. P.E. Seiden, P.M. Grant, Dubrovnik 1978, p. 130 in ref. 2.
92. See f.ex. Ziman, chapter 4.6 and 9.14 in ref. 17.
93. L.O. Gor'kov, I.E. Dzyaloshinskii, JETP Lett. 18, 401 (1973).

94. P.M. Chaikin, J.F. Kwak, A.J. Epstein, Phys. Rev. Lett. 42, 1178 (1979).
95. E.M. Conwell, A.J. Epstein, M.J. Rice, Dubrovnik 1978, o. 204 in ref. 2.
96. See f.ex. N.I. Meyer, Halvledere, Pol. Forl. 1969.
97. A.J. Heeger, Solid St. Phys. 23, 283 (1969).
98. J. Kondo, Solid St. Phys. 23, 183 (1969).
99. See f.ex. Ziman, chap. 9.13 in ref. 17.
100. H. Gutfreund, M. Kaveh, M. Weger, Dubrovnik 1978, p. 105 in ref. 2.
101. A.J. Heeger, M. Weger, M. Kaveh, Dubrovnik 1978, p. 316 in ref. 2.
102 M. Kaveh, H. Gutfreund, M. Weger, Phys. Rev. B18, 7171 (1978).
103. M. Kaveh, Phys. Rev. B15, 3788 (1977).
104. D.B. Tanner, C.S. Jacobsen, A.F. Garito, A.J. Heeger, Phys. Rev. B13, 3381 (1976).
105. C.S. Jacobsen, Dubrovnik 1978, p. 223 in ref. 2.
106. P. Pincus, Low Dim. Cooperative Phen. 1974, p. 1 in ref. 6.
107. F. Denoyer, R. Comes, A.F. Garito, A.J. Heeger, Phys. Rev. Lett. 35, 445 (1975).
108. J. Hubbard, Proc. Roy. Soc. Lond. A276, 238 (1963).
109. A.J. Epstein, E.M. Conwell, D.J. Sandmann, J.S. Miller, Solid State Comm. 23, 355 (1977).
110. G. Beni, Phys. Rev. B10, 2186 (1974).
111. G. Beni, C.F. Coll III, Phys. Rev. B11, 573 (1975).
112. J.F. Kwak, G. Beni, P.M. Chaikin, Phys. Rev. B13, 641 (1976).
113. E.M. Conwell, Phys. Rev. B18, 1818 (1978).
114. P.M. Chaikin, A.F. Garito, A.J. Heeger, Phys. Rev. B5, 4966 (1972 and Jou. Chem. Phys. 58, 2336 (1973).
115. A.N. Bloch, R.B. Weisman, C.M. Varma, Phys. Rev. Lett. 28, 753 (1972).
116. A.J. Epstein, E.M. Conwell, Solid State comm. 24, 627 (1977).
117. N.F. Mott, Phil. Mag. 19, 835 (1977).
118. V.K.S. Shante, Phys. Rev. B16, 2597 (1977).
119. Adam Lewis, Phys. Rev. B13, 1855 (1976).
120. J.F. Kwak, G. Beni, Phys. Rev. B13, 652 (1976).

121. R.A. Bari, Phys. Rev. B9, 4329 (1974) and Phys. Rev. B10, 1560 (1974).
122. P.M. Chaikin, G. Beni, Phys. Rev. B13, 647 (1976).
123. G. Beni, J.F. Kwak, P.M. Chaikin, Solid State Comm. 17, 1549 (1975).
124. D. Ihle, T. Eifrig, Phys. Stat. Solid, b91, 135 (1979).
125. See f.ex. K.-D. Schotte, Zeitsch. Phys. 196, 393 (1966).
126. L.I. Buravov, D.N. Fedutin, I.F. Shchegolev, Sov. Phys. JETP 32, 612 (1971).
127. A.J. Epstein, J.S. Miller, Solid State Comm. 27, 325, (1978).
128. See f.ex Bernard, Chapter 2 in ref. 19.
129. P.M. Chaikin, J.F. Kwak, Rev. Sci. Inst. 46, 218 (1975).
130. L.L. Sparks, R.L. Powell, Temperature, Its measurements and control in science and industry 149, 1569 (1972).
131. J.H. Hust, R.L. Powell, L.L. Sparks, Temperature, Its. measurements and control in Science and Industry 145, 1525 (1972).
132. R.M. Gibbons, Chapt. 12 in "Cryogenic Funda", ed: G.G. Haselden, Academic Press 1971.
133. R.P. Huebener, Phys. Rev. 135, A1281 (1964).
134. A.M. Guénault, D.G. Hawksworth, J. Phys. F, Metal Phys. 7, L219 (1977).
135. See also ref. 39, 61 and 87.
136. Yaffa Tomkiewicz, A.R. Raranko, J.B. Torrance, Phys. Rev. Lett. 36, 751 (1976).
137. A. Andrieux, H.J. Schulz, D. Jerome, K. Bechgaard, Phys. Rev. Lett. 43, 227 (1979) and Jou. Physique Lett. 40, L385 (1979).
138. S.K. Khanna, H.P. Pouget, R. Comes, A.F. Garito, A.J. Heeger, Phys. Rev. B16, 1468 (1977).
139. See f.ex. A.J. Heeger, Bolzano 1976, p. 87 in ref. 8.
140. Kell Mortensen, unpublished results.
141. P.M. Chaikin, R.L. Green, E.M. Engler, Solid State Comm. 25, 1009 (1978).
142. L. Carlsen, K. Bechgaard, C.S. Jacobsen, I. Johanssen, Jou. Chem. Soc. 862, 1979.

143. J.R. Andersen, Thesis: Organic Metals, A study of interstack interactions Risø Reports 379.
144. D. Jérome, M. Weger, Bolzano 1976, p. 341 in ref. 8.
145. The conductivity-measurements were done by Dr. C.S. Jacobsen.
146. D.O. Cowan, A.N. Bloch, T.O. Poehler, T.J. Kistenmacher, J.P. Ferraris, T.E. Philips, K. Bechgaard, R. Gemmer, V.V. Walatka, R.E. Pyle, W. Krug, C. Hu, R. Banks, Bull. Am. Phys. Soc. 20, 415 (1975). Results published by V.K.S. Shante, J. Phys. C. Sol. St. Phys. 11, 2461 (1978).
147. A.N. Bloch, T.F. Carruthers, T.O. Poehler, D.O. Cowan, Bolzano 1976, p. 47 in ref. 8.
148. K. Bechgaard, T.J. Kistenmacher, A.N. Bloch, D.O. Cowan, Acta Crystall B33, 417 (1977).
149. T.E. Philips, T.J. Kistenmacher, A.N. Bloch, J.P. Ferraris, D.O. Cowan, Acta Crystall B33, 422 (1977).
150. G. Rindorf, H. Soling, N. Thorup, Private communication.
151. J.P. Pouget, R. Comés, K. Bechgaard, Tomar 1979, To be published in ref. 9.
152. Y. Tomkiewicz, J.R. Andersen, A.R. Taranko, Phys. Rev. B17, 1579 (1978).
153. A. Andrieux, P.M. Chaikin, C. Doroure, D. Jérome, C. Weyl, K. Bechgaard, J.R. Andersen, Preprint.
154. C. Weyl, E.M. Etemad, K. Bechgaard, G. Jehanno, S. Etemad, Solid State Comm. 19, 925 (1976).
155. R. Comes, Ann. N.Y. Acad. Sci., p. in ref. 4.
156. A.N. Bloch, Tomar 1979.
157. C.S. Jacobsen, J.R. Andersen, K. Bechgaard, C. Berg, Solid State Comm. 19, 1209 (1976).
158. P. Delhaes, C. Coulon, J. Amiel, S. Flandrois, E. Torreilles, J.M. Fabre, L. Giral, Mol. Cryst. Liq. Cryst. 50, 43 (1979).
159. The anisotropy measurements versus T were done using MW-technique by H.J. Pedersen.
160. K. Bechgaard, C.S. Jacobsen, J.R. Andersen, Solid State Comm. 25, 875 (1978).
161. T.J. Kistenmacher, N.Y. Academy of Science 1977, p. 333 in ref. 4.

162. K. Carneiro, Tomar, Poster Session.
163. G. Keryer, J. Amiell, S. Flandrois, P. Delhaes, E. Torreilles, J-M. Fabre, L. Giral, Dubrovnik 1978, p. 65 in ref. 2.
164. D. Chasseau, J. Gaultier, C. Hauer, J-M. Fabre, L. Giral, E. Torreilles, Dubrovnik 1978, p. 359 in ref. 2.
165. C.S. Jacobsen, H.J. Pedersen, Kell Mortensen, K. Bechgaard, J. Phys. C, Solid St. Phys. 13, 3411 (1980).
166. G. Rindorf, H. Soling, N. Thorup, Acta. Cryst. 1980.